Title
THE EXCITATION OF UNNATURAL-PARITY STATES IN 24Mg,20Ne AND 16O BY INELASTIC a SCATTERING.

Author
Reed, Mary.

Publication Date
1968-08-01

University of California

Ernest O. Lawrence Radiation Laboratory

THE EXCITATION OF UNNATURAL-PARITY STATES IN ^{24}Mg, ^{20}Ne AND ^{16}O BY INELASTIC α SCATTERING

Mary Reed
(Ph.D. Thesis)
August 1968

Berkeley, California

UCRL-18414

UNIVERSITY OF CALIFORNIA
Lawrence Radiation Laboratory
Berkeley, California

AEC Contract No. W-7405-eng-48

THE EXCITATION OF UNNATURAL-PARITY STATES IN ^{24}Mg, ^{20}Ne AND ^{16}O BY INELASTIC α SCATTERING

Mary Reed

(Ph. D. Thesis)

August 1968

THE EXCITATION OF UNNATURAL-PARITY STATES IN ^{24}Mg, ^{20}Ne AND ^{16}O BY INELASTIC α SCATTERING

Contents

I. INTRODUCTION

An opportunity to study processes that are normally neglected in direct reaction models is found in the excitation of unnatural-parity states in even-even nuclei by inelastic α scattering. (An unnatural-parity state in an even-even nucleus is one in which the parity $\pi \neq (-)^J$, where J is the spin of the state. For example a 2- or a 3+ state would be of unnatural parity.) The study of the excitation of these states by α particles is particularly useful in the study of reaction mechanisms because the excitation is forbidden under the assumptions that are often made in direct reaction models -- a single scattering involving a central interaction with a well-defined transfer of angular momentum.[1] Spin and parity considerations forbid simple one-step direct interaction mechanisms. Therefore, if these unnatural-parity states are excited it must be by more complicated processes. Since in the excitation of natural-parity states (states in which $\pi = (-)^J$) both simple and complicated processes are involved, the study of unnatural-parity levels will yield a better understanding of inelastic scattering in general. The subject of this research is the study of the excitation of these states with the goal of understanding the reaction mechanisms involved.

Previous work[2-8] has shown that the unnatural-parity 2- levels in ^{16}O and ^{20}Ne and the 3+ levels in ^{24}Mg and ^{28}Si are sometimes made with relatively large cross sections in inelastic scattering of α-particles, even though their excitation by simple single-step interactions is forbidden. The average differential cross sections are a few tenths of millibarns to a few millibarns per steradian. In fact, for large-angle scattering the magnitudes of the differential cross sections are about equal to those of the elastic and natural-parity states. These experimental cross sections and angular distributions have been interpreted by means of various reaction mechanism models. For example, some experimental results suggested that compound nucleus effects dominated the excitation while other experiments indicated a multiple excitation mechanism played an important role. However, there was no one specific mechanism that seemed to explain all the data. In some cases the results suggested that competing reaction mechanisms were involved.

All of these previous experiments were carried out at incident α-particle energies of 42 MeV or below. In the present series of experiments the bombarding energy range was increased in several steps to 80 MeV for ^{16}O and ^{20}Ne and to 120 MeV for ^{24}Mg, in order to gain further information of the means of excitation of unnatural-parity states.

A. Inelastic α Scattering

Inelastic α scattering is of particular interest as a spectroscopic tool for studying excited nuclear energy levels because of its special reaction properties. α particles are spinless projectiles. They are strongly absorbed by the nucleus and thus can lead to compound nucleus reactions. They can also participate in direct surface reactions. (A direct nuclear reaction is one in which the interaction between the projectile and the target takes place in the time necessary for the projectile to travel through the nucleus, or approximately 10^{-22} seconds.) A direct reaction can be contrasted with a compound nucleus reaction, in which the projectile enters the nucleus, shares its energy with the target nucleons, and then the nucleus reemits a particle. Since in direct reactions only one or a few of the degrees of freedom of the nucleus are altered, they are particularly useful in studying low energy nuclear states--states which differ from the ground state in one or a few simple ways.

If the excitation producing a certain state is a simple, one-step mechanism, the spin and parity of the state can often be determined from the angular distribution.[9] For a α scattering at energies well above the Coulomb barrier, the angular distributions are characterized over a large part of the angular range by strong, regular oscillations which arise because α particles are strongly absorbed by the nucleus. The particles that are scattered must therefore have been involved in <u>surface</u> interactions, and the oscillations produced in the angular distributions are analogous to the interference effects seen when light is scattered from the edge of a black disk. A model of inelastic diffraction scattering based on these ideas has been developed by Drozdov[10] and Inopin[11] and extended by Blair.[9]

In Blair's model[9] the differential cross sections for the first few levels are as follows:

$$\frac{d\sigma}{d\Omega}(\text{elastic}) = (k\ R_0^2)^2 \left[\frac{J_1(x)}{x}\right]^2$$

$$\frac{d\sigma}{d\Omega}(0 \to 0+) = (k\ R_0^2)^2\ \frac{\beta_0^2}{4\pi}\ J_0(x)^2$$

$$\frac{d\sigma}{d\Omega}(0 \to 2+) = (k\ R_0^2)^2\ \frac{\beta_2^2}{4\pi} \left\{\frac{1}{4} J_0(x)^2 + \frac{3}{4} J_2(x)^2\right\}$$

$$\frac{d\sigma}{d\Omega}(0 \to 3-) = (k\ R_0^2)^2\ \frac{\beta_3^2}{4\pi} \left\{\frac{3}{8} J_1(x)^2 + \frac{5}{8} J_3(x)^2\right\}$$

$$\frac{d\sigma}{d\Omega}(0 \to 4+) = (k\ R_0^2)^2\ \frac{\beta_4^2}{4\pi} \left\{\frac{9}{64} J_0(x)^2 + \frac{20}{64} J_2(x)^2 + \frac{35}{64} J_4(x)^2\right\}$$

where k is the wave number, R_0 the effective radius, the β's are deformation parameters, the J's are cylindrical Bessel functions and $x = kR\theta$, or more accurately $x = QR_0$, with $Q = |\vec{k}_i - \vec{k}_f|$. The excitation of 1- states by inelastic scattering is forbidden by selection rules. Figure 1 shows these angular distributions. At large angles the odd and even J's approach sines and cosines and thus give rise to different phases in the differential cross sections. If the maxima of the oscillations in the angular distributions for one level correspond to the maxima in another, the distributions are said to be "in-phase". If the maxima of one correspond to the minima of another, the distributions are "out-of-phase." All the positive parity levels will be "in-phase" with each other and "out-of-phase" with the negative parity levels. This is basically a small angle model: nevertheless it still gives good qualitative results even at fairly large angles. It also makes use of the adiabatic assumption. Q is taken to be the same for all energy levels. Thus if the energy of the level is not very small compared with the beam energy, the model will not be applicable without modification.

In the asymptotic region the phase behaviour of the angular distribution can sometimes be used to determine the parity of a level. Blair[9] has pointed out that the differential cross section for a positive parity level produced by a single scattering will oscillate "out-of-phase" with the cross

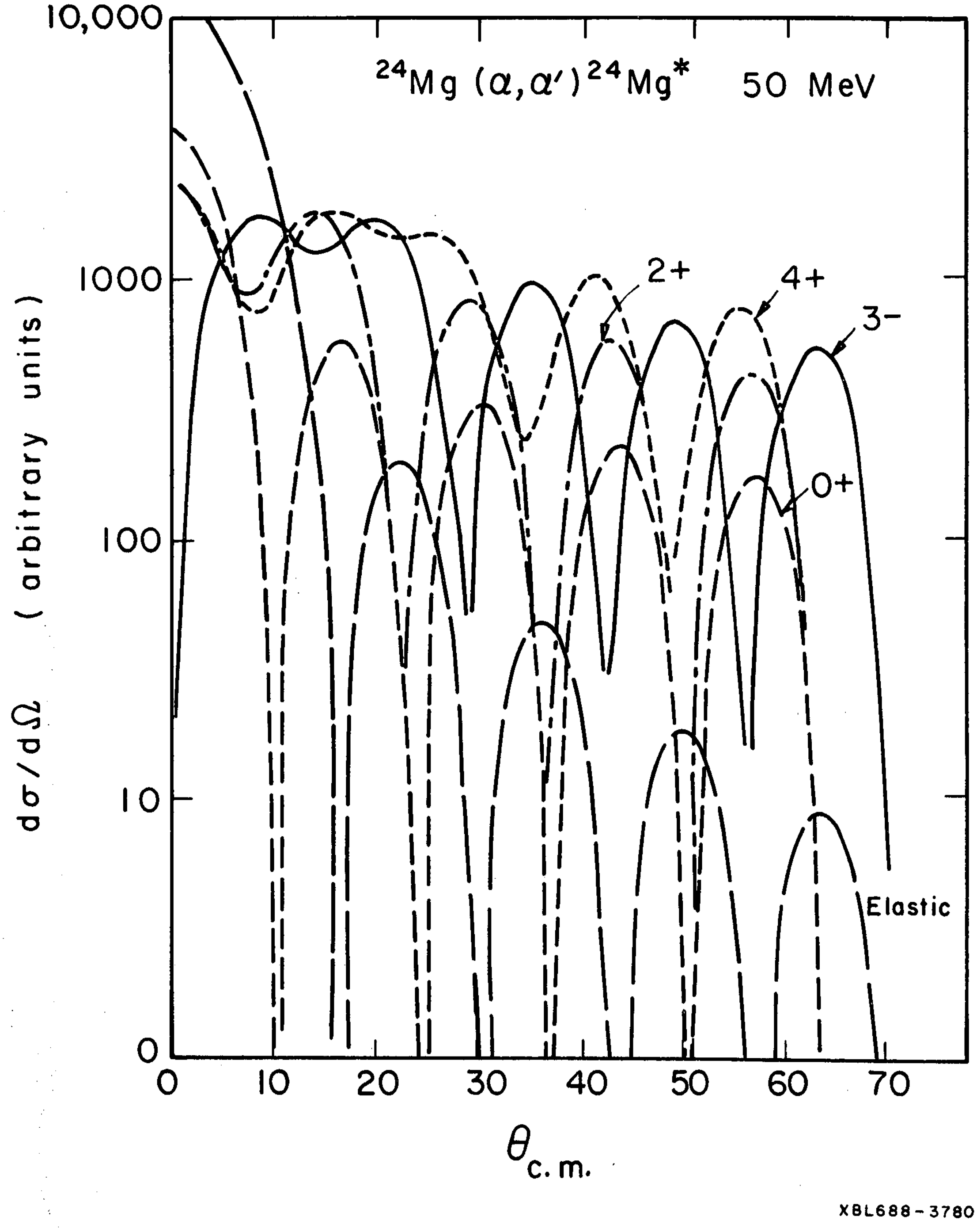

Fig. 1. Blair's inelastic diffraction model cross sections.

section for elastic scattering, and a negative parity level will be "in-phase" with the elastic. If the reaction mechanism is more complicated than a single scattering, these phase relationships will not hold. For light elements, the asymptotic region is not really reached, so the phase behavior will only approach that described above. Also in light elements these pure distributions are even less valid because the adiabatic assumption (here meaning degenerate energy levels) is not well met.

The angular momentum transfer involved in exciting a state can sometimes be determined by the behavior of the first few oscillations in the differential cross section. For a simple, single scattering on an even-even target nucleus this angular momentum transfer will be equal to the spin of the state. In the special case of a medium weight or heavier target, $E_\alpha \geq 30$ MeV, and not too strong coupling between states, the first few oscillations in the differential cross section will behave as follows: The region where the first minimum in the cross section would be expected to fall will be filled for a 2+ state. For a 4+ state the first and second minima positions will be filled in with the cross section breaking into regular oscillations at larger angles. Similar differences at small angles occur between negative parity states of different spins.

Austern and Blair[12] have developed a generalized diffraction model that treats both single and double excitation. This theory is applicable if the projectile is strongly absorbed by the target nucleus and if the angular momentum transfers are much smaller than the angular momenta that are important for the partial wave expansions. Thus it should be a good model for α scattering at medium energies. However in this model the excitation of unnatural-parity states is forbidden to all orders. This model makes an assumption that leads to this selection rule. It approximates the successive steps of angular momentum transfer to the nucleus as taking place at the same angular location. For spinless projectiles it has the consequence that for double excitation as well as for single excitation, only states of natural-parity may be excited. This selection rule results from the fact that the momentum transfer in the first scattering is $|\vec{k}_i - \vec{k}'|$, where k_i is the initial wave number, and k' is the intermediate wave number. The momentum transfer in the second scattering is $|\vec{k}' - \vec{k}_f|$, where k_f is the final wave number. Since both scatterings occur at the same radius R, the degrees of freedom allowed in the scattering are limited. The two angular momenta in the double scattering can add only in such a way as to give natural-parity states.

Rost and Austern[13] and Bassel et al.[14] have interpreted the inelastic scattering of medium energy α particles as a direct reaction using the distorted waves theory. They found that a deformed potential-well interaction based on the collective model of the nucleus gives results in good agreement with experiment. The parameters of the potential well are determined by fitting the elastic scattering. The multipole deformations are then obtained from the magnitudes of the inelastic cross sections. This model describes simple one-step processes. It treats the elastic scattering as the dominant process, and inelastic events are treated as perturbations.

It has been shown by Cohen[15] and many others that inelastic α scattering preferentially excites states which involve collective motions of many nucleons. These are states which involve rotations or vibrations of the nuclear surface. The moment of inertia of the best rotational case is much less than that of a solid body implying that not all of the nucleons take part in the deformation or rotation. A rotation in this sense is a wave of nuclear matter moving around a central core of the nucleus. The type of vibration of interest here is a motion of the nuclear surface. McDaniels et al.[17] have shown that vibrational levels are excited when a nucleus is bombarded with α particles. Experimentally Harvey et al.[16] have shown that rotational levels in ^{152}Sm and ^{154}Sm are excited by inelastic α scattering.

In deformed even-even nuclei the first few levels will correspond to a rotational band having a level sequence 0+, 2+, 4+, etc. with energies approximately proportional to $J(J + 1)$.[18] Rotational bands can also be built on vibrational levels or levels involving the excitations of single nucleons.

B. Unnatural-Parity States

As was mentioned previously, states of unnatural-parity are of particular interest because they cannot be produced in inelastic α scattering by a simple single scattering interaction. This can be illustrated in the following way: The conservation of parity and angular momentum lead to the relationship

$$\pi_f = (-)^L \pi_i$$

where the π's refer to the parity of the initial and final states, and L is the angular momentum transfer. The total spin of the final nucleus, J_f, will be the vector sum of the transferred angular momentum and the spins of the incident particle and target nucleus,

$$\bar{J}_f = \bar{L} + \bar{J}_\alpha + \bar{J}_t$$

Both the α particle and an even-even target nucleus have 0+ (J) ground states. Therefore, $J_f = L$, and the parity of the final state will be

$$\pi_f = (-)^{J_f}$$

giving a natural-parity state.

The cross sections of the unnatural-parity states that have been measured show that sometimes they are produced with fairly large amplitudes. How can this be explained? Eidson and Cramer[1] have pointed out that an unnatural-parity state could theoretically be produced by any mechanism involving the interplay of two different angular momenta. This can be illustrated in the following way. If L_1 and L_2 are the two transfers of angular momentum involved, for an α particle incident on an even-even target nucleus, the final spin and parity will be

$$\overline{J_f} = \overline{L_1} + \overline{L_2} \text{ and } \pi_f = (-)^{L_1+L_2}$$

For example if $L_1 = 2$ and $L_2 = 3$, possible J_f values will be 5, 4, 3, 2 and 1, and the parity would be $(-)^5 = (-)$. In this way a 2- or a 4- unnatural-parity state could be produced.

Eidson and Cramer[1] have suggested several possible processes for the production of unnatural-parity states involving the coupling of two angular momenta:

(1) Double scattering. The two angular momenta would be the angular momentum transfers in the two scatterings. It has been found experimentally that for levels that are known to be made primarily by double excitation the envelope of the angular distribution falls off more slowly with scattering angle than that of the elastic angular distribution or that for a single excitation process. There is also a phase reversal for each simple excitation.

(2) Compound Nucleus formation and decay. Here it would be the initial and final relative orbital angular momenta which are separated in time that could couple to produce the unnatural-parity state. Compound nucleus processes would be expected to give total cross sections and angular distributions that vary greatly with small changes in incident α-particle energy.
(3) A spin-orbit interaction. In this case the coupling would be between the orbital angular momentum of the incident α particle and the spin of one or more of the target nucleons. For example a proton spin flip of $\Delta s = 1$ resulting from a change of orbital of the proton from $d_{5/2}$ to $d_{3/2}$ could couple with an orbital angular momentum $\ell = 1$ or 3 to produce a 2- unnatural parity state in the following way:

$$\vec{J}_f = \vec{\ell} + \vec{s} = 2 \quad \text{and} \quad \pi_f = (-)^{\ell} = (-).$$

(4) An exchange process, e.g. knock-out or target-stripping. Knock-out can be thought of as a coupling of the relative angular momentum of the knocked-out α particle with the angular momentum of the initial system to give the final unnatural-parity state. This would be expected to give a forward peaking in the angular distribution. For target-stripping it would be the angular momentum of the stripped core and α particle which couples with that of the initial system to produce the unnatural-parity state. A target stripping interaction would be expected to give backward peaking for the scattered α particles. Honda and Ui[19] have discussed the exchange effects in the scattering of α particles by light nuclei. They found a weakly angle dependent contribution to the scattering amplitude from heavy particle stripping which would tend to fill in the valleys in the oscillations in the differential cross section and would cause the diffraction peaks to alternate in magnitude.

C. Previous Data

Until recently experimental results have been available at only a few incident α-particle energies, with the work being done at 42 MeV and below. A short summary of this previous work follows: The states of interest will be

$$2- \text{ at } 8.875 \text{ MeV in } {}^{16}O,$$

2- at 4.969 MeV in ^{20}Ne,[20]
3+ at 5.228 MeV in ^{24}Mg,
3+ at 6.27 MeV in ^{28}Si.[21]

(1) Braithwaite et al.[2] have studied ^{24}Mg between E_α = 15.0 and 24.5 MeV. Their results show widely varying angular distribution shapes and large fluctuations in the excitation function indicating possible compound nucleus contributions.

(2) Eidson and Cramer[1] studied ^{24}Mg and ^{28}Si at 22.5 MeV incident α-particle energy. Their angular distributions indicated interference effects, suggesting contributions from both multiple excitation and exchange processes.

(3) Bingham[3] studied ^{28}Si at E_α = 16.2 to 27.0 MeV and his results suggested that a knock-out mechanism may be important in the production of the unnatural-parity state.

(4) Kokame et al.[4] studied all the levels at E_α = 28.5 MeV. Their results indicate multiple excitation in the reaction mechanism.

(5) For ^{24}Mg Vincent, Boschitz and Priest[5] at E_α = 42 MeV found a diffraction pattern in the angular distribution and an enhanced cross section for large angle scattering, suggesting that exchange effects may play a role in this excitation. Recently, a theoretical analysis of their data leads them to consider a multiple excitation process.[6]

(6) Malmin et al.[7] also studied the ^{24}Mg state at 40.175 MeV and found that the angular distribution had pronounced diffraction peaks consistent with the data of Vincent et al.[5]

(7) Work by Blair et al.[8] on ^{16}O suggests large compound nucleus contributions for E_α = 35.4 to 41.0 MeV.

In all cases in this previous work to produce unnatural-parity states by α scattering, the angular distributions showed oscillatory behavior with periods approximately the same as those of the oscillations in the elastic and natural-parity state angular distributions, although the phase relationships were, in general, not clear or consistent at all angles. In order to gain further information on the mechanism of these reactions a study of the unnatural-parity levels in ^{24}Mg, ^{20}Ne and ^{16}O at higher α-particle energies was undertaken.

II. EXPERIMENTAL PROCEDURES

In these experiments the 88-inch Variable Energy Cyclotron at the Lawrence Radiation Laboratory in Berkeley was used to accelerate α particles to the desired energy.[22]

A. Beam Optics

These experiments were done in the 36-inch scattering chamber. Figure 2 shows a layout of the cyclotron and beam transport system. The beam was extracted from the cyclotron and focused at a point midway between the cyclotron and switching magnet by adjusting the currents in a quadrupole doublet magnet. For the quadrupole doublets used in these experiments the first element was radially focusing and vertically defocusing, and the second element was radially defocusing and vertically focusing, giving an overall focusing effect in both planes. The beam was then bent through 57 degrees by the switching and analyzing magnet and focused at the analyzing slit. The switching magnet is a circular pole, uniform field magnet with normal entry and exit. A quartz plate was placed in the beam line at the analyzing slit position, and the fluorescent glow produced when the beam hit it was displayed on a television screen in the cyclotron control room. This made it possible to obtain a good focus at the analyzing slit. The slit was set to a width of approximately 0.060 inches allowing passage of a nearly monoenergetic beam (approximately 0.1% $\Delta E/E$).

The beam then went down the beam pipe through the concrete shielding into Cave 1. A radial focus was then made at the center of the scattering chamber by adjusting the currents in a second quadrupole doublet magnet. The fluorescence of a quartz plate was used to determine the quality of the focus at the target position. The beam was steered to the center of rotation of the scattering chamber by means of a very small correcting field in a magnet placed between the analyzing slit and the quadrupole lens.

The scattering chamber was aligned so that the centered beam fell upon the center of a split Faraday cup approximately four feet beyond the target position. The current readings on each side of the Faraday cup were balanced and held constant during the experiments to minimize any shifts in the beam

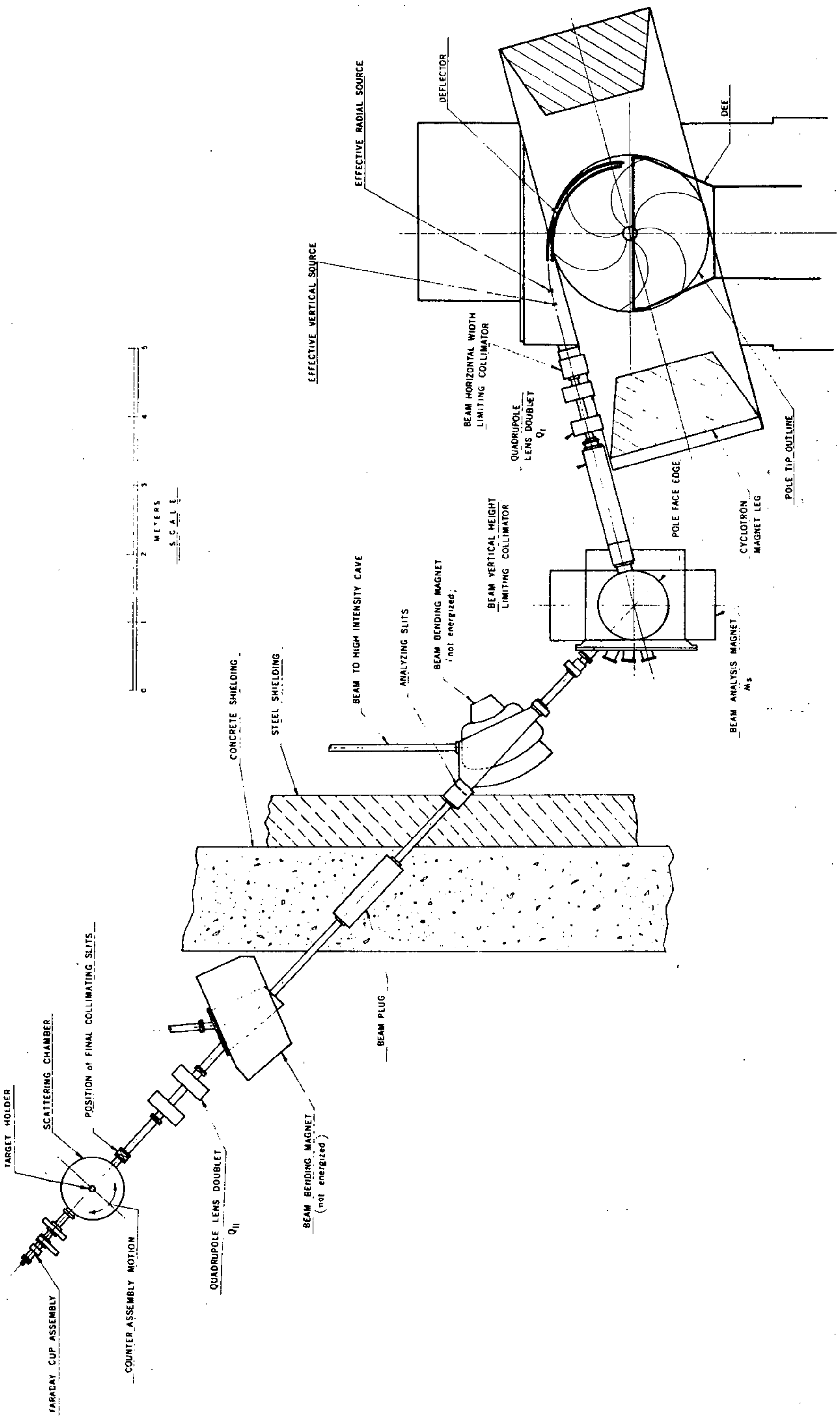

XBL 689-5857

Fig. 2. Diagram of the 88-inch Cyclotron and Cave 1.

angle in passing through the target at the center of the scattering chamber.

The effective source has the following characteristics:[23]

Radial	73.5" upstream from quadrupole 1 (Q1)
	~0.016" = 0.41 mm full width at half maximum intensity
	0.034 radians full angle of divergence
Vertical	~61" upstream from Q1
	0.45" = 11.4 mm full height
	0.0088 radians full angle of divergence.

The beam leaves the cyclotron and is transported down a beam pipe to Q1.

Beam optics calculations are handled by matrix algebra.[24,25] Multiplying the matrix for the beam transport element times the column vector representing the particle will give the new representation of the position and angle of the particle.

The quadrupole excitation ϕ is defined as

$$\phi = L\ ((dB/dx)/B\rho)^{1/2}$$

where $B\rho = \dfrac{\text{momentum of particle}}{\text{charge of particle}}$

and dB/dx = Field gradient in gauss/inch.

To account for the fringing field of the elements of the quadrupole doublet the magnetic field was assumed to extend one inch on either side of each element. For the switching magnet the field was assumed to extend 2.5 inches beyond the physical pole edge on either side.

The matrices representing the first quadrupole doublet, Q1, with the quadrupole excitations $\phi_1 = 0.667$ and $\phi_2 = 0.580$ are, in the radial plane (r)

$$M_r = \begin{pmatrix} .0014 & 28.40 \\ -.0351 & 1.531 \end{pmatrix}$$

and in the vertical plane (v)

$$M_v = \begin{pmatrix} 1.882 & 30.92 \\ -.0143 & .2964 \end{pmatrix}$$

The matrices for the switching magnet are

$$M_r = \begin{pmatrix} .5446 & 34.64 \\ -.0203 & .5446 \end{pmatrix}$$

and

$$M_v = \begin{pmatrix} 1 & 41.09 \\ 0 & 1 \end{pmatrix}$$

The overall matrices from the effective sources to the focus near the analyzing slit are

$$M_r = \begin{pmatrix} 1.906 & .1974 \\ .0382 & .5267 \end{pmatrix}$$

and

$$M_v = \begin{pmatrix} -1.773 & .260 \\ -.0143 & -.5616 \end{pmatrix}$$

The top right hand elements should be zero for a focus; however these calculations were carried out by hand and represent only an approximate fit to the physical situation. This accounts for the small, but non-zero values in the matrices. These elements give a magnification of 1.906 in the radial plane and -1.773 in the vertical plane.

The matrices for the quadrupole doublet in Cave 1, Q11, with the excitations $\phi_1 = 0.494$ and $\phi_2 = 0.496$ are

$$M_r = \begin{pmatrix} .4385 & 29.88 \\ -.0098 & 1.463 \end{pmatrix}$$

$$M_v = \begin{pmatrix} 1.456 & 29.83 \\ -.0102 & .4777 \end{pmatrix}$$

The matrices from the focus near the analyzing slit to the focus in the scattering chamber are

$$M_r = \begin{pmatrix} -1.379 & -.290 \\ -.0098 & -.7273 \end{pmatrix}$$

and

$$M_v = \begin{pmatrix} -.584 & .700 \\ -.0102 & -1.700 \end{pmatrix}$$

The overall matrices from the source to the focus in the scattering chamber are

$$M_r = \begin{pmatrix} -2.639 & -.4249 \\ -.0465 & -.3850 \end{pmatrix}$$

$$M_v = \begin{pmatrix} 1.025 & -.5449 \\ .0424 & .9520 \end{pmatrix}$$

These give magnifications at the target of -2.639 in the radial plane and 1.025 in the vertical plane. Figure 3 shows the results of the beam optics calculations.

In phase space the particles can be characterized by an emittance, e, which is equal to 4rr' in the radial plane, where r is the particle's distance from the optic axis and r' is the angle it makes with the axis. In the vertical plane the emittance is 4vv' where the v's have similar definitions. At the source we have

$$e_r = 13.8 \text{ mm-mradians.}$$

and

$$e_v = 100.7 \text{ mm-mradians.}$$

Using a radial collimator width of 3/4 inch 65 inches from the effective radial source and a vertical collimator 1 inch in height 110 inches from the radial source gives the radial emittance at the target

$$e_r = 3.17 \text{ mm-mradians.}$$

The vertical collimator does not limit the beam so its emittance remains the same as that at the source

$$e_v = 100.7 \text{ mm-mradians.}$$

The energy resolution of the beam can be calculated using the formula[24]

$$\frac{\Delta E}{E} = \frac{2MS}{R(1 - \cos\theta) + d\sin\theta}$$

where M is the magnification from the effective source to the analyzing slit, S is the radial width of the effective source, R is the radius of curvature of the trajectory in the analyzing magnet, θ is the angle of

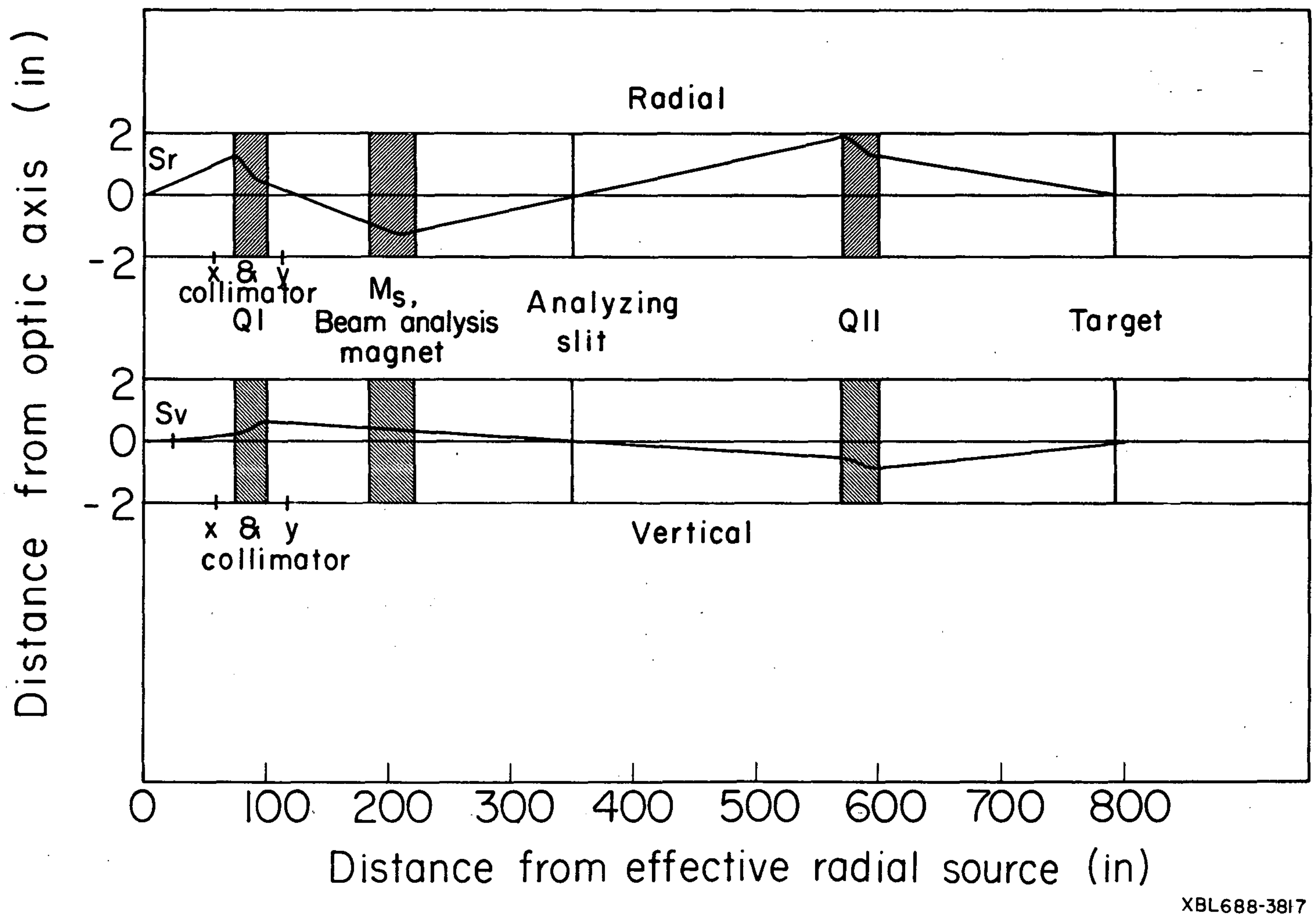

Fig. 3. Beam optics for Cave 1.

deflection through the magnet and d is the distance from the magnet to the analyzing slit. Substituting in the numbers used in these experiments gives

$$\frac{\Delta E}{E} = \frac{2 \times 1.906 \times .016}{41.3(1 - .5446) + 125 \times .8390} = 4.931 \times 10^{-4}$$

or

$$\frac{\Delta E}{E} = .0493\%$$

This gives 25 keV resolution for a 50 MeV α-particle beam. Experimentally, a resolution better than 0.08% has never been observed for the Cave 1 beam. Almost certainly the discrepancy is due to the large uncertainty in the width of the effective radial source.

B. Scattering Chamber

The scattering chamber was 36 inches in diameter and approximately 12 inches high. A diagram of it and associated equipment is shown in Figure 4. Either a solid target holder or a gas target could be placed at the center of the chamber. The detectors were in boxes that were clamped to a circular ring on the floor of the chamber which rotated about the center of the chamber. The detector boxes were thermally connected to a freon refrigeration system with the expansion tube in the scattering chamber. The compressor and the remainder of the system were outside the chamber, and the freon was fed into the expansion tube by flexible hoses. The target height and angle and the counter angle could be changed by remote controls from the counting area. The monitor detector was placed in a port in the equatorial plane at an angle of 20° to the beam direction. A foil wheel in the beam line between the scattering chamber and the Faraday cup was used to determine the beam energy by measuring the ranges of the α particles in aluminum. The range was taken to be the thickness of aluminum where the beam transmitted through the absorbers was one-half of its maximum value. The range-energy tables of Williamson, Boujot and Picard[26] were used. The tables were considered accurate to 2%.

C. Targets

For the ^{24}Mg experiments the targets were self-supporting foils of

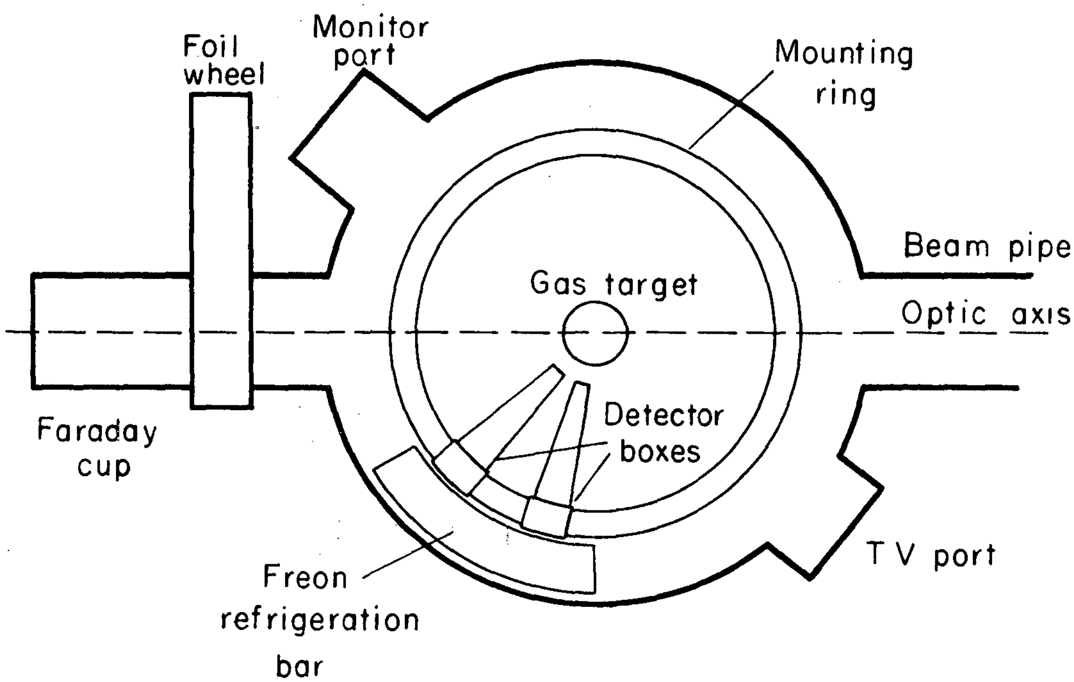

XBL 688-3768

Fig. 4. Diagram of the 36-inch scattering chamber and equipment.

isotopically enriched (to 99.96%) ^{24}Mg from .4 to 1.6 mg/cm^2 thick prepared at our laboratory by evaporation techniques. The separated isotope was obtained from Oak Ridge. For the ^{20}Ne and ^{16}O experiments gas targets were used. The neon was isotopically enriched (99.2% ^{20}Ne), obtained from Mound Laboratories, and the oxygen was reagent grade natural oxygen (99.8% ^{16}O), obtained from the Linde Company. The gas target assemblies were cylindrical. They consisted of a stainless steel frame surrounded by 0.0001" thick havar foil.* The pressure of the gas in the cell could be controlled from outside the scattering chamber. Typically a pressure of 1/3 atmosphere was used. Four solid targets or one gas target and one solid target could be placed in the chamber at one time. These different targets could be placed in the beam at the center of the chamber by means of remote controls in the counting area. The major impurities in the gases were carbon and oxygen; however, their peaks in the energy spectra could be separated from the target peaks at most angles.

D. Detectors

The angular distributions of the α particles scattered from the target were measured by using lithium-drifted silicon detectors.[27,28] They were mounted on a table in the chamber which could be rotated to any desired angle. A single collimator near the detector was used in the solid target experiments, while a double collimator was used with the gas target system. The detectors were cooled to -25° C during the experiments with the freon refrigeration system. Lithium-drifted silicon detectors produce a pulse proportional to the energy of the particle they absorb; thus they give a measure of both the scattering angle and the energy of the particle. The detectors used varied in thickness from 1.5 - 3.0 mm depending on the energy of the α-particle beam in the experiment. They were made especially for these experiments at our laboratory.[29] Two detectors 20° apart were used simultaneously in the chamber for the gas target experiments, and four detectors 2° apart were used for the ^{24}Mg experiments.

*Hamilton Watch Company

E. Electronics

Figure 5 is a block diagram of the electronics system. The pulses produced in the detector were amplified first by a pre-amplifier inside the scattering chamber, then they were amplified further by a linear amplifier. They were then put through a biased amplifier where the bottom of the signal was cut off and they were amplified five times, increasing the sensitivity of the system. The linear amplifier was an 11 × 1980P-2 Goulding-Landis system.[30] Since more than one detector was in use, the signals were fed through a mixer and then routed into one of the 1024 channel groups of a 4096 Channel Nuclear Data 160 pulse height analyzer. Thus four energy spectra (data for four angles) could be measured simultaneously. The dead time in the detector and electronics system was measured by feeding pulses from a pulser into each preamplifier. The pulser was triggered by the monitor detector, and the percent dead time was determined by summing the number of counts in the pulser peaks in the spectrum and comparing this to the number of pulses put into the system, recorded by a scaler.

F. Data Analysis

The spectra were then transferred from the pulse height analyzer into a small computer -- a PDP-5 manufactured by Digital Equipment Corporation. The memory size was 8000 12-bit words. Once the data were transferred to the computer the pulse height analyzer was free to accumulate further data while initial data reduction was carried out with the computer. A Cal-Comp plotter was used in connection with the computer to plot the energy spectra. The computer also displayed the spectra on an oscilloscope screen, and a light pen was used to sum the counts in the individual peaks and to type out the number of counts in the separate channels. The differential cross sections in the center-of-mass system were obtained from the number of counts in an individual peak and the number of microcoulombs collected in the Faraday cup by using the formula

$$\left(\frac{d\sigma}{d\Omega}\right)_{C.M.} = \frac{\text{counts}}{\mu\text{coulomb}} \times J \times G \quad \text{mb/sr}$$

where J is the Jacobian for the transformation from the laboratory to the

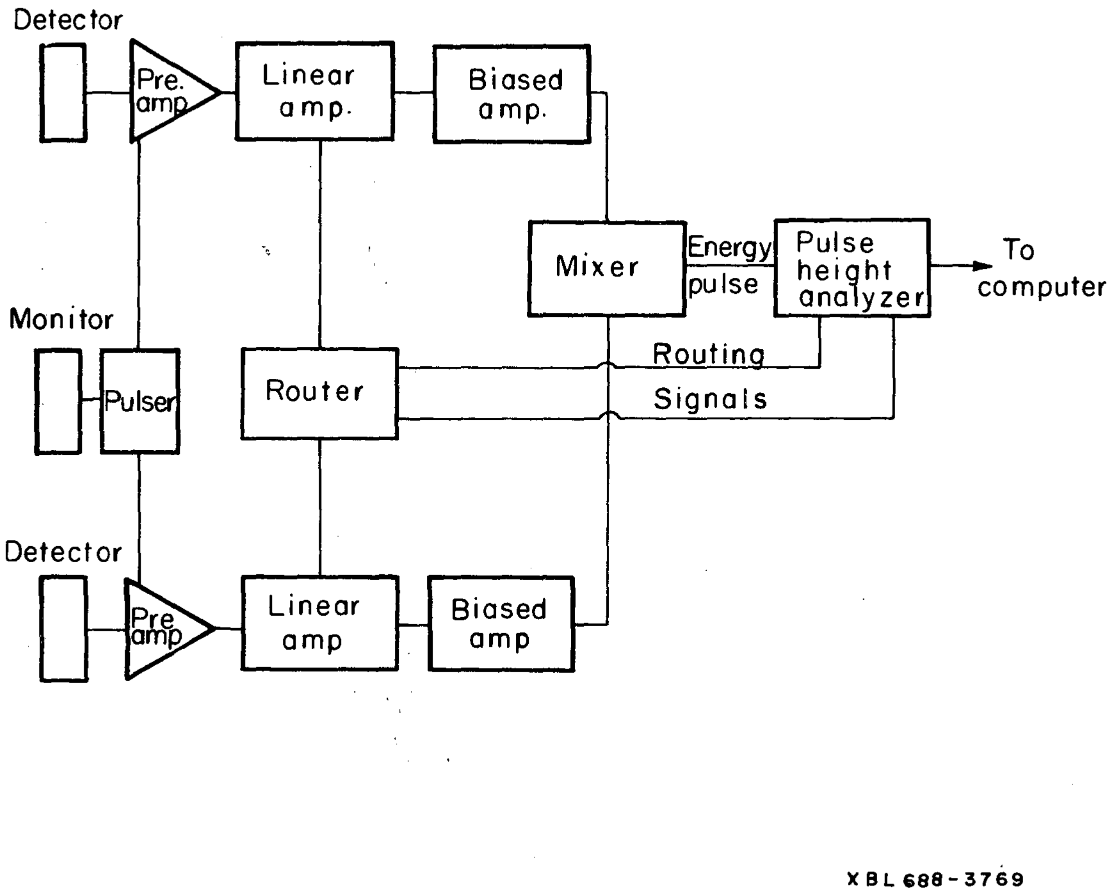

Fig. 5. Block diagram of electronics system used in α-scattering experiments.

center-of-mass system and G is the geometry and target thickness factor.

(1) Solid target. The geometry factor is given by

$$G = 5.32 \times 10^{-7} \left(\frac{1}{\Omega}\right) \frac{A \cos \phi}{T}$$

where Ω is the solid angle of the counter collimator, A is the atomic weight of the target, ϕ is the angle of the target with respect to the beam direction, and T is the target thickness in mg/cm^2.

(2) Gas target. The geometry factor is given by

$$G = 3.32 \times 10^{-6} \frac{(t + 273)(\ell_1 + \ell_2)^2 \sin \theta}{Pn\, w_1\, w_2\, h_2\, (1 + \ell_1/\ell_2)}$$

where t is the gas temperature in degrees Centigrade, ℓ_1 is the distance from the center of the gas target to the rear of the front collimator, ℓ_2 is the distance from the rear of the front collimator to the front of the counter collimator, θ is the laboratory scattering angle, P is the pressure in cm of mercury, n is the number of target atoms per molecule, w_1 and w_2 are the widths of the front and rear collimators and h_2 is the height of the rear collimator.

The approximations made in the derivation of the gas target geometry factor are (1) that the widths of the two collimators are approximately equal, (2) that the lengths ℓ_1 and ℓ_2 are approximately equal and much larger than the collimator widths and thicknesses, (3) that the scattering angle θ is much greater than $\tan^{-1} \frac{w_1 + w_2}{2\,\ell_2}$ which is itself greater than $\tan^{-1} \frac{w_2 - w_1}{2\ell_2}$ and that (4) $\ell_1 \sin\theta$ is much greater than $\ell_1 \cos \theta$.[31] Using these approximations in the exact formula reduces it to that given above.

Fortran programs were used to calculate these differential cross sections on the computer. If the peaks were not fully resolved an IBM-7094 computer program[32] was used to fit Gaussian peaks to the components and obtain the number of counts in each peak. By plotting the differential cross sections at the various angles, angular distributions of the scattered α particles were obtained.

G. Energy Resolution

There are many factors which influence the energy resolution obtained in an experiment. Moss and Ball have discussed most of them and given formulas for their calculation.[33] The factors which were taken into account in these calculations were the spread in the beam energy obtained from the cyclotron (see section IIA), beam convergence and beam width at the target, counter collimator slit width, target thickness, energy straggling in the target, multiple scattering and electronic noise. Of these beam convergence, beam width, collimator slit width and target thickness depend upon kinematics. For thin solid targets the contributions from target thickness introducing an angular spread at the detector is negligible.

Comparisons of theoretical contributions to energy resolution and experimentally determined values for both 50 and 120 MeV α particles are given in Table 1. In calculating the energy spread of the beam the best experimental value for the resolution, 0.08%, was used. The contributions from the different sources were added as the sum of their squares. The square root was then assumed to be the theoretical value. Since all of the contributions are not gaussian this method introduced errors in the calculated energy resolution. The rather large discrepancies found between the theoretical values and the experimental values could arise from several factors. In the 120 MeV experiment two 3 mm silicon detectors in series were used to measure the energy of the scattered α particles. The particles had to pass through the dead layer of the first counter to reach the sensitive region of the detectors. The dead layer has been estimated to be 0.015 - 0.030 mm in thickness. Undoubtedly the energy straggling and multiple scattering in this dead layer are the major factors in the large discrepancies between experimental and theoretical energy resolution for the 120 MeV case. The quality of the beam in a particular experiment may not have been as good as the best obtained value. The beam width may have been larger than the calculated value. The 120 MeV experiment was done in a different beam line. An additional bend and a closer quadrupole doublet magnet gave a larger value for the beam convergence and a correspondingly larger energy spread. The counting rate may have been high enough to give pile-up of pulses in the electronics system and subsequent loss of

Table I. Contributions to energy resolution.

Case	1	2	3	4
Beam Energy (MeV)	50	50	120	120
Target Angle with Respect to Beam (deg)	90	45	90	60
Effective Target Thickness (mg/cm^2)	1.62	2.29	1.62	1.87
Scattering angle (deg)	30	76	30	76
Contributing Factor (keV)				
Beam Energy Spread (.08%)	40	40	96	96
Beam Convergence (.26°)	36	57	87	182
Beam Width (.042 in.)	24	51	58	123
Collimator Slit Width (.060 in.)	38	60	91	144
Target Thickness (<.0006 in.)	~0	~0	~0	~0
Energy Straggling in Target	53	63	53	57
Multiple Scattering in Target	17	33	17	30
Electronic Noise	50	50	70	70
$\Delta E_{theoretical}$	103	136	191	295
$\Delta E_{experimental}$	115	162	305	456

resolution. The detectors used could have been of poor quality. A bad detector can cause as many as several hundred keV spread in the peaks in an energy spectrum.

III. EXPERIMENTAL RESULTS

A. ^{24}Mg

The reaction $^{24}Mg(\alpha,\alpha')^{24}Mg^*$ was studied at α-particle energies of 50.0, 65.7, 81.0 and 119.7 MeV. Figure 6 shows the energy level diagram for the low-lying states of ^{24}Mg.[34,35] A typical energy spectrum for the 50 MeV case can be seen in Figure 7. The peaks can be seen to be fairly well resolved. The energy resolution is 180 keV full-width-at-half-maximum. The experimental angular distributions for the lowest-lying energy levels at the various energies are shown in Figures 8 to 11. The 50 MeV data of Hendrie et al.[36] are included. They used a thin target (~350 μg/cm^2) and were able to separate the 2+, 4+ doublet at 4.12 and 4.23 MeV. In the experiments described here a thick target (1.62 mg/cm^2) was used to obtain the necessary statistics for the weakly excited unnatural-parity 3+ state. The cross sections for scattering particles of the various energies to the elastic, first 2+, second 4+ and unnatural-parity 3+ are shown in Figures 10-13 plotted versus momentum transfer times the interaction radius, $|\vec{k}_i - \vec{k}_f| \times R$, or QR. In Blair's formulas[9] for the differential cross sections for single excitation α scattering, the argument of the Bessel function is QR. (See section II.A.) The oscillatory behavior of the cross section is determined completely by the Bessel functions. If the differential cross sections to make the same final state for different α particle bombarding energies are plotted versus QR, the oscillations in the cross section should lie at the same values of QR. Thus compatible curves will be obtained. In this way different incident α-particle energy results can be compared directly. Figure 12 shows that the elastic angular distributions line up very well when plotted in this way. Figure 13 shows that similar agreement is obtained for a natural-parity level that is made primarily by a simple single-step interaction. For a 4+ state which is expected to be made primarily by double excitation the oscillations also line up very well as can be seen in Figure 14. However, for the 3+ state, Figure 15, no such agreement is found. The 42 MeV data of Vincent, Boshitz and Priest[5] are also included here. It can be seen that the rather pronounced large-angle oscillations at 42 MeV tend to become damped out and then two very broad peaks appear

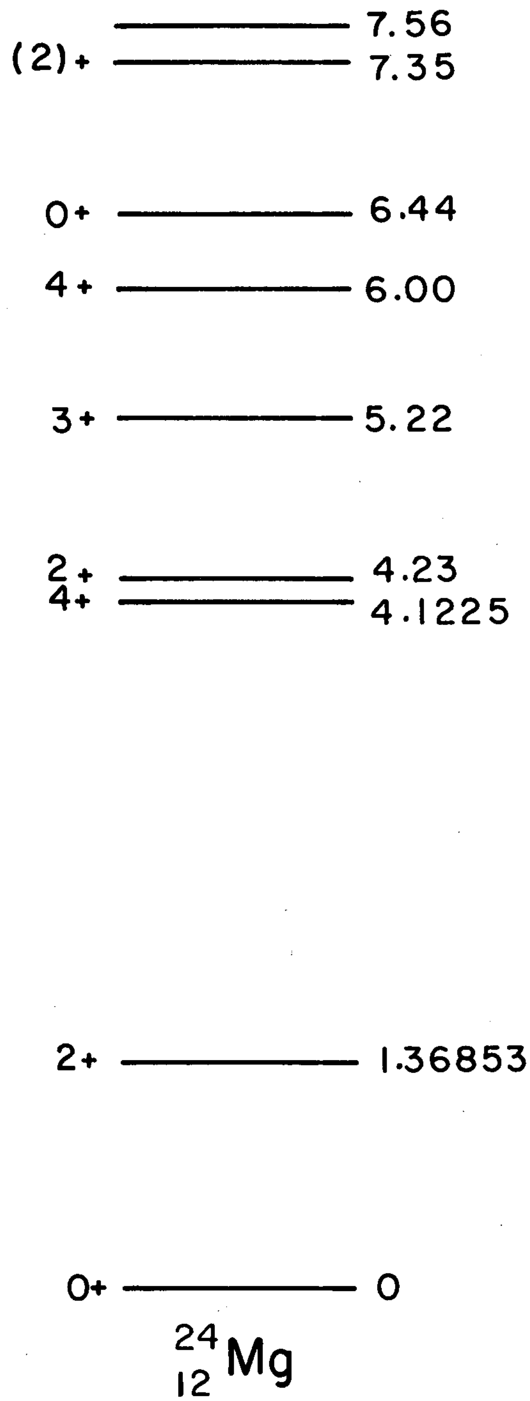

Fig. 6. ^{24}Mg energy level diagram.

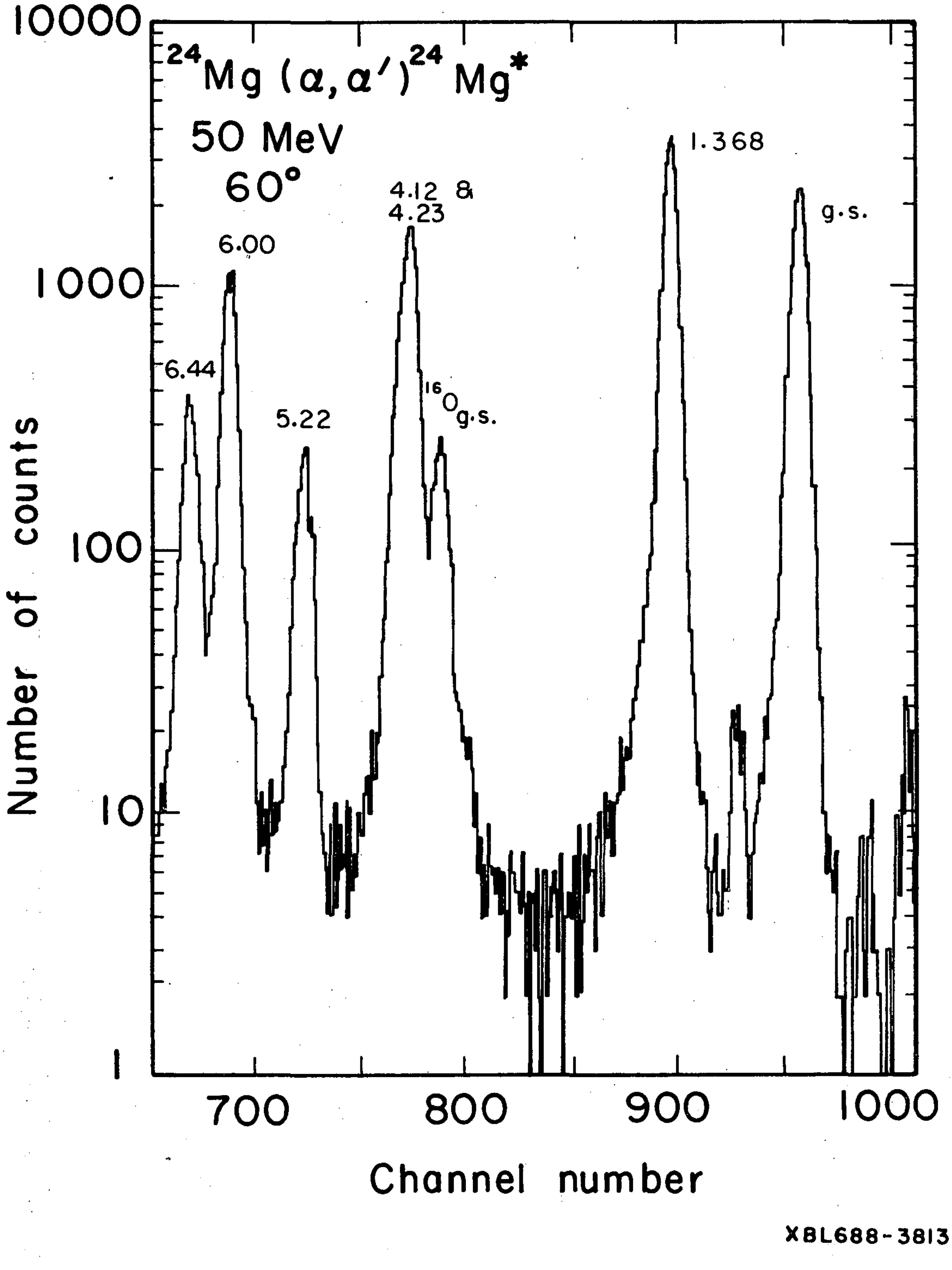

Fig. 7. $^{24}Mg(\alpha,\alpha')^{24}Mg^*$ energy spectrum for E_α = 50 MeV.

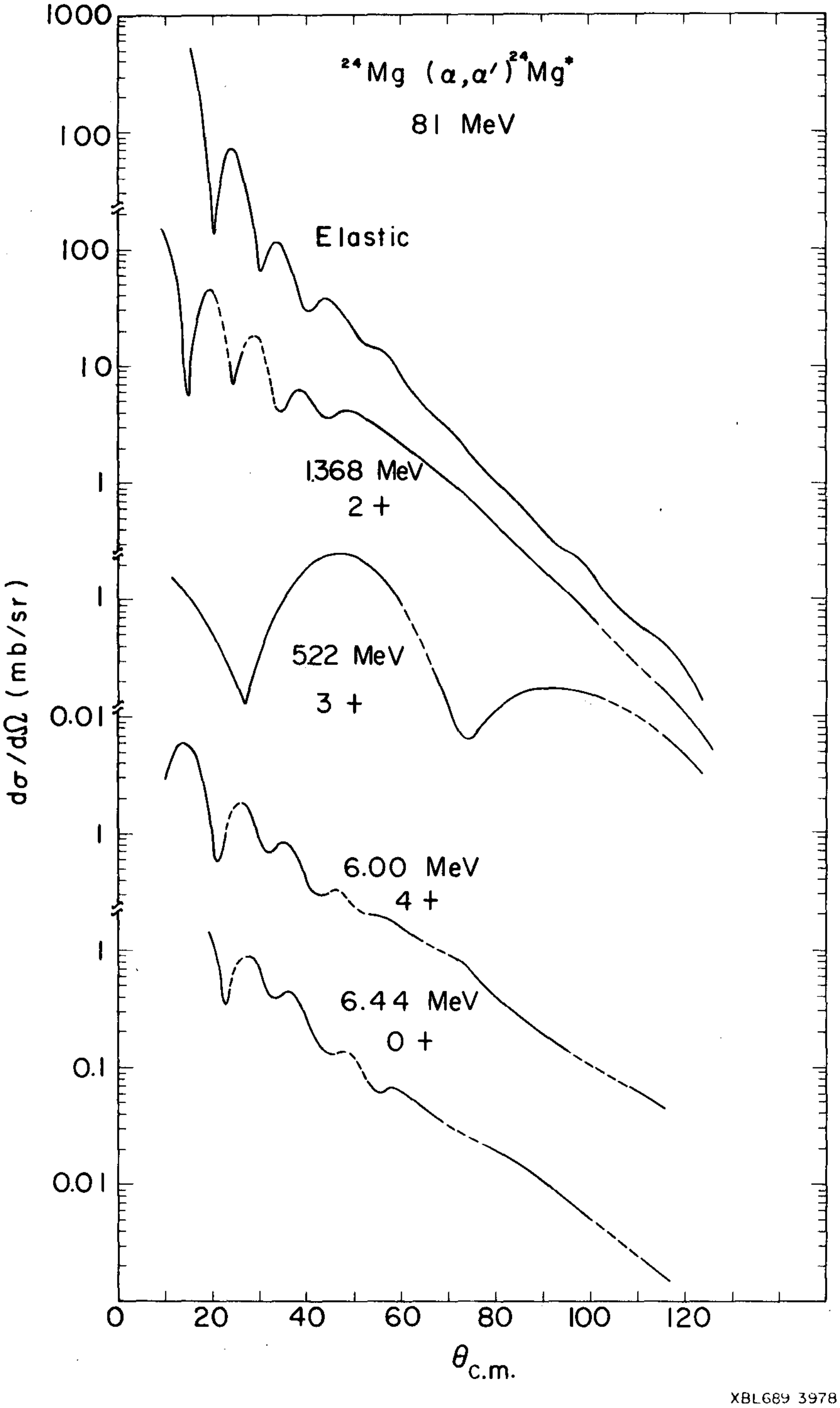

Fig. 10. $^{24}Mg(\alpha,\alpha')^{24}Mg^{*}$ 81 MeV angular distribution.

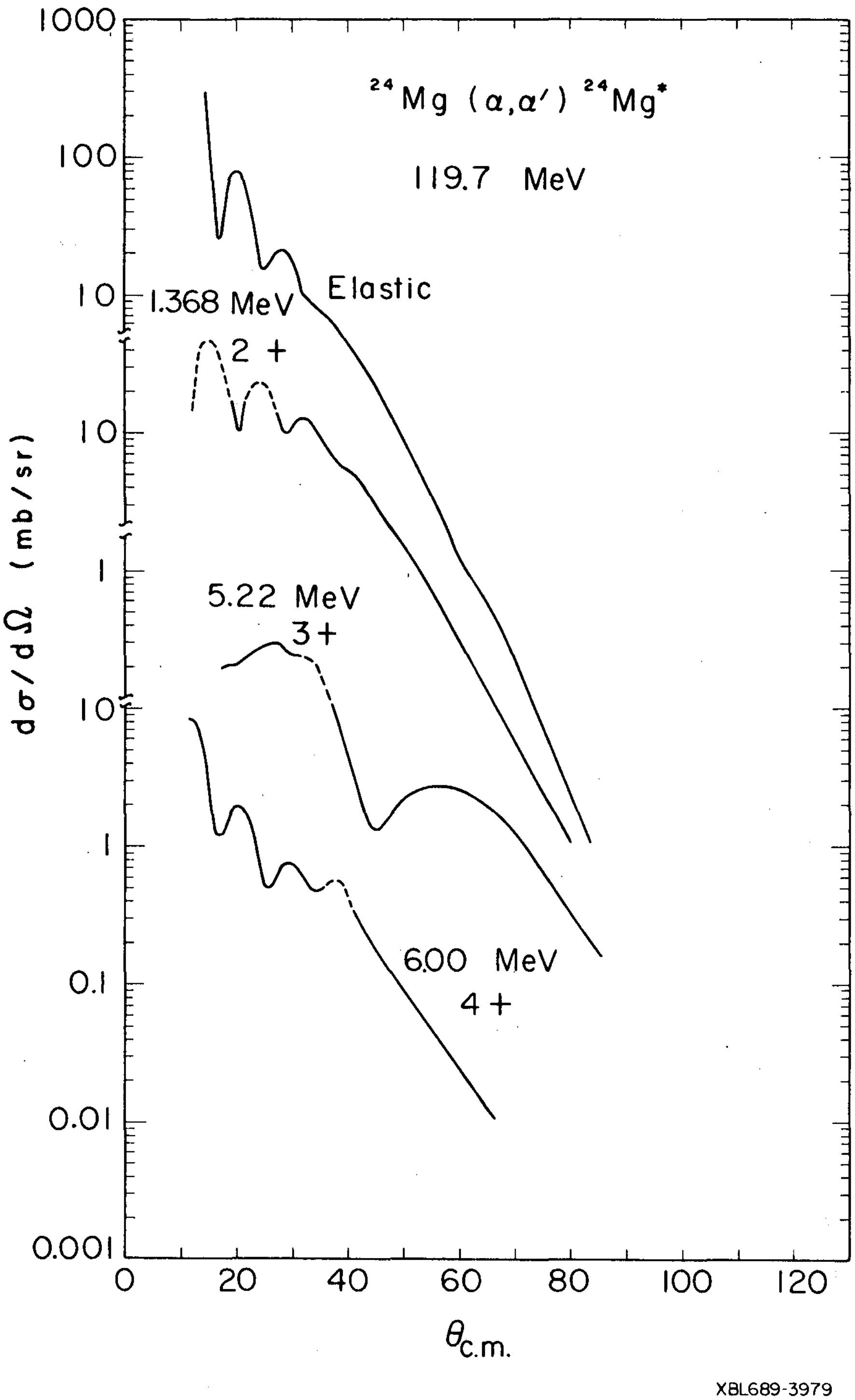

Fig. 11. $^{24}Mg(\alpha,\alpha')^{24}Mg^*$ 119.7 MeV angular distribution.

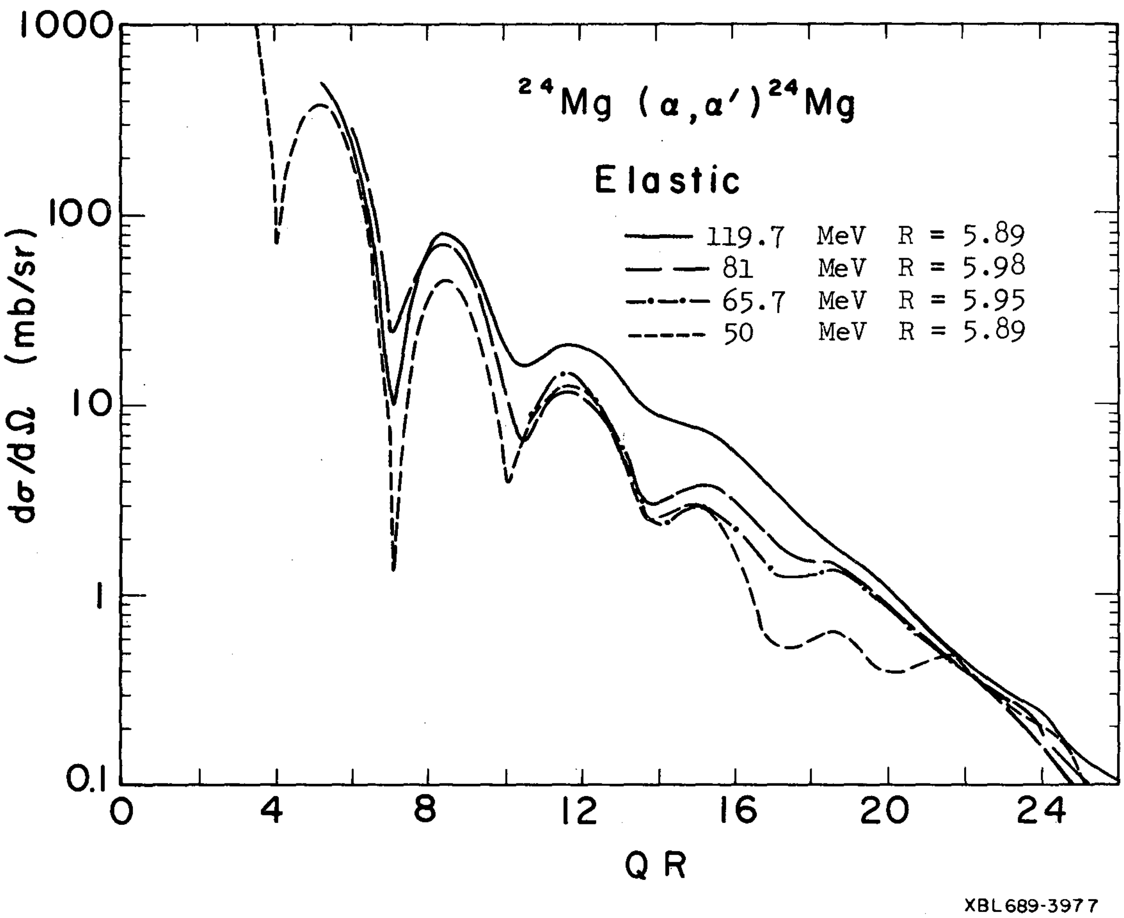

Fig. 12. $^{24}Mg(\alpha,\alpha')^{24}Mg^*$ elastic angular distributions plotted versus QR.

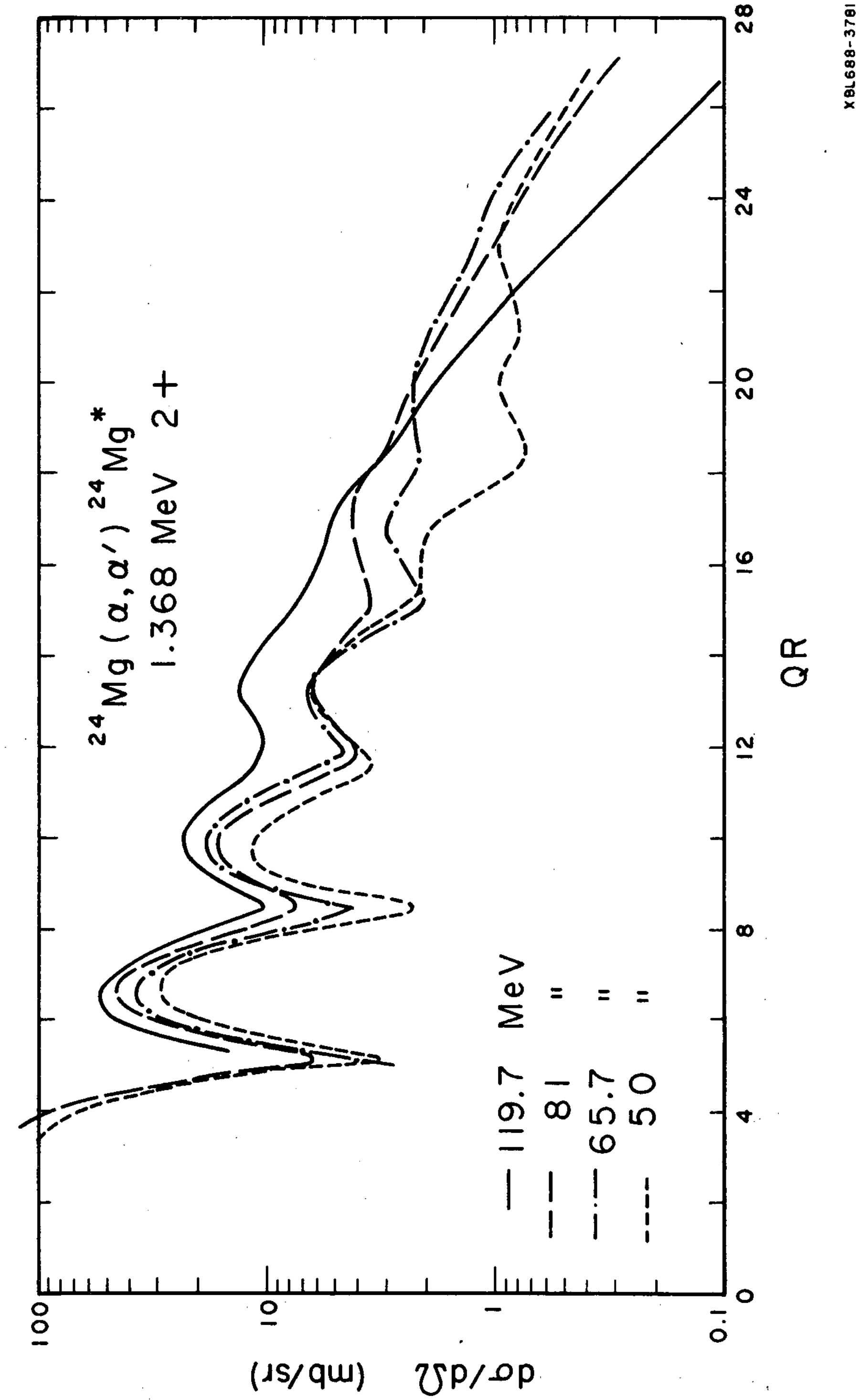

Fig. 13. $^{24}Mg(\alpha,\alpha')^{24}Mg^*$ first 2+ angular distributions versus QR.

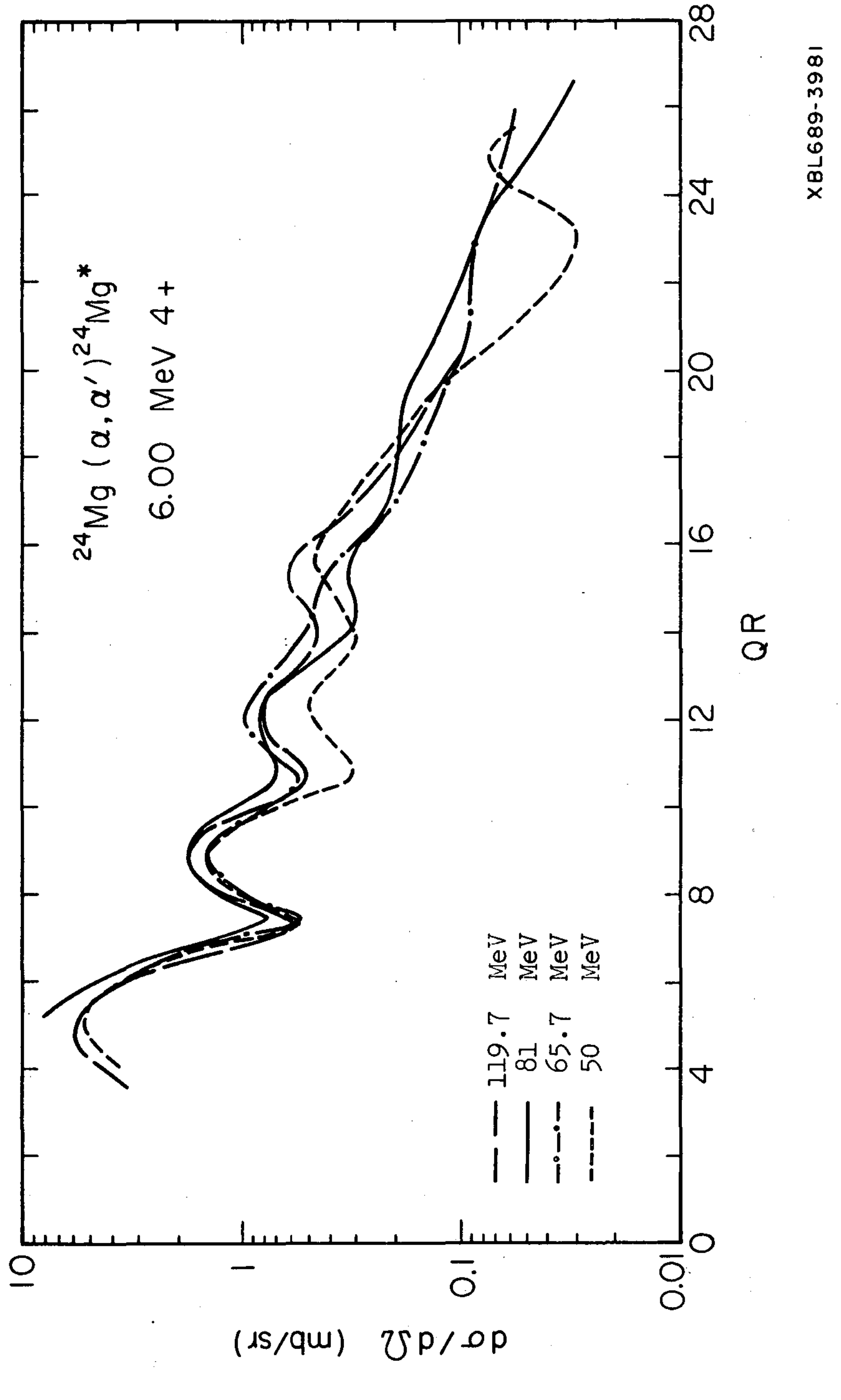

Fig. 14. $^{24}Mg(\alpha,\alpha')^{24}Mg^*$ second 4+ angular distributions versus QR.

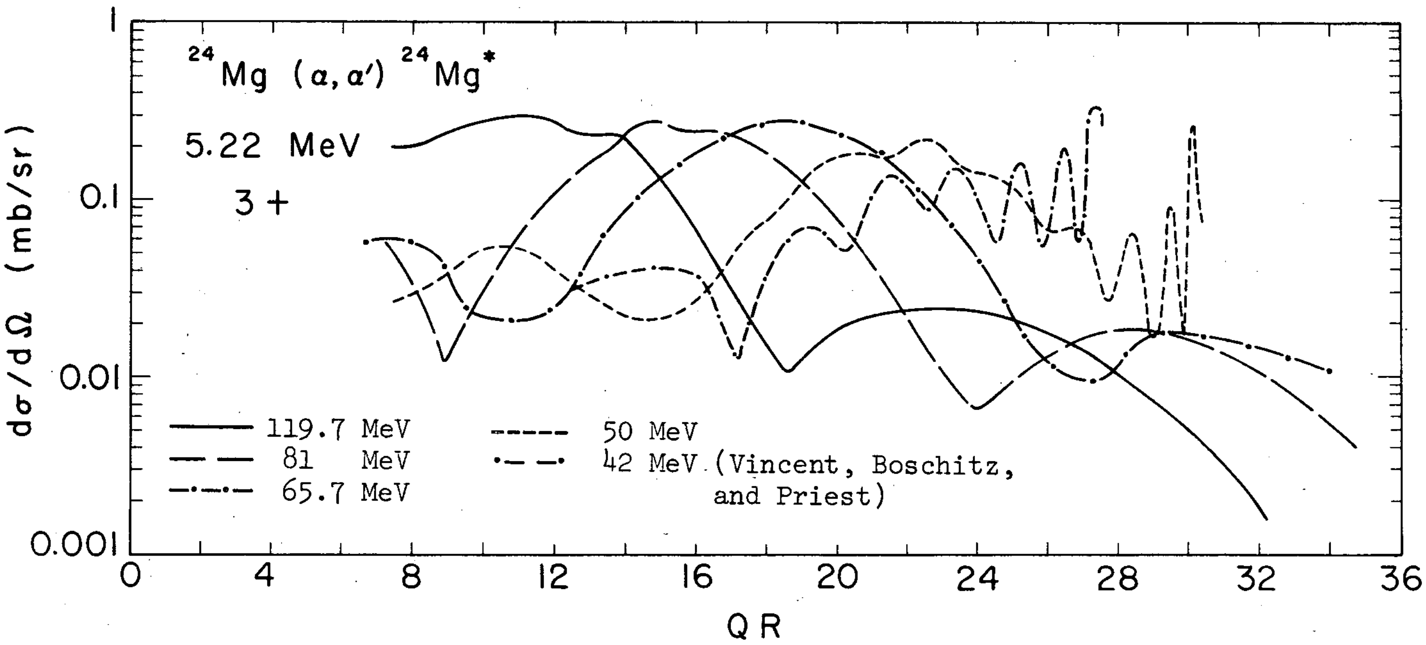

XBL689-3980

Fig. 15. ^{24}Mg(α,α′)^{24}Mg* 3+ angular distributions versus QR.

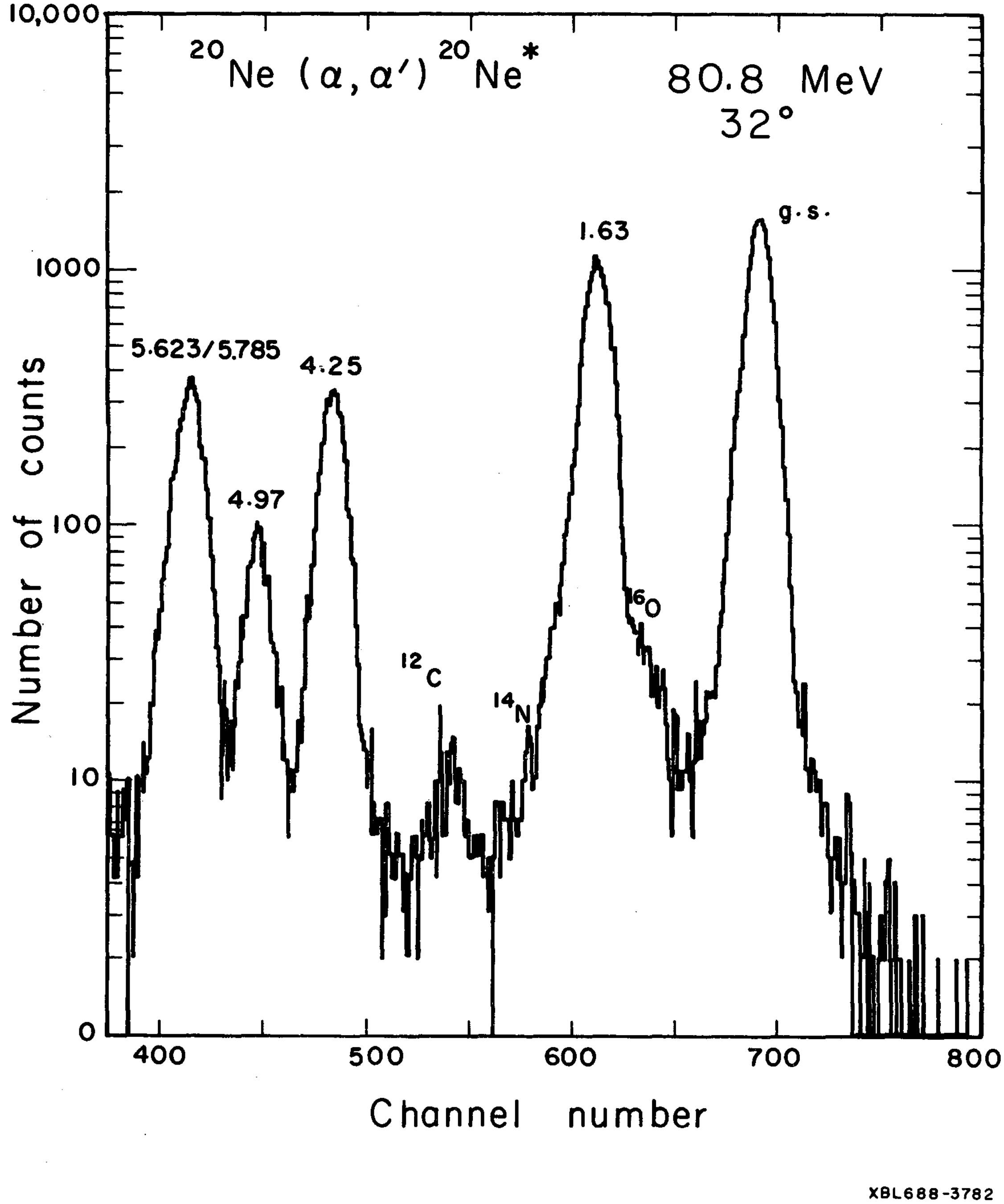

Fig. 17. ^{20}Ne(α,α')^{20}Ne* energy spectrum.

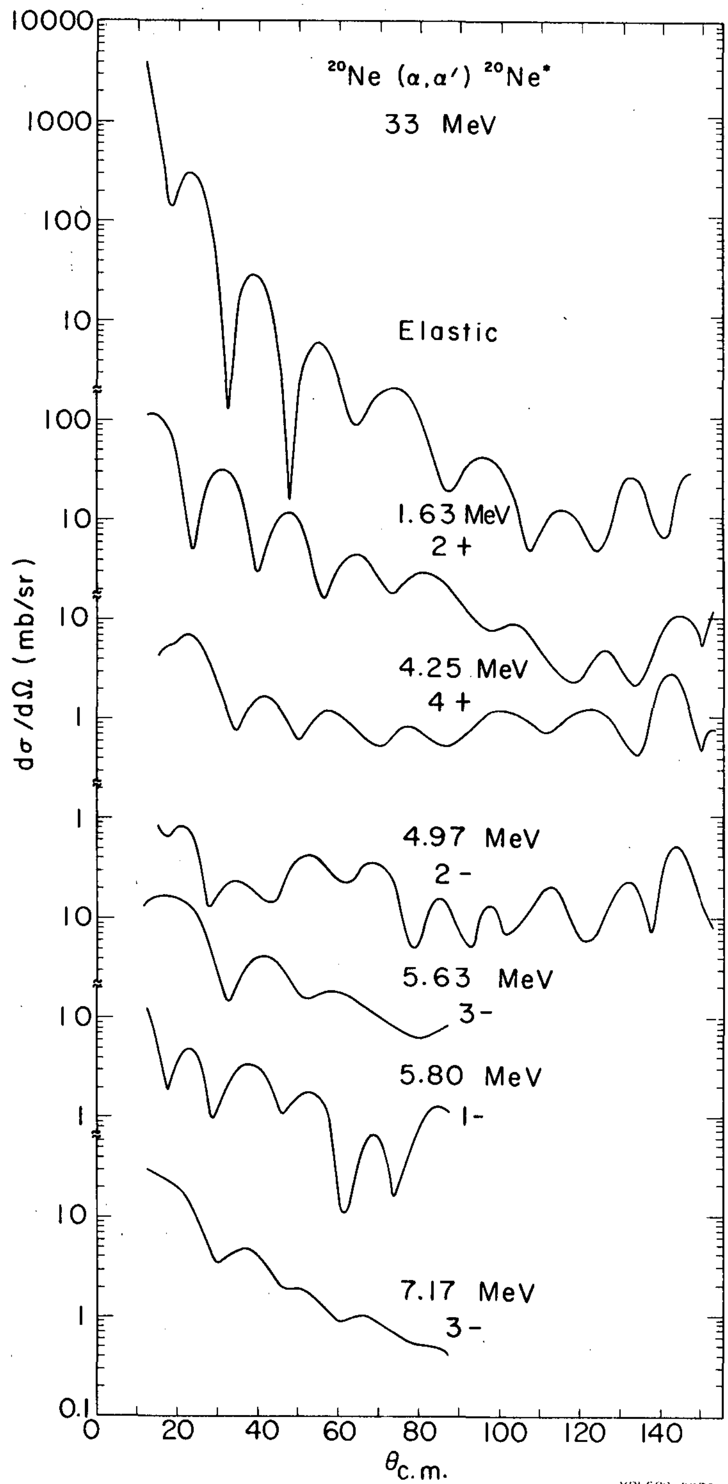

Fig. 18. $^{20}Ne(\alpha,\alpha')^{20}Ne^*$ 33 MeV angular distributions.

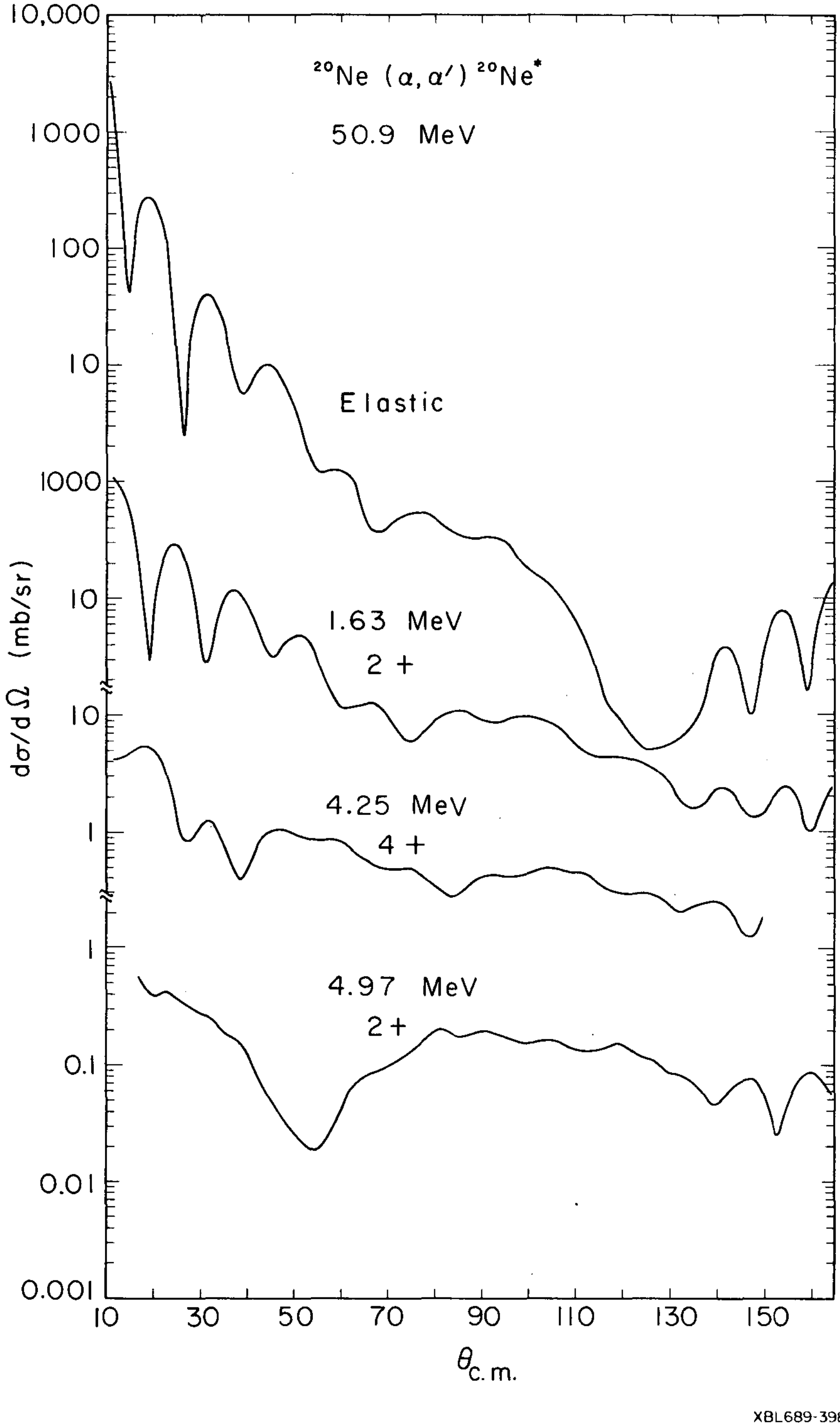

Fig. 19. $^{20}Ne(\alpha,\alpha')^{20}Ne^*$ 50 MeV angular distributions.

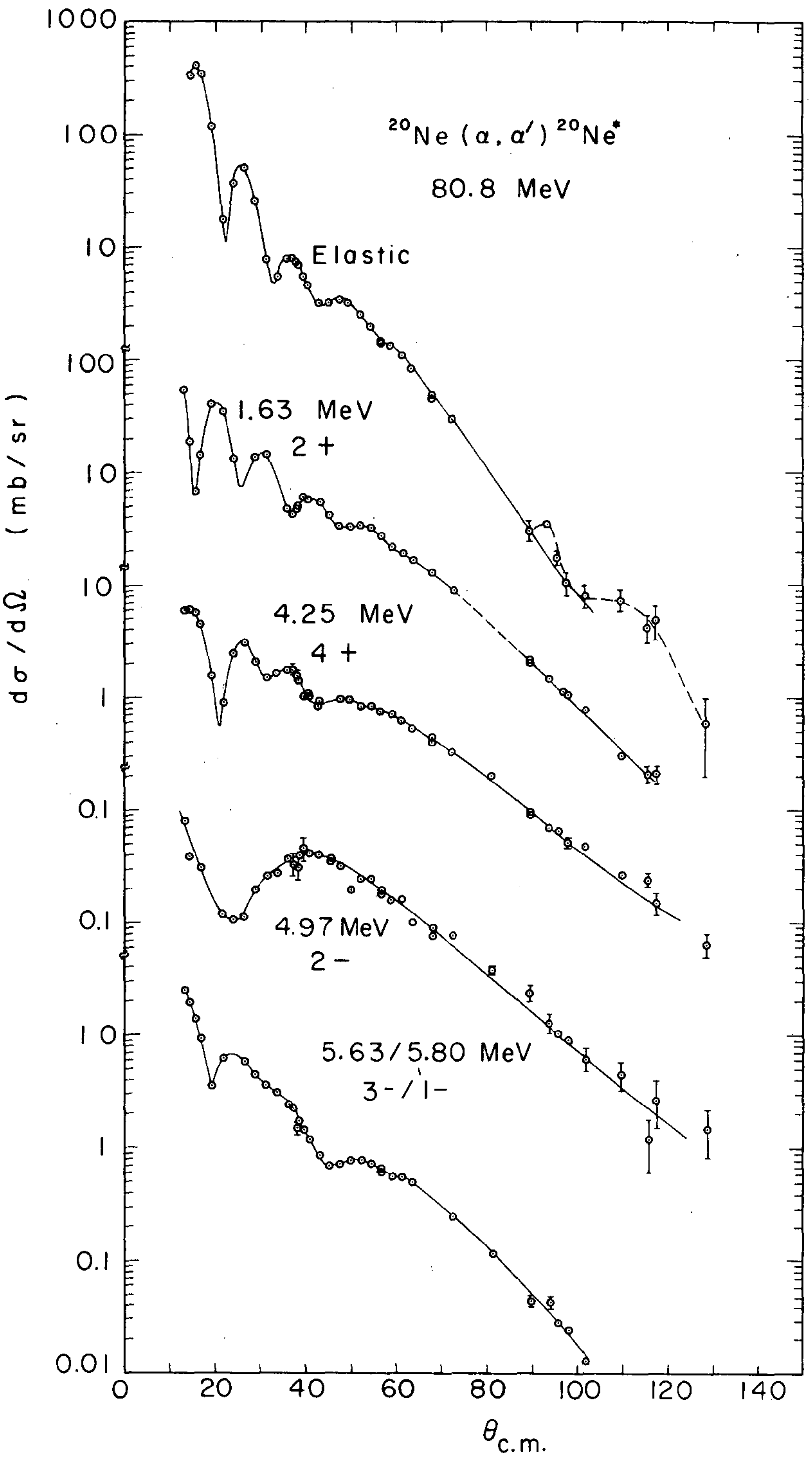

Fig. 20. $^{20}Ne(\alpha,\alpha')^{20}Ne^*$ 80.8 MeV angular distributions.

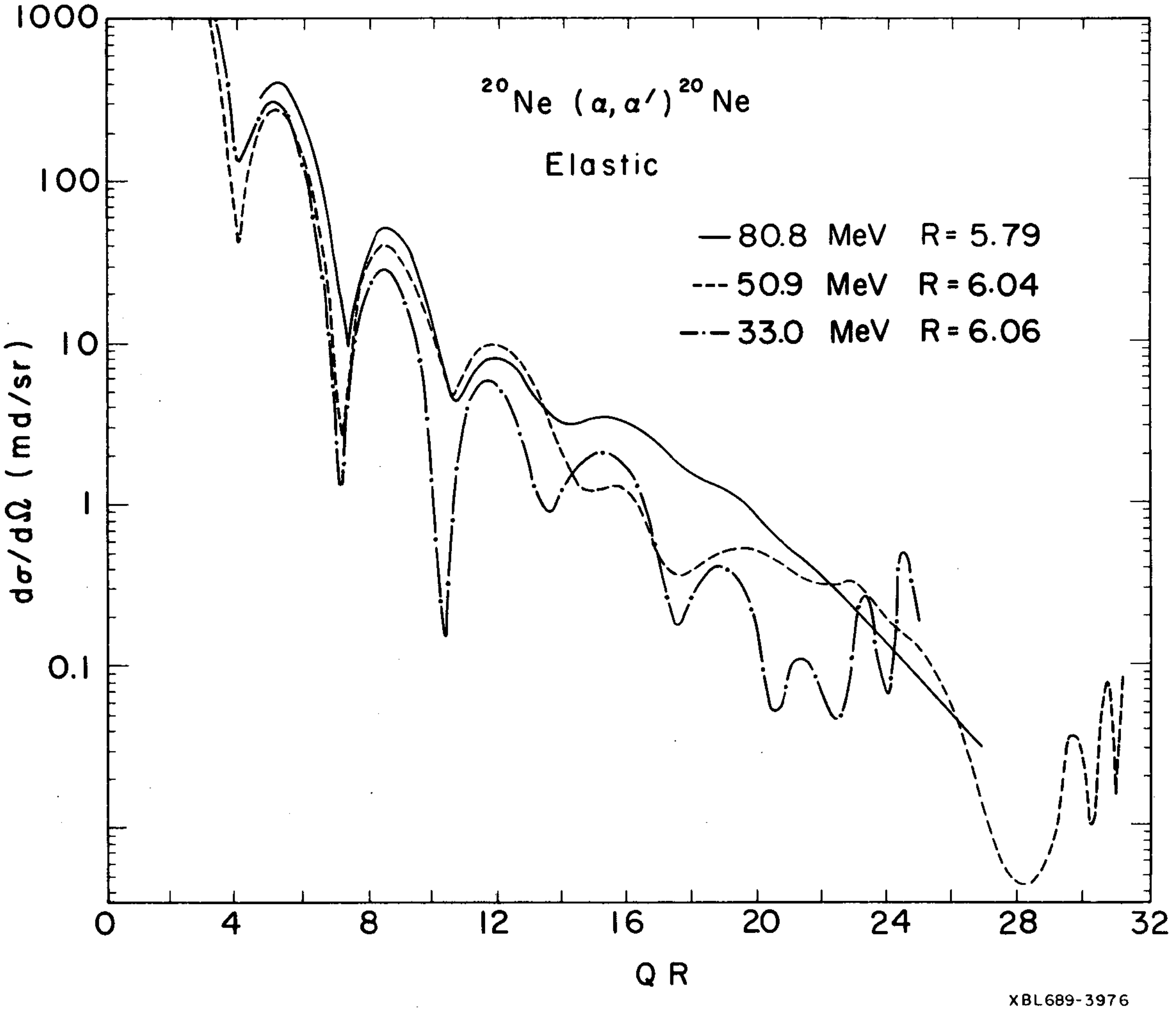

Fig. 21. $^{20}Ne(\alpha,\alpha')\,^{20}Ne^{*}$ elastic angular distributions versus QR.

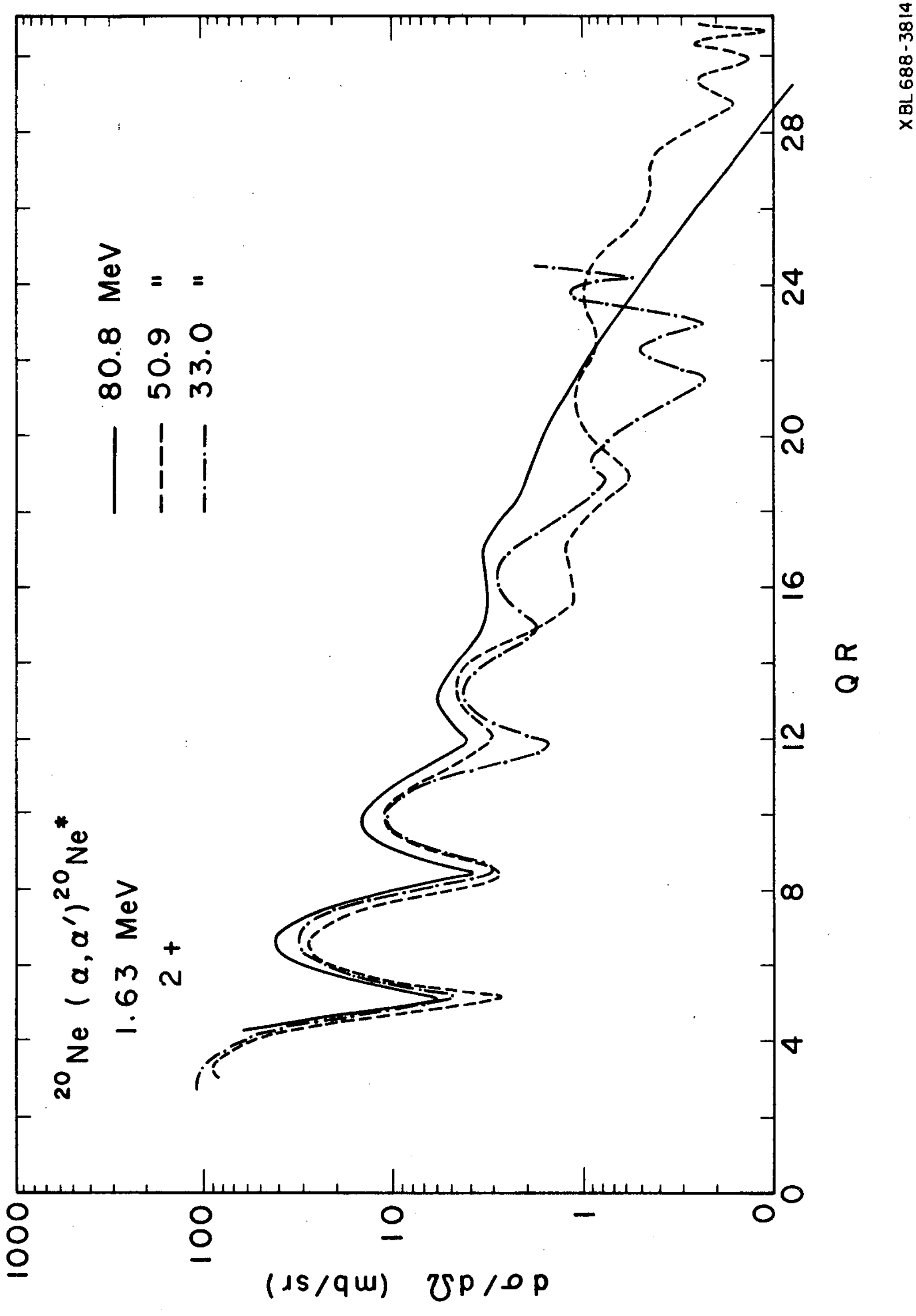

Fig. 22. $^{20}Ne(\alpha,\alpha')^{20}Ne^*$ 2+ angular distributions versus QR.

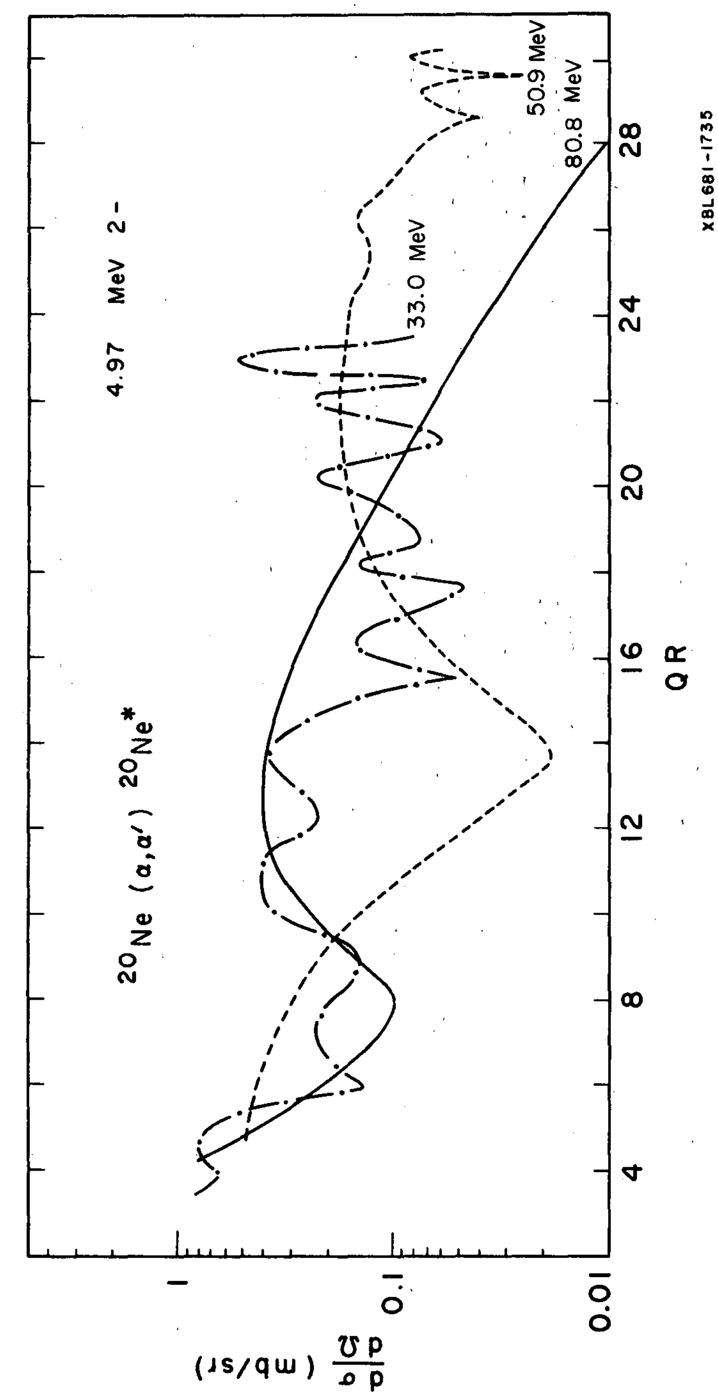

Fig. 23. $^{20}Ne(\alpha,\alpha')^{20}Ne^*$ 2- angular distributions versus QR.

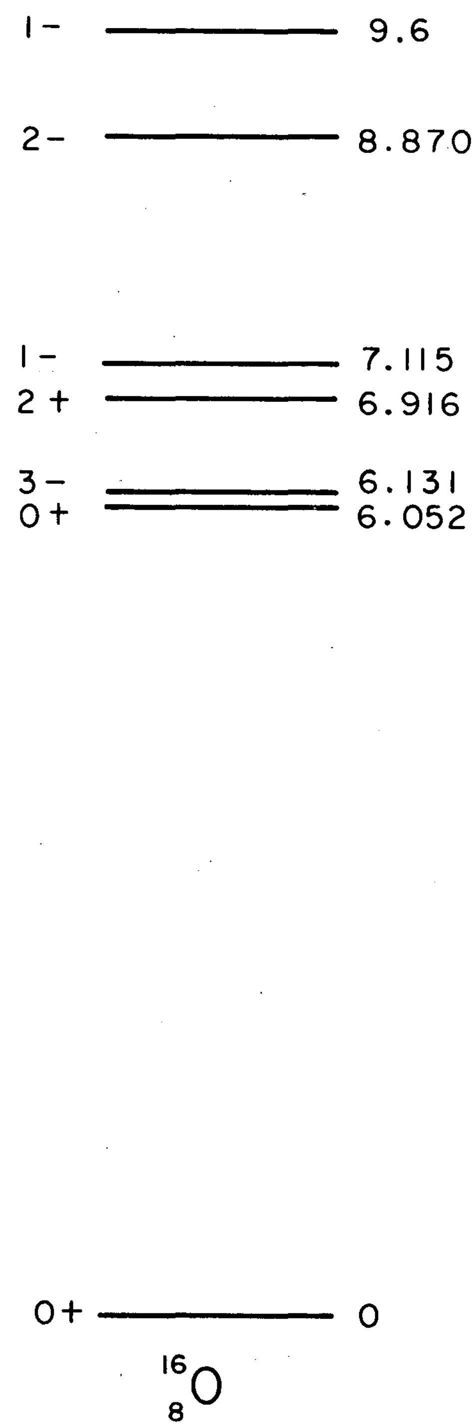

XBL688-3778

Fig. 24. ^{16}O level diagram.

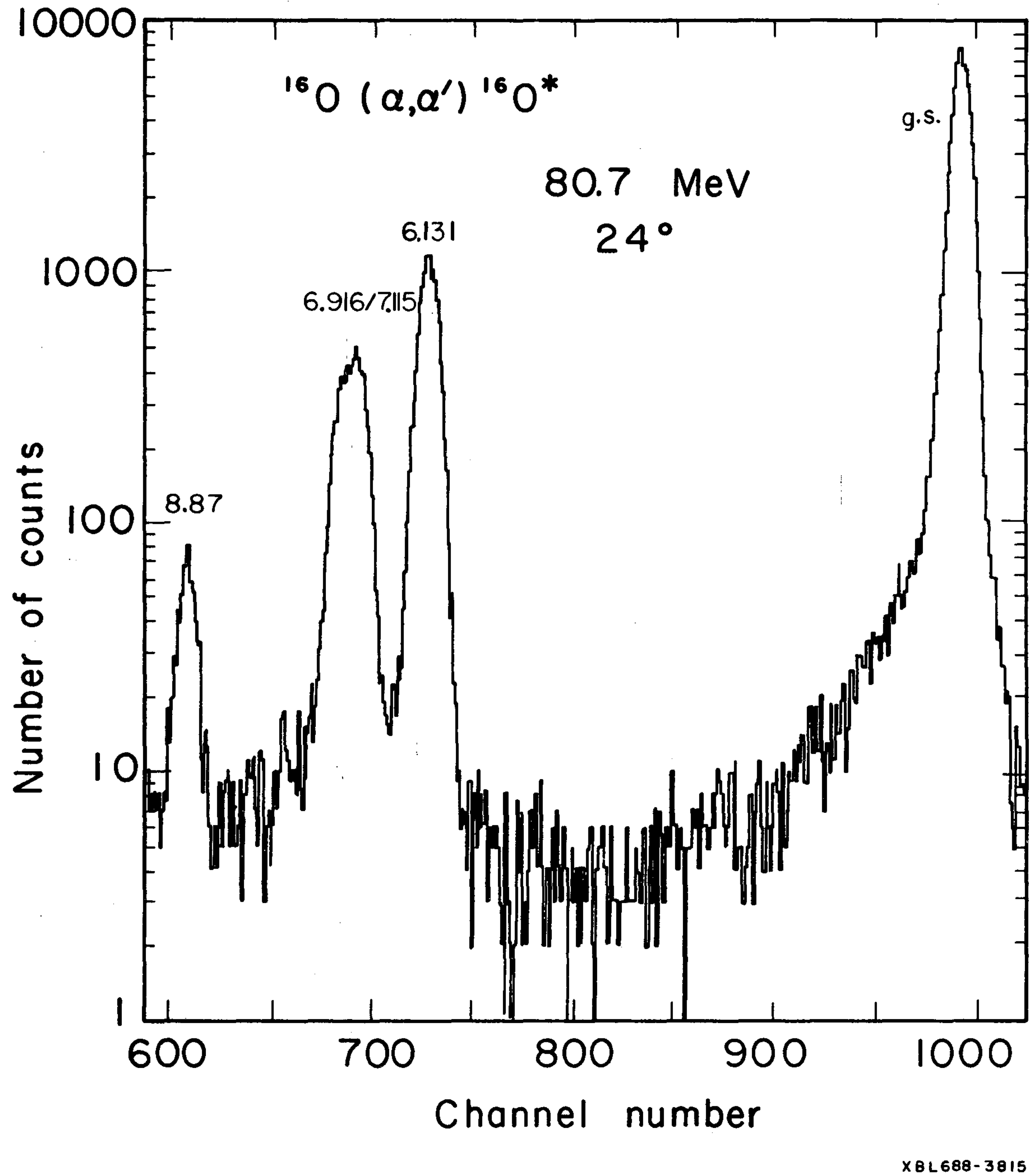

Fig. 25. ^{16}O energy spectrum.

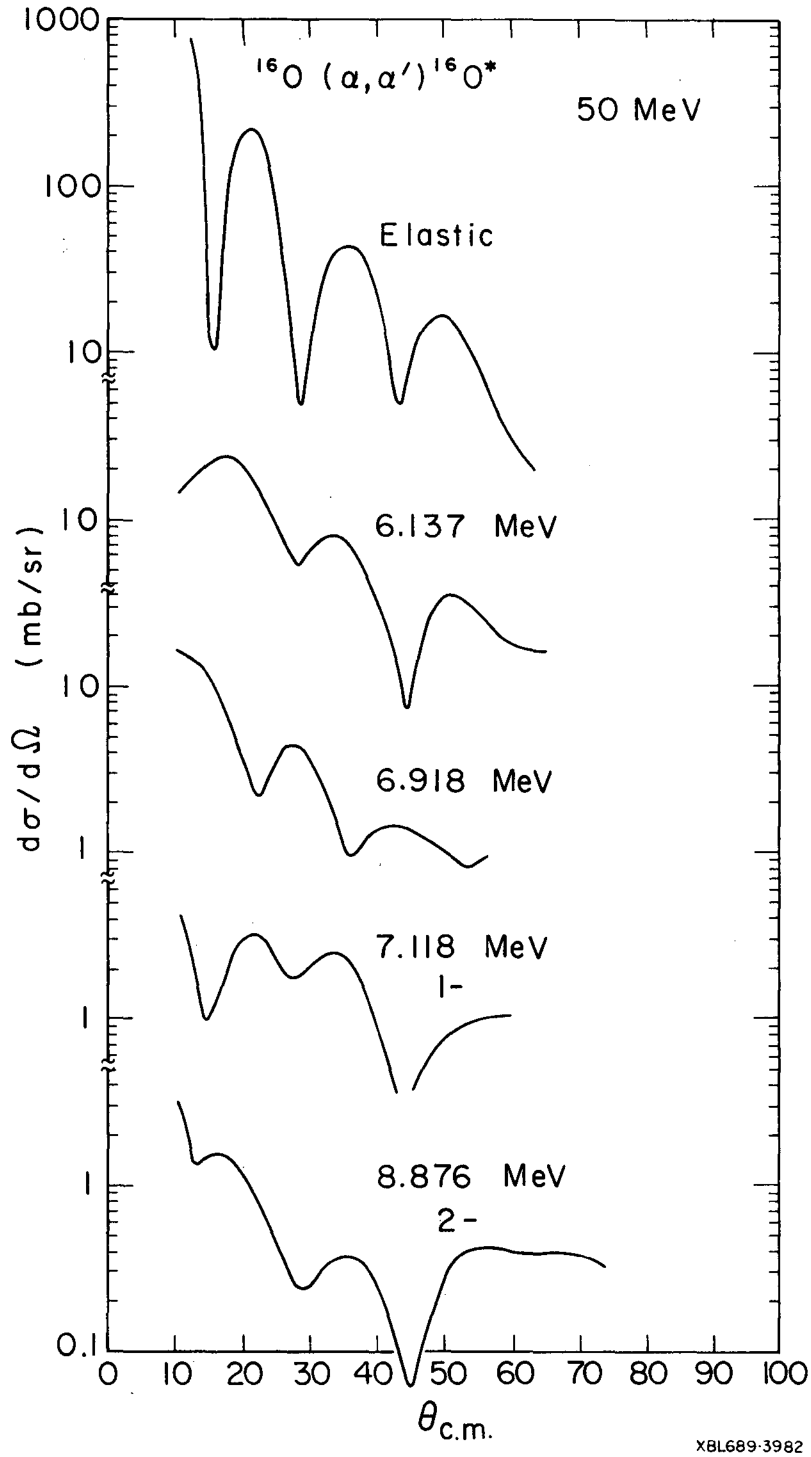

Fig. 26. $^{16}O(\alpha,\alpha')^{16}O^*$ 50 MeV angular distributions.

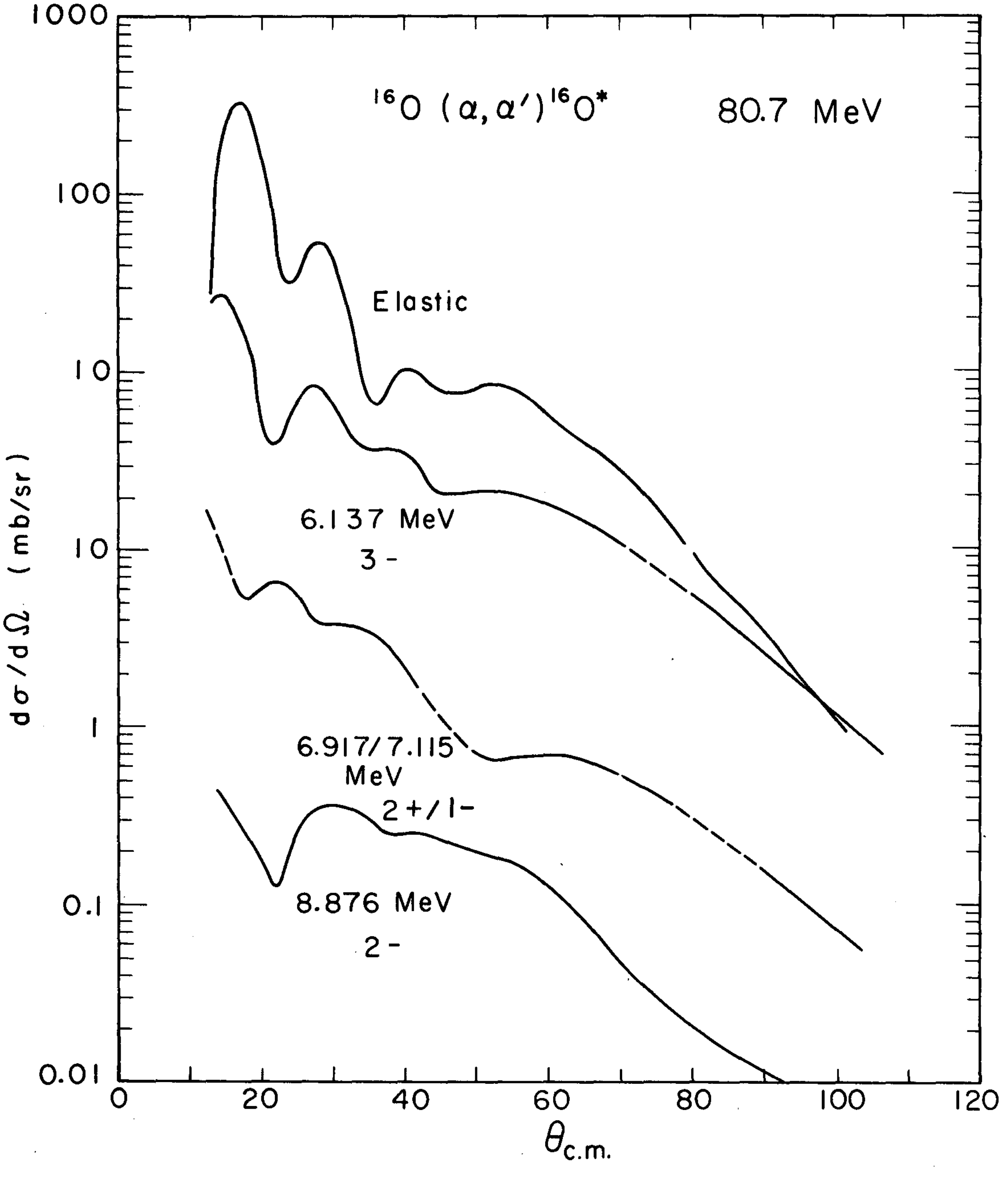

Fig. 27. $^{16}O(\alpha,\alpha')^{16}O^*$ 80.7 MeV angular distributions.

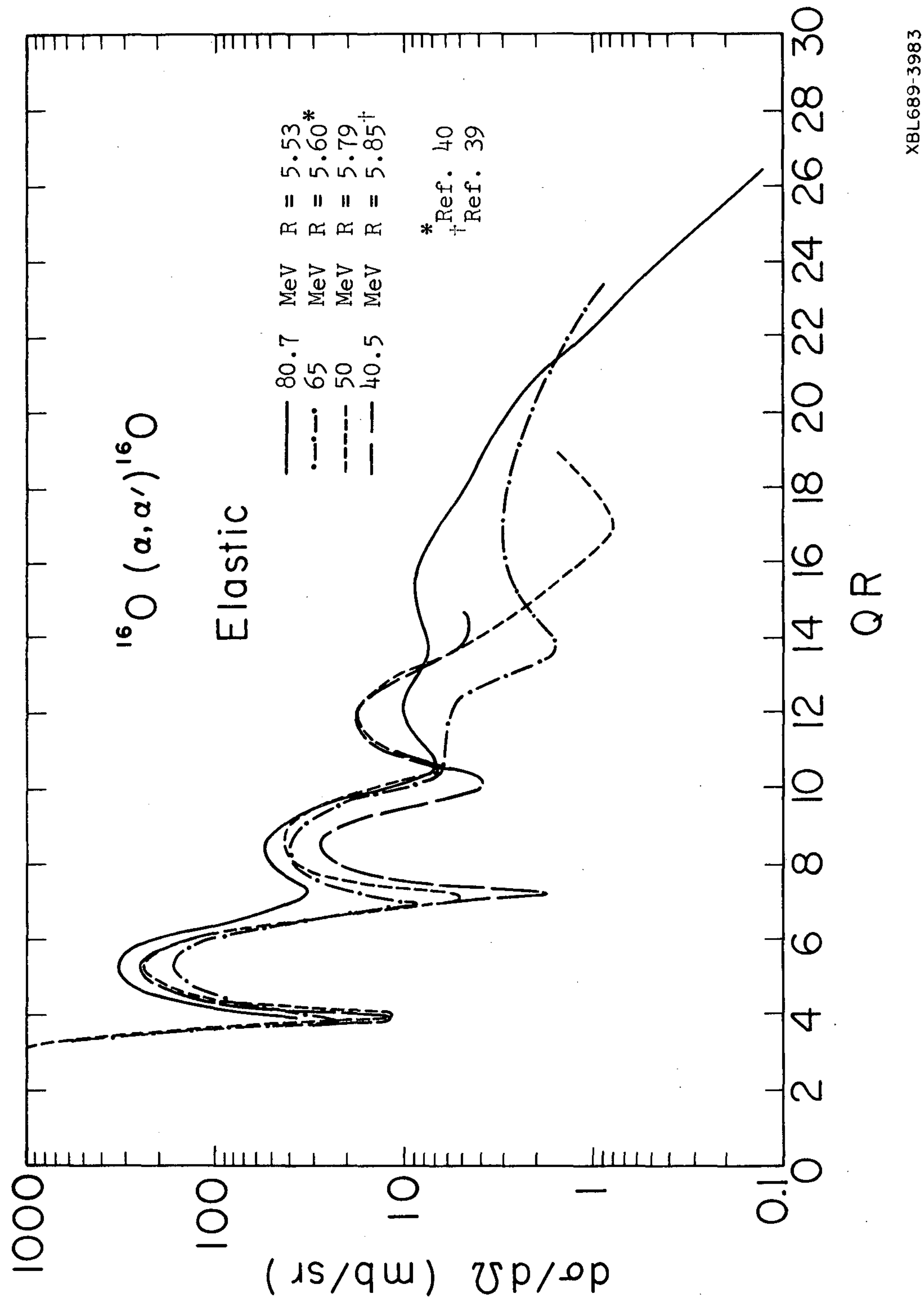

Fig. 28. $^{16}O(\alpha,\alpha')^{16}O^*$ elastic angular distribution versus QR.

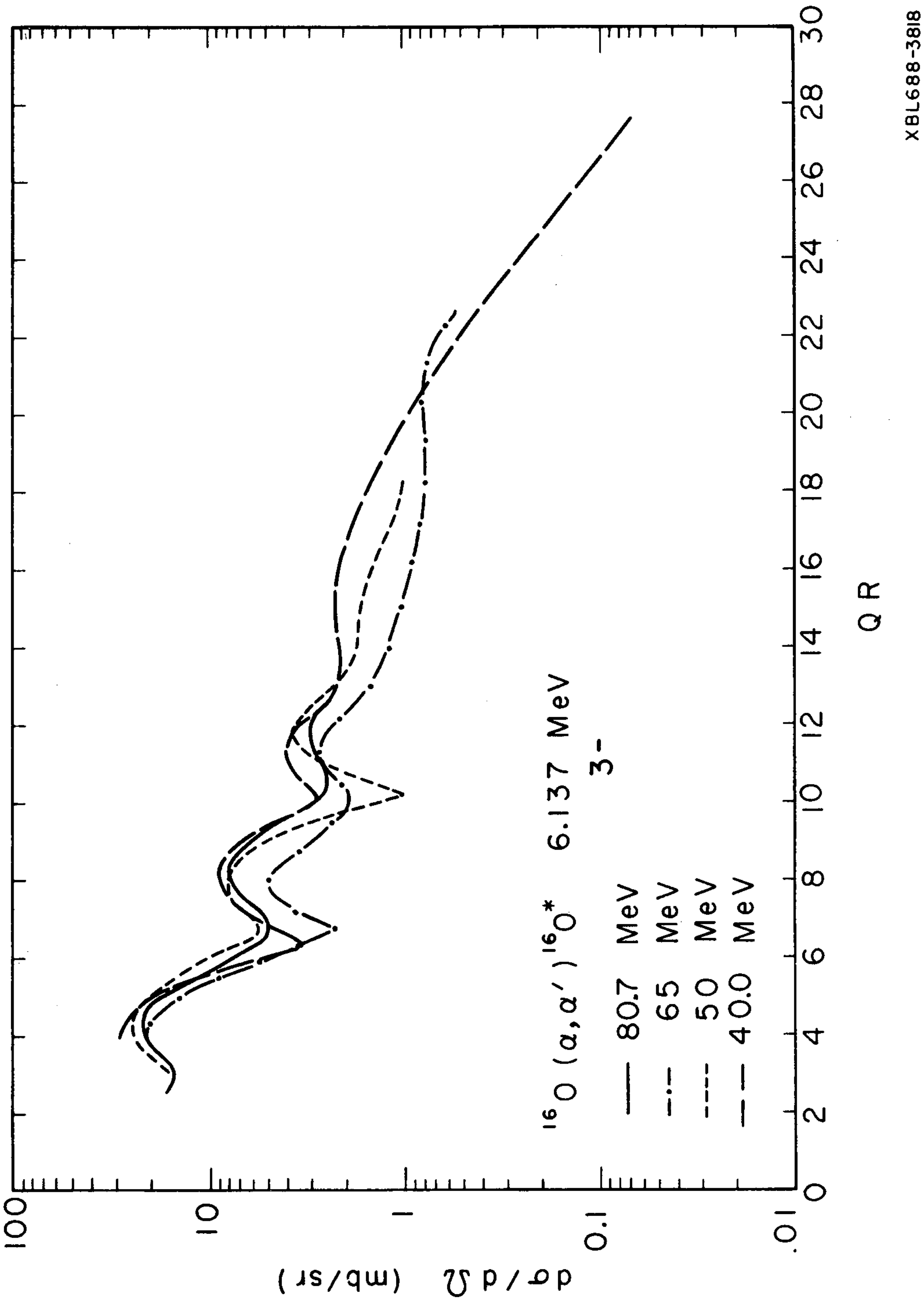

Fig. 29. $^{16}O(\alpha,\alpha')^{16}O^*$ 3- angular distribution versus QR.

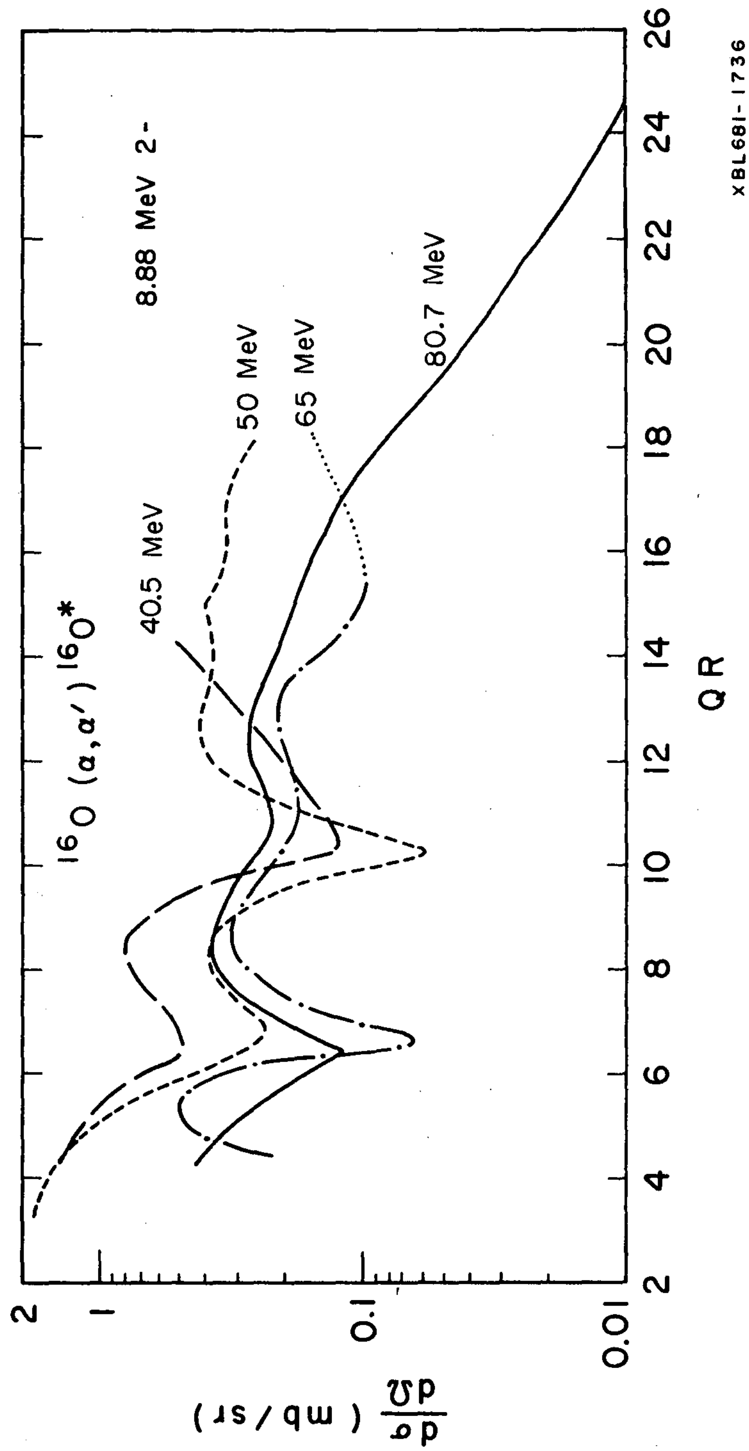

Fig. 30. $^{16}O(\alpha,\alpha')^{16}O^*$ 2- angular distribution versus QR.

the cross sections show behavior very similar to that found for natural-parity states.

D. Discussion

The low-lying states of ^{24}Mg can be interpreted as members of two rotational bands. The first 2+ and 4+ levels are described as members of the ground state rotational band. Kuehner and Almquist[41] used coincidence γ-ray spectra to locate the high spin members of the collective bands in ^{24}Mg by the reaction $^{12}C(^{16}O,\alpha\gamma)^{24}Mg$ and $^{25}Mg(^{3}He,\alpha\gamma)^{24}Mg$. Their results suggested that the 8.12 and 13.2 MeV levels are the 6+ and 8+ members of the ground state rotational band. They found that the levels at 8.81 and 9.52 MeV are the 5+ and 6+ members of the K = 2 rotational band based on the 2+ level at 4.23 MeV. The unnatural-parity 3+ at 5.22 MeV is the second member of this band. Further evidence for the existence of rotational bands in ^{24}Mg has been put forth by Cohen and Cookson[42]. They found that the ground state and first two excited states obey the relationship

$$E_J = AJ(J + 1) - B(J(J + 1))^2$$

with A = 237 keV and B = 1.56 keV. They also found that the observed decay modes indicate that the band mixing is less than about 2%.

Litherland et al.[43] divided the low-lying energy levels of ^{20}Ne into several rotational bands by using the relationship

$$E_J \propto J(J + 1).$$

The unnatural-parity 2- level is the first member of a K = 2 negative parity rotational band.

Brink and Nash[44] have classified the low-lying excited states of ^{16}O by the SU3 coupling scheme. The 0+ state at 6.06 MeV and the 2+ state at 6.91 MeV are interpreted as being the two lowest-lying states of a rotational band. The 3-, 1- and 2- states at 6.14, 7.12 and 8.87 MeV are classified as a rotational band strongly distorted by a decoupling effect. Alternatively, the unnatural-parity state at 8.87 MeV is described in terms of the shell model as a $(p_{1/2}^{-1}\ d_{5/2})_{2-}$ configuration.[45]

Another indication of the degree of collectively of a nucleus is the value of the reduced transition probability, $B(E2)/e^2$, for the excitation of the first 2+ level. These $B(E2)/e^2$ values are related to the deformation parameter for the nucleus by the formula[46]

$$B(E2)/e^2 = \beta_2^2 \left[3ZR_0^2/4\pi\right]^2.$$

Table 2 gives the values for the reduced transition probabilities and the deformation parameters for the nuclei of interest here. Values of the $B(E\lambda)/e^2$'s and the B_λ's for some of the other low-lying levels are also included here. The values for both $B(E2)/e^2$ and β_2 for ^{16}O are much smaller than those of ^{24}Mg and ^{20}Ne. These results are in accord with the idea that ^{20}Ne and ^{24}Mg are highly deformed nuclei, while ^{16}O is close to spherical in its ground state.

A possible mechanism is multiple excitation. The small slopes of the envelopes of the experimental angular distributions are indicative of this process, which would be expected to be enhanced in a deformed nucleus where the coupling strengths and $B(E\lambda)$'s between levels are quite large. Since ^{16}O is nearly spherical in its ground state and has small $B(E\lambda)$ values, while ^{24}Mg and ^{20}Ne are deformed nuclei, a multiple excitation process would be expected to differentiate between the two cases.

Table II. Values for the reduced transition probabilities and deformation parameters.

Nucleus	Level	Spin	$\frac{B(E_\lambda;\ 0+ \rightarrow \lambda)}{e^2}$ fermi$^{2\lambda}$	β_λ
^{16}O	6.923	2+	2.15 ± .54[a]	0.084
	6.131	3-	630[c]	
^{20}Ne	1.63	2+	480 ± 90[a]	0.87
	4.25	4+	56700[b]	0.10
	5.63	3-	3150[b]	0.23
	7.17	3-	3150[b]	0.23
^{24}Mg	1.368	2+	510 ± 80[a]	0.65

[a]Ref. 46.
[b]Ref. 32.
[c]Ref. 39

IV. CALCULATIONS

Calculations assuming the compound nucleus and multiple excitation mechanisms have been carried out for the 3+ state in ^{24}Mg at the various α-particle energies. No theory has yet been formulated for the spin-flip mechanism.

A. Compound Nucleus

A Hauser-Feshbach computer code[47-49] was used to calculate differential cross sections for the $^{24}Mg(\alpha,\alpha')^{24}Mg^*$ reaction assuming the compound nucleus mechanism. In these calculations it is assumed that the compound nucleus is sufficiently excited so that the statistical model may be applied. Only a few levels of the residual nucleus are assumed to be excited. In this case the angular distributions will be anisotropic and symmetric about 90°.

The scattering process can be considered in two parts, first, the formation of the compound nucleus by the incoming projectile and the target nucleus, and then the decay of the compound nucleus by particle emission. The compound nuclear state exists long enough for the energy of the incident particle to be shared with the target nucleons.

The Hauser-Feshbach integrated cross section[47] is calculated as follows:

$$\sigma = \frac{\pi A_0}{k^2(2J_1 + 1)(2s_1 + 1)}$$

where

$$A_0 = \sum_{J\pi} \frac{(2J + 1)}{D_{J\pi}} \left[\sum_{\ell_1 j_1} T_{\ell_1 j_1}\right]\left[\sum_{\ell_2 j_2} T_{\ell_2 j_2}\right]$$

and

$$D_{J\pi} = \sum_{k,\ell_k,j_k} T_{\ell_k j_k} .$$

The subscript k = 1 refers to the incoming channel and k = 2 to the observed outgoing channel. J is the compound nucleus spin, s is the particle spin, and $T_{\ell_k j_k}$ is the penetrability in channel k for the partial wave ℓ_k and the total spin j_k.[50] $D_{J\pi}$ is the sum over all penetrabilities with subscripts which can be coupled to form a compound state with spin J and parity π. The penetrability $T_{\ell_k j_k}$ is the probability that the particle of angular momentum ℓ_k enters into the nucleus forming a compound system. The influence of the potential barrier, centrifugal and Coulomb, is included in the penetrability. The formula for $T_{\ell_k j_k}$ is

$$T_{\ell_k j_k} = \frac{4\rho X |A_\ell|^{-2}}{X^2 + (2\rho X + \rho X^2 |A'_\ell|^2)|A_\ell|^{-2}}$$

where $\rho = kR$ and $X = KR$ and the incident wave has the form e^{ikz}. While inside the nucleus the wave is of the form e^{iKr}, where K is the wave number corresponding to the kinetic energy in the interior of the nucleus, $K \approx 10^{13}\ \mathrm{cm}^{-1}$. Also $A_\ell = G_\ell + iF_\ell$ where F_ℓ is the regular coulomb wave function and G_ℓ is the irregular wave function, and A'_ℓ is the derivative of A_ℓ with respect to kr.

The differential cross section is given by

$$\frac{d\sigma}{d\Omega} = \frac{1}{4k^2(2J_1+1)(2s_1+1)} \sum_\nu A_\nu P_\nu(\cos\theta)$$

where

$$A_\nu = \sum_{J\pi} \frac{(2J+1)}{D_{J\pi}} \left[\sum_{\ell_1 j_1} \beta_\nu^{J_1 s_1}(\ell_1 j_1 J) T_{\ell_1 j_1}\right]\left[\sum_{\ell_2 j_2} \beta_\nu^{J_2 s_2}(\ell_2 j_2 J) T_{\ell_2 j_2}\right]$$

The $\beta_\nu^{J_k s_k}(\ell_k j_k J)$'s are angular momentum coupling coefficients which are calculated by means of a recursion relation for Racah coefficients and an explicit expression for Clebsch-Gordan coefficients. The $P_\nu(\cos\theta)$ are the Legendre Polynomials.

The calculations were carried out with the Fortran computer program Liana written by W. R. Smith[49] which was modified for the Control Data Corporation-6600 computer. Twenty-five open channels were assumed for the nuclear reaction. These included the (α,p), (α,n), $(\alpha,^3He)$, (α,t) and (α,α') reactions to the first five excited states of the product nuclei. Figure 31 shows the results for the 3+ state in ^{24}Mg at $E_\alpha = 50$ MeV. The

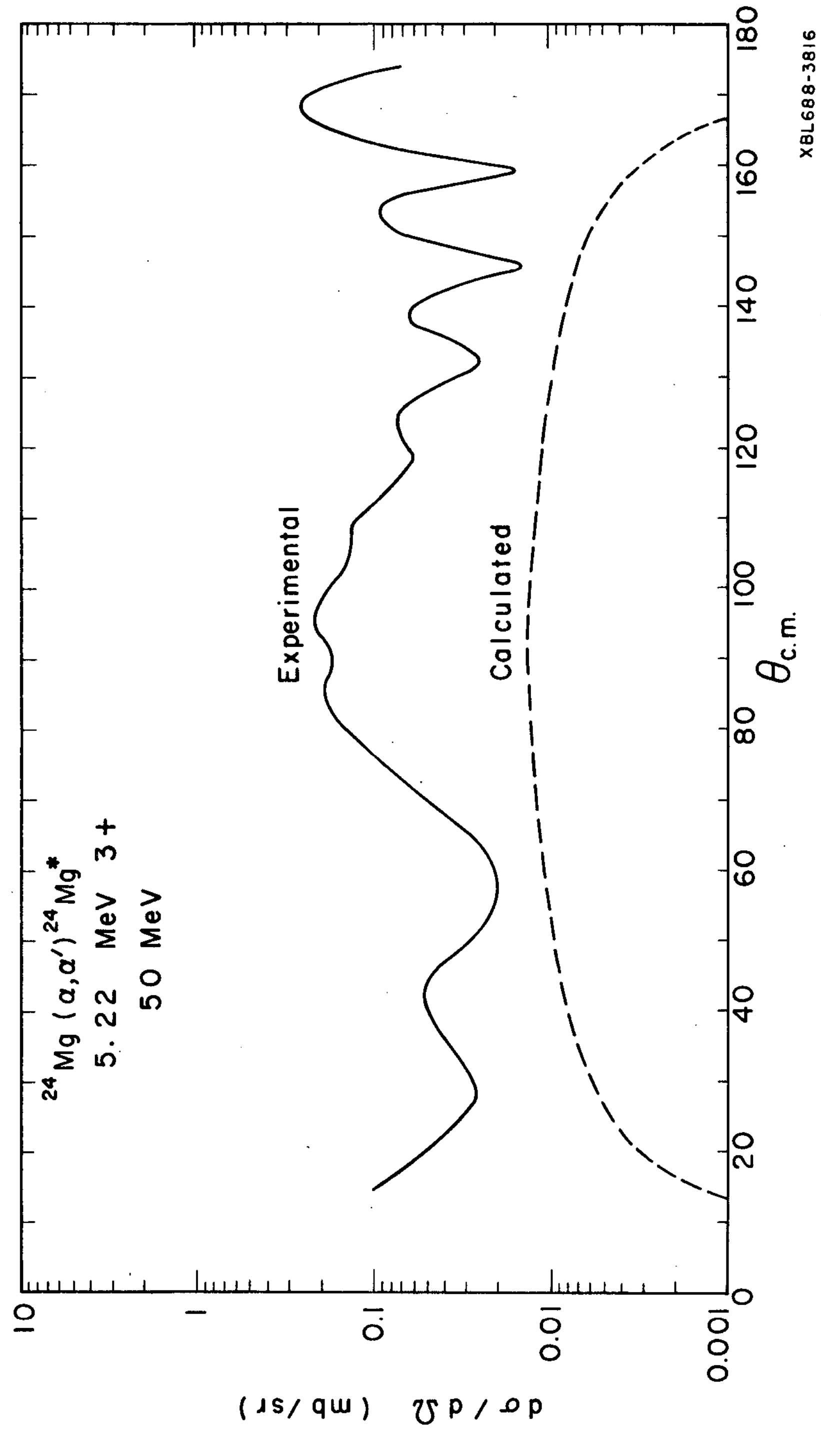

Fig. 31. $^{24}Mg(\alpha,\alpha')^{24}Mg^*$ 3+ state with compound nucleus cross section.

calculated number of channels that should be open at this excitation energy for the decay of the compound nucleus is 10^6. This number was obtained by integrating the formula for level density[51]

$$w(E) = C\, e^{2\sqrt{aE}}$$

where C and a are constants with the values 0.5 and 0.45 MeV^{-1} for the ^{24}Mg case. The average number of energy levels with energies up to the excitation energy of the compound nucleus in a nucleus with atomic weight equal to approximately 24 was calculated to be 1.7×10^5. The channels considered included the emission of several particle types. Thus the number of open channels for particle emission by the compound nucleus is approximately 10^6. The actual cross section to any given state should therefore be much less than that calculated using only 25 open channels. The small calculated cross sections indicate that this mechanism does not play an important role in the excitation of this unnatural-parity state at 50 MeV. Also the relatively smooth transition in the shape of the QR plot with increasing energy is indicative that the compound nucleus mechanism is not important. Direct reactions characteristically show only small changes in the shapes of angular distributions for small changes in incident particle energy.

The number of open channels in the scattering of α particles from ^{20}Ne and ^{16}O is of the same order of magnitude as those for ^{24}Mg. Even if this number is overestimated, it is still so large that the compound nucleus mechanism should play a very small role in the excitation of states at α-particle energies of 50 MeV or greater.

B. Multiple Excitations

The multiple excitation mechanism was investigated by means of a coupled-channel computer code written by Glendenning.[52] The coupled-channel formalism corresponds to the physical situation in which a nuclear level is produced by both single excitation, if allowed, and all the possible combinations of multiple excitations, both nuclear and Coulomb.[53] For example, the 2- states in ^{16}O and ^{20}Ne may be made by $\ell = 2$ plus $\ell = 3$ double excitation, while the 3+ in ^{24}Mg may be $\ell = 2$ plus $\ell = 2$ excitation, since quadrupole and octupole transitions would be expected. Coupled-channel calculations have been carried out for the deformed nucleus ^{24}Mg.

For the purpose of this calculation, the low-lying states of ^{24}Mg are assumed to belong to a ground state ($K = 0$) rotational band and to a second band based on a static non-axially symmetric deformation. This second band is usually described as a rotational band based on a quadrupole γ-vibration.[41] However Glendenning's code treats K as a good quantum number, as it should for a vibration but should not for a non-axially symmetric deformation. Since α-scattering differential cross sections and angular distributions are determined almost entirely by the coupling strengths and by the angular momentum transfers respectively, it is quite unlikely that this unusual and self-inconsistent model used for the levels of the second rotational band will introduce more than minor errors.

The nucleus is assumed to be a perfect rotor. The wave functions are taken as an internal nuclear part, which is the same for all members of the same rotational band, and a D function which describes the state of rotation of the nucleus.[54] The model assumes the scattering is from a non-axially symmetric deformed complex well. The calculation is an exact solution of the Schrödinger equation within the number of channels considered. The coupled channel formalism is not as restricted as the Austen-Blair Model, and the excitation of unnatural parity states is allowed to second and higher order.

The physical process involved in exciting rotational states in deformed nuclei is an interaction with the part of the nuclear field arising from the deformation. The scattering problem is defined by the Schrödinger equation

$$(H - E)\Psi(\overline{r},\overline{A}) = 0$$

The solution will be in the form of an expansion in terms of the nuclear wave functions $\Phi_{\alpha J}(\vec{A})$, where

$$(H_A - E_{\alpha J})\,\Phi_{\alpha J}(\vec{A}) = 0$$

and H_A is the nuclear rotor model Hamiltonian.

Let Ψ be the wave function of the particle. For a particular channel with total angular momentum I and parity π the wave function will be

$$\phi = \left[\Psi \Phi_{\alpha J}\right]^{I}_{M}$$

Let c denote the collection of quantum numbers which define the intrinsic state of the nucleus and particle and their relative angular momenta before the collision, and let c' denote some other state of intrinsic or relative motion resulting from the collision. The solution for the Schrödinger equation will be

$$\Psi(\vec{r},\vec{A}) = \frac{1}{r} \sum_{c'} u_{c'}(r)\ \phi$$

where u(r) is a radial wave function.

Inserting Ψ into the Schrödinger equation gives a set of coupled equations for each channel c' for the radial wave functions of the scattered particle.

$$(T_{c'} + V_{c'c'} - E_{c'})\ u_{c'}(r) = -\sum_{c''\neq c'} V_{c'c''}\ u_{c''}(r)$$

where

$$T_c = \frac{\hbar^2}{2m}\left(-\frac{d^2}{dr^2} + \frac{\ell(\ell+1)}{r^2}\right)$$

and

$$E_c = E - E_{\alpha J}$$

when E is the bombarding energy. Also

$$V_{c'c''} = \langle \phi_{c'} | V(\vec{r},\vec{A}) | \phi_{c''} \rangle$$

To make the number of equations finite, consider only those terms corresponding to the lowest-lying states of the target nucleus. When certain boundary conditions are met the set of coupled equations can be solved. They are (1) each u_c must vanish at the origin and (2) in the exterior region, where the nuclear potentials have fallen to zero, the equations become uncoupled

$$u_c \to \alpha F_c + \beta G_c$$

where F and G are the regular and irregular Coulomb functions. Instead of F and G the combinations of these functions which behave asymptotically like outgoing and incoming spherical waves, O_ℓ and I_ℓ, are used.

$$I^*_\ell = O_\ell = G_\ell + iF_\ell$$

In the channel c there are both incoming and outgoing spherical waves at infinity, corresponding to the fact that there is an incident wave in this channel. In all other channels there are only outgoing waves.

$$u_{c'} \rightarrow \delta_{c'c}\, I_c - \left(\frac{k_c}{k_{c'}}\right)^{1/2} S_{c'c}\, O_{c'}$$

where $S_{c'c}$ is the scattering matrix element. Because the integration had to be started at the origin, in general the integrated solutions will have both incoming and outgoing waves in all channels at infinity. Therefore a linearly independent set of solutions must be generated. Number the various channels c' by 1, 2, ..., N with 1 the target channel c. Place 2 subscripts on each solution, u_{kp} where k is the channel and p is the boundary condition with respect to which the system is solved. By solving the system N times with boundary conditions p = 1,..., N gives N distinct sets of solutions, some linear combination of which satisfies the required boundary conditions at an arbitrary exterior point R. The linear algebraic equations are

$$a_1u_{11} + a_2u_{12} + \ldots a_Nu_{1N} + S_1O_{\ell_1} + 0 + \ldots + 0 = I_{\ell_1}$$

$$a_1u_{21} + a_2u_{22} + \ldots a_Nu_{2N} + 0 + S_2O_{\ell_2} + \ldots + 0 = 0$$

$$\vdots$$

$$a_1u_{N1} + a_2u_{N2} + \ldots a_Nu_{NN} + 0 \ldots\ldots + S_NO_{\ell_N} = 0$$

where all functions are evaluated at R. These equations and their derivatives give 2N equations which can be solved for the a's and the S's, the scattering matrix elements. Thus we have for the asymptotic behavior of the wave function for one channel

$$\Psi \rightarrow \frac{1}{r} \sum_{c'} \phi_{c'} \left\{\delta_{c'c}(I_c - O_c) + \left(\frac{k_c}{k_{c'}}\right)^{1/2} (\delta_{c'c} - S^I_{c'c})\, O_{c'}\right\}$$

The total wave function is

$$\Psi_T = \sum A\,\Psi$$

where the A's are chosen so that there is a plane (or Coulomb distorted) wave in the target channel. Including the Coulomb field and the asymptotic expressions for O_c and I_c gives the general form

$$\Psi_T \rightarrow \Psi_c^{M,m} + \sum_{\alpha' J' M' m'} \frac{e^{i(k'r-\eta' \ell n(2kr))}}{r} f^N \Phi \Psi$$

where the first term has a Coulomb scattered wave and the second represents the scattered waves arising from the nuclear interactions.

The flux through the surface $r^2 d\Omega$ in the direction Ω is $|f|^2 \nu' d\Omega$ and the incident flux is ν, so that the differential cross section is

$$\frac{d\sigma}{d\Omega} = \frac{1}{2(2J+1)}\left(\frac{\nu'}{\nu}\right) \sum_{MmM'm'} |f|^2$$

where

$$f = f^c + f^N$$

with f^c the Coulomb amplitude and f^N the nuclear amplitude.

A modification of the optical model computer program SEEK[55] was used to fit the elastic angular distribution in order to obtain the starting optical model parameters. These were V, the real potential well depth, W the imaginary potential well depth, r and r_i the real and imaginary radii, r_c the Coulomb radius and a and a_i the real and imaginary diffuseness parameters.

The nuclear shape was defined by

$$R = R_0\left[1 + \sum_{\substack{\lambda=2,4 \\ K \text{ even}}} \alpha_{\lambda K} Y_{\lambda K}(\theta', \phi')\right] = R_0 + \delta R$$

where the prime refers to the body-fixed axis. Five independent α's can be written in terms of the constants $\hat{\beta}_\lambda$.

$$\alpha_{2,0} = \hat{\beta}_2 \cos \hat{\beta}_1$$

$$\alpha_{2,2} = \alpha_{2,-2} = \frac{1}{\sqrt{2}} \hat{\beta}_2 \sin \hat{\beta}_1$$

$$\alpha_{4,0} = \hat{\beta}_4 \cos \hat{\beta}_3$$

$$\alpha_{4,2} = \alpha_{4,-2} = \frac{1}{\sqrt{2}} \hat{\beta}_4 \sin \hat{\beta}_3 \cos \hat{\beta}_5$$

$$\alpha_{4,4} = \alpha_{4,-4} = \frac{1}{\sqrt{2}} \hat{\beta}_4 \sin \hat{\beta}_3 \sin \hat{\beta}_5$$

where $\hat{\beta}_2$ and $\hat{\beta}_4$ are the deformation parameters, $\hat{\beta}_1$ corresponds to γ, which describes the deviation from rotational symmetry and $\hat{\beta}_3$ and $\hat{\beta}_5$ are azimuthal asymmetry parameters in the $\lambda = 4$ deformations.

Expanding the potential in a Taylor series about the spherical shape gives

$$V(r-R) = V(r-R_0) + \sum_{s=1}^{\infty} \frac{(-\delta R)^s}{s!} \frac{\delta^s V}{\delta r^s}$$

The first term is merely a spherical optical potential giving rise only to elastic scattering and the second, non-spherical part, gives rise to excitations of the nucleus from one rotational state to another.

With the nuclear shape parameterized as above, the α's that contribute to the in-band transitions between the 0+ and the 2+ states will be $\alpha_{2,0}$, $\alpha_{2,0}^2$, $\alpha_{4,0}^2$, $\alpha_{2,0}\alpha_{4,0}$ and higher order terms. The expansion was carried to eighth order. For the $\ell = 4$ transition to the 4+ state in the ground state rotational band the major contributions will be from the $\alpha_{4,0}$, $\alpha_{2,0}^2$, $\alpha_{2,0}\alpha_{4,0}$ and the $\alpha_{4,0}^2$. For the interband transitions to the K = 2 rotational band 2+ level the main contributing terms will be $\alpha_{2,2}$ and $\alpha_{2,-2}$. Since the unnatural-parity 3+ state cannot be made by a direct transition, the terms contributing will be those that go through the various possible intermediate states.

The optical model parameters as well as the nuclear shape parameters were then put into the coupled-channel program and adjusted as necessary to give the best overall fit to both the shapes and magnitudes of the experimental angular distributions. The code calculates absolute cross sections. The results obtained for the 50 MeV case are shown in Figure 32. The results for the higher energies are given in Figures 33 to 35. Figure 36 shows the shape of the nucleus with the given $\hat{\beta}_2$ and $\hat{\beta}_4$ values.

Table 3 gives the optical model parameters obtained in fitting the elastic angular distributions with the program SEEK[55] and the parameters

Table III. $^{24}Mg(\alpha,\alpha')^{24}Mg$.*

Optical Model Parameters

Elastic Fits*

E	V	w	r	r_i	r_c	a	a_i
50	100	27.6	1.47	1.6	1.3	.58	.57
65.7	100	40.1	1.44	1.6	1.3	.66	.48
81	100	31.7	1.38	1.6	1.3	.69	.58
119.7	100	23.8	1.28	1.6	1.3	.78	.71

Coupled Channel Fits

E	V	w	r	r_i	r_c	a	a_i
50	100	16	1.38	1.45	1.3	.69	.58
65.7	100	18	1.38	1.45	1.3	.69	.58
81	100	17	1.38	1.6	1.3	.69	.58
119.7	100	23	1.38	1.6	1.3	.69	.58

E	$\hat{\beta}_1$	$\hat{\beta}_2$	$\hat{\beta}_3$	$\hat{\beta}_4$
50	.29	.35	1.571	.12
65.7	.29	.35	1.571	.12
81	.29	.35	1.571	.12
119.7	.29	.35	1.571	.12

*Ref. 56.

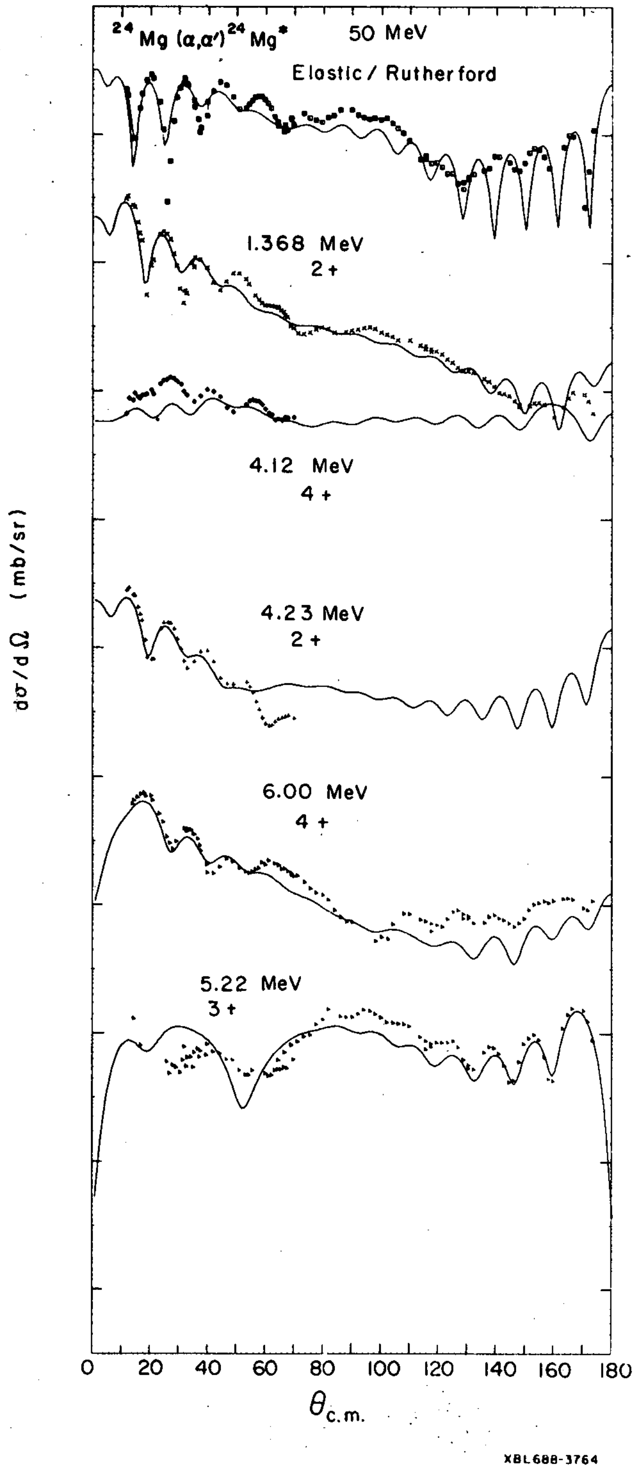

Fig. 32. $^{24}Mg(\alpha,\alpha')^{24}Mg^{*}$ cross sections with coupled-channel results for 50 MeV.

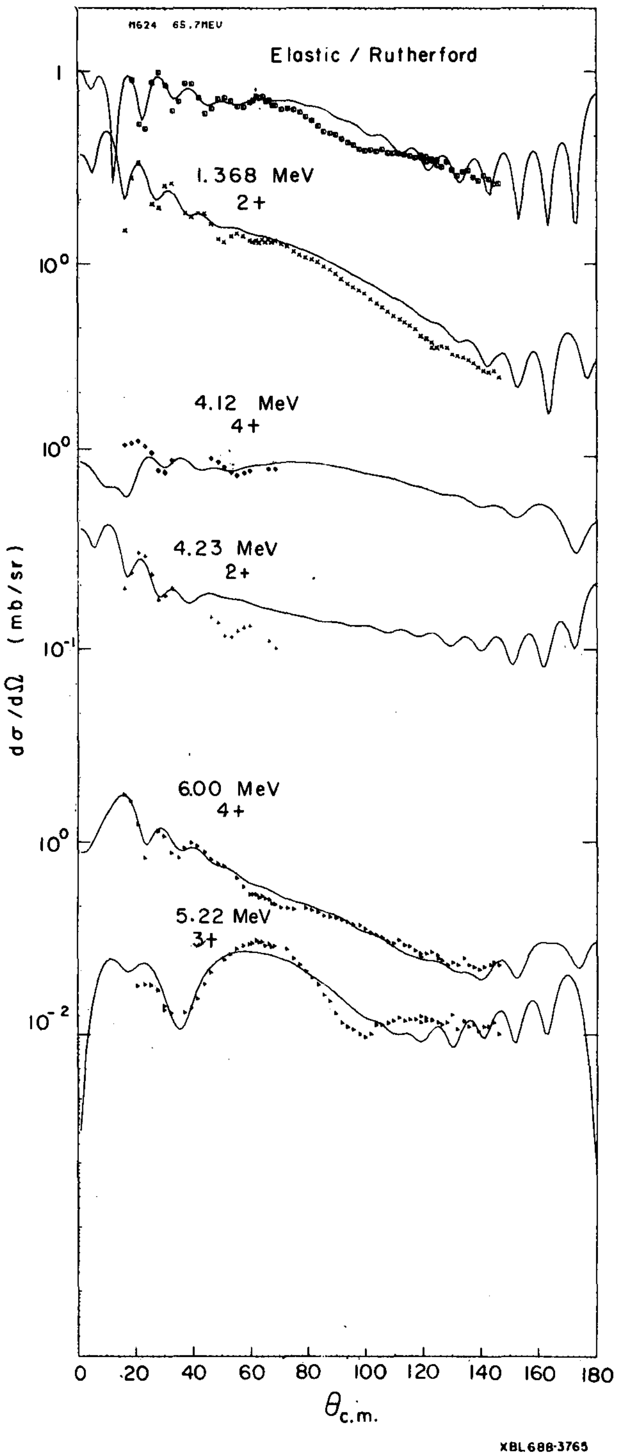

Fig. 33. $^{24}Mg(\alpha,\alpha')^{24}Mg^*$ cross sections with coupled-channel results for 65 MeV.

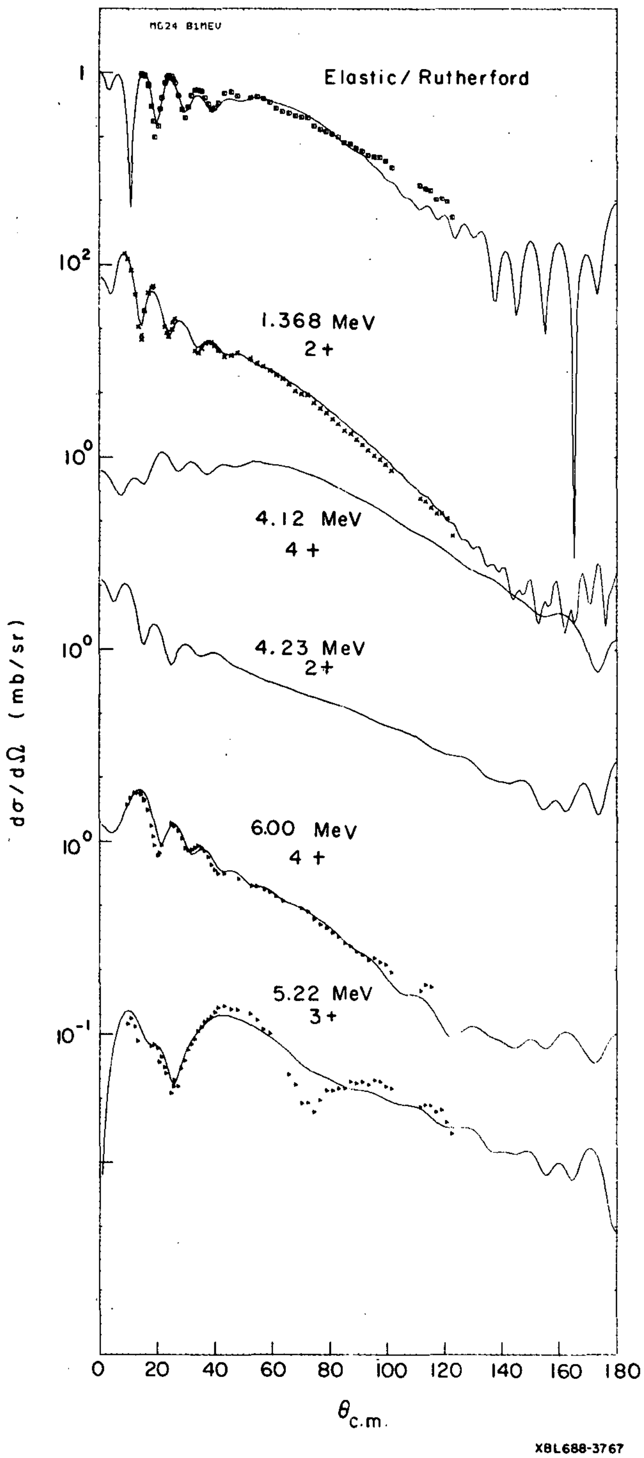

Fig. 34. $^{24}Mg(\alpha,\alpha')^{24}Mg^*$ cross sections with coupled-channel results for 81 MeV.

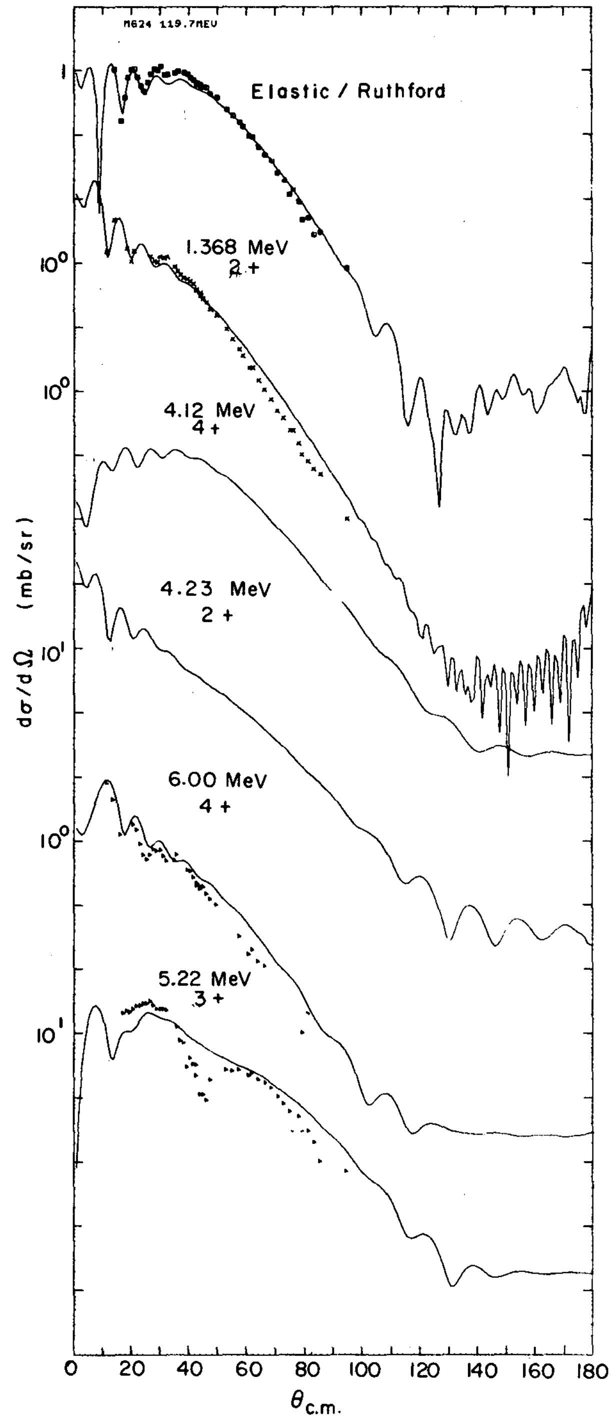

Fig. 35. $^{24}Mg(\alpha,\alpha')^{24}Mg^{*}$ cross sections with coupled-channel results for 119.7 MeV.

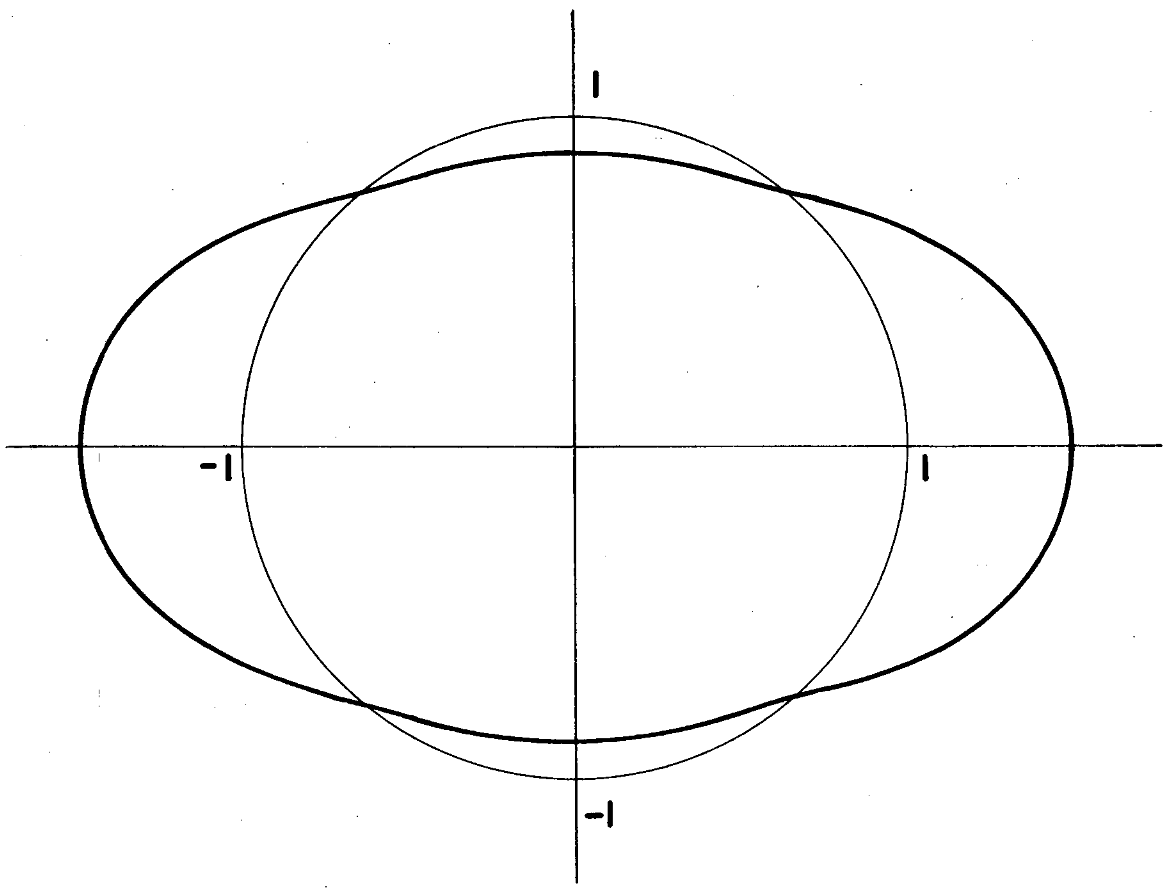

XBL 688-3783

Fig. 36. Diagram of nuclear shape using given β_2 and β_4 values.

obtained in the coupled-channel fits. The major change in the parameterization when the excited states are coupled to the ground state is a decrease in W, the imaginary potential well depth. This is as would be expected since W measures the nuclear reactions taking place, and in the coupled-channel calculation, some of these reactions are inserted explicitly through the $\hat{\beta}_\lambda$'s. The table shows that a consistent set of optical model and coupling parameters can be obtained with the coupled-channel program.

To show that the 3+ excitation is explained by the multiple excitation process, the parameters used in the calculations must also reproduce the cross sections to the states which can be produced through single excitation processes. The figures show that the fits to all the levels are quite good.

Cohen and Cookson[42] found a value of .38 for γ. This should be compared to our $\hat{\beta}_1$ value of .29. The values for the $\alpha_{\lambda\mu}$'s corrected for nuclear radius correspond to the β_λ's used by other authors in the expansion of the nuclear shape. Table 4 compares these values. My values include only first order effects while those of other workers include higher order terms. This can be seen in the expansion of the nuclear shape:

$$\beta_2 Y_2^0 + (\beta_2 Y_2^0)^2 + \ldots = \beta_2 Y_2^0 + \beta_2^2 \, (Y_0^0 + Y_2^0 + Y_4^0) + \ldots$$

My value is the β_2 in the first term. Other authors use the sum of all the β_2 terms. Thus my values would be expected to be smaller. It can be seen that in general the agreement is fairly good, and the nuclear model used in the coupled-channel program gives parameters consistent with those found by other authors using different methods. Some of the other values were obtained by coulomb excitation studies; however Naqib[57] obtained his from inelastic α scattering at 42 MeV.

The parameters used in the coupled channel program were such that $\alpha_{4,0}$ equaled zero, eliminating any direct component in the excitation of the first 4+ state. $\alpha_{4,2}$ was non-zero giving some direct excitation to the K = 2 band 4+ state, as was found necessary by Naqib in his work. This direct component to the 4+ in the γ band indicates some band mixing.

The lifetimes of the states and the branching ratios for γ-decay were

Table IV. ^{24}Mg deformation parameters.

Level	Spin	K	Present Work β_λ [a]	Other Work β_λ [b]	Reference
1.368	2+	0	.39	.65	46
1.368	2+	0	.39	.48	57
4.12	4+	0	0		
4.23	2+	2	.082		
6.00	4+	2	.098	.17	57
6.44	0+	0		.12	57

[a] $\beta_\lambda = \alpha_{\lambda\mu} \times \frac{1.38A^{1/3}}{1.20A^{1/3}}$

[b] $\beta_\lambda = \frac{\delta_\lambda}{1.2 \times A^{1/3}}$ where δ_λ is the deformation distance reported in reference 57.

calculated using a β value of .42. This value includes the higher order contributions to the deformation parameter. The lifetimes and branching ratios obtained in this way give fairly good agreement with values obtained by other experimenters. In these calculations only the major components of the wave functions were used. Other reasons for discrepancies include the fact that K is not a good quantum number in this case and that there is mixing between the K = 0 and K = 2 bands.

The shapes and magnitudes for the 3^+ angular distributions are fit well enough to suggest very strongly that a multiple excitation mechanism is able to account for the experimental results. Tamura[58] used the ^{24}Mg data of Kokame et al.[4] at 28.5 MeV in similar calculations and concluded that the multiple excitation process can account for the excitation of the unnatural-parity state. Vincent, Boschitz and Priest[6] have also used this formalism for comparison to their 42 MeV data and found fairly good agreement. Thus these results allow us to conclude that the multiple excitation process accounts for the major part of the excitation of the unnatural-parity state in ^{24}Mg at these α-particle energies.

V. CONCLUSIONS

The good agreement obtained using the coupled-channel program of Glendenning [52] allows us to conclude that the multiple excitation mechanism does account for the production of the 3+ state in ^{24}Mg at medium and high α-particle energies.

The strange behavior of the ^{24}Mg 3+ QR plots at the different energies is reproduced by the coupled-channel program. It seems likely that it arises from a change with energy of the major excitation path for the production of the unnatural-parity state. For instance the excitation may be mainly through the first 2+ at lower α-particle energies and mainly through the K = 2 2+ at higher energies. There may be interference effects between these two paths giving rise to the moving peaks on the QR plots. Unfortunately it is not possible to select the path and use only this in the coupled-channel program. Gruhn and Wall[59] have studied the energy dependence of elastic scattering of α's by ^{40}Ca. They found that for the large angle data the last few maxima in the oscillatory pattern remained relatively fixed in angle as the α-particle energy was changed. The intermediate angular region appeared to result from an interference between the large angle oscillatory pattern and the forward angle diffraction pattern. This type of interference effect may give rise to the observed behavior in ^{24}Mg and ^{20}Ne.

The small compound nucleus cross sections calculated for the ^{24}Mg 50 MeV incident α-particle energy make it unlikely that this mechanism makes an important contribution to the reaction mechanism at this energy or above. At the α-particle energies studied, the number of open channels for all the nuclei studied is so large that decay to any one state is very unlikely. The compound nucleus mechanism can therefore be ruled out for the production of states in the nuclei studied here.

The similar behavior of the 2+ QR plots for ^{20}Ne as for the ^{24}Mg case suggests that the multiple excitation mechanism will also be able to explain the excitation in the ^{20}Ne case. The different behavior of the 2- QR plots for ^{16}O make it unlikely that the reaction mechanism is the same. Unfortunately the wave functions of ^{20}Ne and ^{16}O are not of a form that can be used in the coupled-channel program at this time. The actual mechanisms for the excitation of the unnatural-parity states in these nuclei therefore remain to be investigated. The spin-flip mechanism, where the orbital angular momentum of the incoming α particle couples with a spin-flip of one or more of the target nucleons may be an important mechanism in the ^{16}O case. The 2- state is described as a $p_{1/2}$ hole and a $d_{5/2}$ particle. When the particle is promoted to the $d_{5/2}$ orbital a spin flip may occur.

The knock-out or target-stripping mechanisms seem unlikely because in all the cases studied the angular distributions for the unnatural-parity states are not strongly forward or backward peaked. Also the large angle behavior described by Honda and Ui[19] is not observed in these cases.

ACKNOWLEDGMENTS

I would like to thank my research director, Dr. Bernard G. Harvey, for suggesting this topic and for all his help during the experiments and the writing of this thesis. I would also like to thank Dr. David L. Hendrie for his help with the calculations and thesis, Dr. John R. Meriwether for his help in the initial stages of the experiments, and Dr. Norman K. Glendenning for the use of his computer code.

I would like to thank my fellow graduate students, Mr. Joel Moss, Dr. Arthur Springer, Dr. Nolan Mangelson, Dr. Chi Chang Lu and Mr. Michael Zisman, for their help in the execution of these experiments.

I would also like to thank Dr. Joseph Cerny III, Dr. Gilbert Butler, Mr. Creve Maples, Mr. John Esterl, Mr. George Goth, and Mr. Gordon Wazniak.

I am extremely grateful to the entire crew of the 88-inch cyclotron, especially to Mr. John Bowen and the operators and to Mr. John Meneghetti and his crew.

This work was done under the auspices of the U. S. Atomic Energy Commission.

APPENDIX

$Mg^{24}(\alpha,\alpha')$

50 MeV

Elastic

θ_L (deg)	θ_{cm} (deg)	$d\sigma/d\Omega$ (mb/sr)	Δ (mb/sr)	θ_L (deg)	θ_{cm} (deg)	$d\sigma/d\Omega$ (mb/sr)	Δ (mb/sr)
10.8	12.6	1127	3	106.1	115.4	.033	.002
12.8	14.9	106.5	.8	106.1	115.4	.037	.002
14.8	17.3	337.9	1.4	108.1	117.3	.027	.002
17.7	20.6	338.6	1.4	108.1	117.3	.027	.002
27.7	32.2	50.32	.32	110.1	119.1	.027	.002
28.7	33.3	34.96	.08	112.1	121.0	.022	.001
29.7	34.5	25.69	.23	114.1	122.9	.017	.001
30.7	35.6	12.33	.05	116.0	124.7	.016	.001
31.7	36.8	6.95	.12	118.0	126.5	.011	.001
32.7	37.7	4.73	.03	120.0	128.4	.0086	.0011
34.7	40.1	9.31	.04	120.0	128.4	.011	.001
56.6	64.6	.667	.011	122.0	130.2	.012	.001
58.6	66.8	.606	.010	122.0	130.2	.013	.001
60.6	69.0	.705	.011	124.0	132.0	.014	.001
60.6	69.0	.686	.005	128.0	135.7	.015	.002
64.6	73.3	.681	.005	130.0	137.4	.016	.002
66.5	75.3	.526	.004	132.0	139.2	.024	.002
68.5	77.5	.440	.011	133.9	140.8	.023	.001
70.5	79.6	.381	.010	135.9	142.6	.019	.001
72.5	81.7	.405	.011	137.9	144.4	.018	.001
74.5	83.8	.400	.011	139.9	146.1	.014	.001
76.5	85.9	.452	.009	141.9	147.8	.013	.001
78.4	87.8	.447	.008	143.9	149.6	.017	.001
80.4	89.9	.392	.008	145.9	151.3	.024	.001
82.4	92.0	.303	.007	147.9	153.0	.028	.002
84.4	94.0	.260	.006	149.9	154.7	.026	.002
86.4	96.0	.230	.005	151.9	156.4	.020	.002
88.3	97.9	.223	.005	153.9	158.1	.013	.001
90.3	100.0	.201	.005	155.9	159.8	.011	.001
92.3	101.9	.198	.005	159.9	163.2	.027	.002
94.3	103.9	.157	.004	161.9	164.9	.041	.002
96.2	105.8	.124	.005	163.8	166.5	.039	.002
98.2	107.8	.099	.004	168.2	170.2	.0030	.0008
100.2	109.8	.072	.003	170.2	171.9	.011	.002
104.1	113.5	.034	.002	172.2	173.5	.048	.003

(continued)

50 MeV (continued)

1.368 MeV 2+

θ_L (deg)	θ_{cm} (deg)	dσ/dΩ (mb/sr)	Δ (mb/sr)	θ_L (deg)	θ_{cm} (deg)	dσ/dΩ (mb/sr)	Δ (mb/sr)
10.8	12.6	104.1	.8	106.1	115.5	.441	.009
12.8	15.0	71.20	.64	106.1	115.5	.491	.008
13.8	16.1	40.92	.48	108.1	117.4	.401	.008
14.8	17.3	21.60	.35	108.1	117.4	.443	.008
15.8	18.5	6.04	.18	110.1	119.3	.410	.008
17.7	20.7	8.94	.22	112.1	121.2	.366	.003
27.7	32.3	3.53	.08	114.1	123.1	.306	.002
28.7	33.4	5.98	.03	116.0	124.8	.273	.002
29.7	34.6	9.63	.14	118.0	126.6	.228	.005
30.7	35.7	11.67	.05	120.0	128.5	.199	.005
56.6	64.7	1.91	.02	120.0	128.5	.207	.005
58.6	66.9	1.47	.02	122.0	130.3	.198	.005
60.6	69.1	1.03	.01	122.0	130.3	.207	.005
60.6	69.1	1.00	.01	124.0	132.1	.189	.005
62.6	71.3	.775	.005	128.0	135.8	.150	.005
64.6	73.4	.745	.005	130.0	137.5	.139	.004
66.5	75.5	.790	.005	132.0	139.3	.114	.004
68.5	77.6	.884	.016	133.9	141.0	.092	.003
70.5	79.7	.957	.017	135.9	142.7	.089	.003
72.5	81.8	.908	.017	137.9	144.5	.082	.003
74.5	83.9	.799	.016	139.9	146.2	.069	.003
76.5	86.0	.773	.011	141.9	147.9	.059	.002
78.4	88.0	.814	.012	143.9	149.7	.056	.002
80.4	90.0	.848	.012	145.9	151.4	.058	.002
82.4	92.1	.893	.012	147.9	153.1	.064	.003
84.4	94.2	.946	.010	149.9	154.8	.065	.003
86.4	96.2	.982	.010	151.9	156.5	.060	.003
88.3	98.1	.897	.010	153.9	158.2	.055	.002
90.3	100.1	.800	.009	155.9	159.9	.038	.002
92.3	102.1	.735	.009	159.9	163.3	.056	.003
94.3	104.0	.687	.008	161.9	164.9	.076	.003
96.2	106.0	.601	.008	163.8	166.5	.094	.003
98.2	108.0	.631	.008	168.2	170.2	.087	.005
100.2	110.0	.604	.008	170.2	171.9	.069	.004
104.1	113.6	.500	.009	172.2	173.5	.044	.003

(continued)

50 MeV (continued)

	4.12 MeV 4+				4.23 MeV 2+		
θ_L (deg)	θ_{cm} (deg)	$d\sigma/d\Omega$ (mb/sr)	Δ (mb/sr)	θ_L (deg)	θ_{cm} (deg)	$d\sigma/d\Omega$ (mb/sr)	Δ (mb/sr)
10.8	12.7	.753	.065	10.8	12.7	8.39	.22
12.8	15.0	.910	.072	12.8	15.0	6.36	.19
13.8	16.2	.786	.066	13.8	16.2	4.18	.15
14.8	17.4	.837	.069	14.8	17.4	2.57	.12
15.8	18.6	.850	.068	15.8	18.6	1.28	.08
17.7	20.8	1.01	.08	17.7	20.8	.636	.059

(continued)

50 MeV (continued)

5.22 MeV 3+

θ_L (deg)	θ_{cm} (deg)	$d\sigma/d\Omega$ (mb/sr)	Δ (mb/sr)	θ_L (deg)	θ_{cm} (deg)	$d\sigma/d\Omega$ (mb/sr)	Δ (mb/sr)
12.8	15.1	.116	.026	106.1	116.0	.055	.003
14.8	17.4	.064	.019	106.1	116.0	.074	.003
27.7	32.5	.063	.011	108.1	117.9	.060	.003
28.7	33.6	.041	.003	108.1	117.9	.067	.003
29.7	34.8	.042	.009	110.1	119.8	.070	.003
30.7	35.9	.049	.003	112.1	121.6	.070	.001
31.7	37.1	.056	.011	114.1	123.5	.070	.001
32.7	38.1	.052	.003	116.0	125.3	.074	.001
34.7	40.4	.066	.004	118.0	127.1	.059	.003
56.6	65.1	.037	.003	120.0	128.9	.037	.002
58.6	67.3	.049	.003	120.0	128.9	.039	.002
60.6	69.5	.065	.003	122.0	130.7	.028	.002
60.6	69.5	.064	.001	122.0	130.7	.031	.005
62.6	71.7	.073	.002	124.0	132.5	.027	.002
64.6	73.9	.087	.002	128.0	136.2	.049	.003
66.5	75.9	.092	.002	130.0	137.9	.063	.003
68.5	78.0	.135	.006	132.0	139.6	.058	.003
70.5	80.2	.161	.007	133.9	141.3	.047	.002
72.5	82.3	.232	.008	135.9	143.1	.031	.002
76.5	86.5	.180	.005	137.9	144.8	.017	.001
78.4	88.5	.177	.005	139.9	146.5	.018	.001
80.4	90.6	.176	.005	141.9	148.2	.035	.002
82.4	92.6	.196	.006	143.9	149.9	.067	.003
84.4	94.6	.225	.005	145.9	151.7	.082	.003
86.4	96.7	.217	.005	147.9	153.4	.094	.003
88.3	98.6	.195	.005	149.9	155.0	.078	.003
90.3	100.6	.173	.005	151.9	156.7	.042	.002
92.3	102.6	.146	.004	153.9	158.4	.019	.001
94.3	104.6	.143	.004	155.9	160.0	.018	.001
96.2	106.5	.138	.004	159.9	163.4	.117	.004
98.2	108.4	.135	.004	161.9	165.1	.194	.005
100.2	110.3	.125	.004	163.8	166.6	.245	.005
104.1	114.1	.086	.004	168.2	170.3	.221	.007
				170.2	172.0	.150	.006
				172.2	173.6	.077	.005

(continued)

50 MeV (continued)

6.00 MeV 4+

θ_L (deg)	θ_{cm} (deg)	dσ/dΩ (mb/sr)	Δ (mb/sr)	θ_L (deg)	θ_{cm} (deg)	dσ/dΩ (mb/sr)	Δ (mb/sr)
12.8	15.1	4.18	.15	106.1	116.1	.055	.003
13.8	16.3	4.62	.16	108.1	118.0	.039	.003
14.8	17.5	5.22	.17	108.1	118.0	.050	.003
15.8	18.6	5.42	.17	110.1	119.9	.047	.003
17.7	20.9	4.88	.16	112.1	121.7	.045	.001
27.7	32.5	1.54	.05	114.1	123.6	.059	.001
28.7	33.7	1.49	.02	116.0	125.4	.077	.001
29.7	34.9	1.46	.05	118.0	127.2	.081	.003
30.7	36.0	1.24	.02	120.0	129.0	.071	.003
31.7	37.2	1.04	.05	120.0	129.0	.063	.003
32.7	38.2	.686	.011	122.0	130.8	.066	.003
34.7	40.5	.313	.008	122.0	130.8	.062	.003
56.6	65.2	.410	.009	124.0	132.6	.051	.003
58.6	67.4	.352	.008	128.0	136.3	.052	.003
60.6	69.6	.303	.008	130.0	138.0	.065	.003
60.6	69.6	.283	.003	132.0	139.7	.069	.003
62.6	71.8	.277	.003	133.9	141.4	.062	.002
64.6	74.0	.222	.003	135.9	143.1	.057	.002
66.5	76.0	.174	.003	137.9	144.9	.051	.002
68.5	78.1	.150	.007	139.9	146.6	.045	.002
70.5	80.3	.140	.006	141.9	148.3	.051	.002
72.5	82.4	.117	.006	143.9	150.0	.063	.003
74.5	84.5	.081	.005	145.9	151.7	.083	.003
76.5	86.6	.064	.003	147.9	153.4	.100	.003
78.4	88.6	.054	.003	149.9	155.1	.107	.003
80.4	90.7	.053	.003	151.9	156.8	.113	.004
88.3	98.7	.027	.002	153.9	158.5	.106	.003
90.3	100.7	.031	.002	155.9	160.1	.114	.004
92.3	102.7	.029	.002	159.9	163.5	.124	.004
94.3	104.7	.049	.002	161.9	165.1	.125	.004
96.2	106.6	.052	.002	163.8	166.7	.122	.004
98.2	108.5	.073	.003	168.2	170.3	.088	.005
100.2	110.5	.071	.003	170.2	172.0	.082	.005
104.1	114.2	.058	.003	172.2	173.6	.115	.005
106.1	116.1	.055	.003				

(continued)

50 MeV (continued)

6.44 MeV 0+

θ_L (deg)	θ_{cm} (deg)	dσ/dΩ (mb/sr)	Δ (mb/sr)	θ_L (deg)	θ_{cm} (deg)	dσ/dΩ (mb/sr)	Δ (mb/sr)
12.8	15.1	2.17	.11	104.1	114.2	.016	.002
27.7	32.6	.385	.027	106.1	116.1	.010	.001
31.7	37.2	.531	.032	106.1	116.1	.014	.001
32.7	38.2	.403	.009	108.1	118.0	.012	.002
34.7	40.5	.200	.006	108.1	118.0	.014	.001
58.6	67.5	.118	.005	110.1	119.9	.012	.001
60.6	69.7	.097	.004	112.1	121.8	.010	.001
60.6	69.7	.091	.002	116.0	125.4	.0048	.0003
62.6	71.8	.087	.002	120.0	129.1	.0074	.0010
64.6	74.0	.072	.002	120.0	129.1	.0084	.0012
66.5	76.1	.058	.002	122.0	130.9	.012	.001
68.5	78.2	.068	.005	122.0	130.9	.011	.001
70.5	80.4	.055	.004	124.0	132.6	.010	.001
72.5	82.5	.050	.004	133.9	141.4	.0023	.0005
74.5	84.6	.041	.004	135.9	143.2	.0028	.0005
76.5	86.7	.031	.002	137.9	144.9	.0044	.0007
78.4	88.7	.031	.002	139.9	146.6	.0051	.0008
80.4	90.7	.029	.002	141.9	148.3	.0022	.0005
82.4	92.8	.020	.002	143.9	150.1	.0017	.0005
94.3	104.8	.013	.001	149.9	155.1	.0028	.0006
96.2	106.6	.013	.001	151.9	156.8	.0006	.0003
98.2	108.6	.019	.001	153.9	158.5	.0048	.0007
100.2	110.5	.016	.001				

$Mg^{24}(\alpha,\alpha')$

65.7 MeV

Elastic

θ_L (deg)	θ_{cm} (deg)	dσ/dΩ (mb/sr)	Δ (mb/sr)	θ_L (deg)	θ_{cm} (deg)	dσ/dΩ (mb/sr)	Δ (mb/sr)
16.1	18.8	243.1	.3	76.1	85.5	.127	.003
18.1	21.1	31.44	.12	78.1	87.6	.111	.002
20.1	23.4	17.89	.09	80.1	89.6	.098	.002
22.1	25.7	64.35	.10	82.1	91.7	.079	.002
22.1	25.7	65.27	.11	84.1	93.7	.065	.002
24.1	28.0	66.59	.10	86.1	95.8	.055	.001
24.1	28.0	67.51	.11	88.1	97.8	.046	.001
26.1	30.3	30.69	.07	90.1	99.8	.040	.001
26.1	30.3	31.04	.08	92.1	101.8	.039	.001
28.1	32.6	9.189	.037	94.1	103.8	.035	.001
30.1	34.9	9.984	.026	96.1	105.7	.036	.001
32.1	37.2	14.67	.03	98.1	107.7	.030	.001
34.1	39.5	11.55	.03	100.1	109.6	.028	.001
36.1	41.8	5.675	.020	102.1	111.6	.026	.001
38.1	44.1	2.615	.013	104.1	113.5	.024	.001
40.1	46.3	2.572	.013	106.1	115.4	.022	.001
42.1	48.6	3.054	.014	108.1	117.3	.020	.001
44.1	50.8	2.697	.014	110.1	119.2	.019	.001
46.1	53.1	2.034	.012	110.1	119.2	.021	.001
48.1	55.3	1.439	.010	112.1	121.1	.019	.001
50.1	57.5	1.227	.009	112.1	121.1	.016	.001
52.1	59.7	1.264	.009	114.1	122.9	.016	.001
53.1	60.8	1.275	.010	114.1	122.9	.017	.001
54.1	61.9	1.378	.008	116.1	124.8	.013	.001
55.1	63.0	1.226	.009	116.1	124.8	.016	.001
56.1	64.1	1.224	.008	117.9	126.4	.012	.001
57.1	65.2	.971	.008	119.9	128.3	.014	.002
58.1	66.3	.945	.007	121.9	130.1	.010	.001
59.1	67.4	.746	.007	123.9	131.9	.008	.001
60.1	68.5	.701	.006	126.1	133.9	.009	.001
62.1	70.6	.547	.004	128.1	135.7	.009	.001
64.1	72.8	.496	.004	130.1	137.5	.007	.001
66.1	74.9	.434	.004	132.1	139.3	.006	.001
68.1	77.1	.363	.004	134.1	141.0	.007	.001
70.1	79.2	.282	.004	136.1	142.8	.006	.001
72.1	81.3	.224	.003	138.1	144.5	.005	.001
74.1	83.4	.169	.003	140.1	146.3	.005	.001

(continued)

65.7 MeV (continued)

1.368 MeV 2+

θ_L (deg)	θ_{cm} (deg)	$d\sigma/d\Omega$ (mb/sr)	Δ (mb/sr)	θ_L (deg)	θ_{cm} (deg)	$d\sigma/d\Omega$ (mb/sr)	Δ (mb/sr)
14.1	16.5	3.295	.039	78.1	87.7	.801	.005
16.1	18.8	21.65	.10	80.1	89.8	.681	.005
18.1	21.1	37.94	.13	82.1	91.8	.572	.005
22.1	25.8	8.397	.035	84.1	93.8	.480	.004
22.1	25.8	8.517	.039	86.1	95.9	.422	.003
24.1	28.1	7.413	.033	88.1	97.9	.384	.003
24.1	28.1	7.532	.037	90.1	99.9	.338	.003
26.1	30.4	16.22	.05	92.1	101.9	.278	.003
26.1	30.4	16.44	.06	94.1	103.9	.240	.002
28.1	32.7	17.80	.05	96.1	105.8	.206	.002
32.1	37.3	6.209	.021	98.1	107.8	.179	.002
34.1	39.6	5.249	.019	100.1	109.7	.154	.002
36.1	41.9	6.308	.021	102.1	111.7	.132	.001
38.1	44.1	5.988	.020	104.1	113.6	.119	.001
40.1	46.4	4.117	.017	106.1	115.5	.106	.001
42.1	48.7	2.421	.013	108.1	117.4	.094	.001
44.1	50.9	2.156	.012	110.1	119.3	.074	.002
46.1	53.2	2.665	.013	110.1	119.3	.073	.003
48.1	55.4	2.960	.014	112.1	121.2	.066	.002
50.1	57.6	2.665	.014	112.1	121.2	.067	.003
52.1	59.8	2.254	.012	114.1	123.0	.058	.002
53.1	60.9	2.140	.012	114.1	123.0	.048	.003
54.1	62.0	2.277	.011	116.1	124.9	.048	.002
55.1	63.1	2.106	.012	116.1	124.9	.048	.003
56.1	64.2	2.338	.011	117.9	126.5	.051	.003
57.1	65.3	2.144	.013	119.9	128.4	.048	.003
58.1	66.4	2.370	.011	121.9	130.2	.038	.003
59.1	67.5	2.149	.013	123.9	132.0	.036	.003
60.1	68.6	2.278	.011	126.1	134.0	.034	.002
62.1	70.8	2.032	.008	128.1	135.8	.031	.001
64.1	72.9	1.850	.008	130.1	137.6	.028	.001
66.1	75.1	1.572	.008	132.1	139.3	.024	.001
68.1	77.2	1.351	.007	134.1	141.1	.021	.002
70.1	79.3	1.229	.008	136.1	142.9	.020	.002
72.1	81.4	1.150	.008	138.1	144.6	.021	.002
74.1	83.5	1.042	.008	140.1	146.4	.017	.002
76.1	85.6	.894	.007				

(continued)

65.7 MeV (continued)

4.12 MeV 4+				4.23 MeV 2+			
θ_L (deg)	θ_{cm} (deg)	$d\sigma/d\Omega$ (mb/sr)	Δ (mb/sr)	θ_L (deg)	θ_{cm} (deg)	$d\sigma/d\Omega$ (mb/sr)	Δ (mb/sr)
14.1	16.5	1.483	.026	14.1	16.5	.874	.020
16.1	18.9	1.593	.027	16.1	18.9	1.564	.027
18.1	21.2	1.716	.028	18.1	21.2	3.165	.039
20.1	23.5	1.429	.026	20.1	23.5	2.767	.036
22.1	25.9	1.125	.013	22.1	25.9	1.431	.014
22.1	25.9	1.142	.014	22.1	25.9	1.454	.016
24.1	28.2	.625	.011	24.1	28.2	.579	.009
24.1	28.2	.630	.011	24.1	28.2	.590	.010
26.1	30.5	.553	.009	26.1	30.5	.676	.010
26.1	30.5	.565	.010	26.1	30.5	.680	.011
28.1	32.8	.863	.011	28.1	32.8	.904	.012
40.1	46.6	.914	.008	40.1	46.6	.313	.005
42.1	48.8	.808	.007	42.1	48.8	.253	.004
44.1	51.1	.675	.007	44.1	51.1	.159	.003
46.1	53.3	.555	.006	46.1	53.3	.156	.003
48.1	55.6	.505	.006	48.1	55.6	.189	.004
50.1	57.8	.548	.006	50.1	57.8	.213	.004
52.1	60.0	.593	.006	52.1	60.0	.228	.004
58.1	66.6	.632	.006	58.1	66.6	.133	.003
60.1	68.8	.637	.006	60.1	68.8	.102	.002

(continued)

65.7 MeV (continued)

5.22 MeV 3+

θ_L (deg)	θ_{cm} (deg)	$d\sigma/d\Omega$ (mb/sr)	Δ (mb/sr)	θ_L (deg)	θ_{cm} (deg)	$d\sigma/d\Omega$ (mb/sr)	Δ (mb/sr)
18.1	21.2	.057	.005	80.1	90.1	.021	.001
20.1	23.6	.060	.005	82.1	92.2	.015	.001
22.1	25.9	.058	.003	84.1	94.2	.013	.001
22.1	25.9	.059	.003	86.1	96.2	.012	.001
24.1	28.2	.050	.003	88.1	98.3	.010	.001
24.1	28.2	.048	.003	90.1	100.3	.009	.001
26.1	30.6	.028	.002	92.1	102.3	.010	.001
26.1	30.6	.025	.002	94.1	104.2	.014	.001
28.1	32.9	.022	.002	96.1	106.2	.014	.001
32.1	37.5	.022	.001	98.1	108.2	.015	.001
34.1	39.8	.026	.001	100.1	110.1	.016	.001
36.1	42.1	.036	.002	102.1	112.0	.018	.001
38.1	44.4	.063	.002	104.1	114.0	.016	.001
40.1	46.6	.092	.002	106.1	115.9	.017	.001
44.1	51.2	.147	.003	108.1	117.8	.017	.001
46.1	53.4	.177	.003	110.1	119.6	.015	.001
48.1	55.7	.214	.004	110.1	119.6	.019	.001
50.1	57.9	.243	.004	112.1	121.5	.018	.001
52.1	60.1	.253	.004	112.1	121.5	.016	.001
53.1	61.2	.264	.004	114.1	123.4	.017	.001
54.1	62.3	.294	.004	114.1	123.4	.016	.001
55.1	63.4	.272	.004	116.1	125.2	.015	.001
56.1	64.5	.279	.004	116.1	125.2	.015	.001
57.1	65.6	.250	.004	117.9	126.9	.014	.001
58.1	66.7	.258	.004	119.9	128.7	.015	.002
59.1	67.8	.231	.004	121.9	130.5	.020	.002
60.1	68.9	.239	.004	123.9	132.3	.012	.001
64.1	73.2	.210	.003	126.1	134.3	.016	.001
66.1	75.4	.155	.002	128.1	136.1	.013	.001
68.1	77.5	.121	.002	130.1	137.9	.014	.001
70.1	79.7	.097	.002	132.1	139.6	.011	.001
72.1	81.8	.077	.002	134.1	141.4	.013	.002
74.1	83.9	.059	.002	136.1	143.1	.013	.002
76.1	86.0	.041	.001	138.1	144.9	.015	.002
78.1	88.0	.033	.001	140.1	146.6	.010	.001

(continued)

65.7 MeV (continued)

6.00 MeV 4+

θ_L (deg)	θ_{cm} (deg)	$d\sigma/d\Omega$ (mb/sr)	Δ (mb/sr)	θ_L (deg)	θ_{cm} (deg)	$d\sigma/d\Omega$ (mb/sr)	Δ (mb/sr)
14.1	16.6	5.411	.050	78.1	88.1	.067	.002
16.1	18.9	4.332	.045	80.1	90.2	.065	.002
18.1	21.3	1.858	.029	82.1	92.2	.060	.001
20.1	23.6	.561	.016	84.1	94.3	.056	.001
24.1	28.3	1.453	.015	86.1	96.3	.051	.001
24.1	28.3	1.475	.016	88.1	98.3	.050	.001
26.1	30.6	1.207	.013	90.1	100.3	.044	.001
26.1	30.6	1.219	.015	92.1	102.3	.038	.001
28.1	32.9	.679	.010	94.1	104.3	.035	.001
30.1	35.2	.560	.006	96.1	106.3	.032	.001
32.1	37.5	.793	.007	98.1	108.2	.028	.001
34.1	39.8	.967	.008	100.1	110.2	.026	.001
36.1	42.1	.857	.008	102.1	112.1	.029	.001
38.1	44.4	.680	.007	104.1	114.0	.025	.001
40.1	46.7	.532	.006	106.1	115.9	.023	.001
42.1	49.0	.460	.006	108.1	117.8	.020	.001
44.1	51.2	.417	.005	110.1	119.7	.018	.001
48.1	55.7	.272	.004	110.1	119.7	.016	.001
50.1	57.9	.198	.004	112.1	121.6	.018	.001
52.1	60.2	.154	.003	114.1	123.4	.019	.001
53.1	61.3	.153	.003	116.1	125.3	.015	.001
54.1	62.4	.151	.003	116.1	125.3	.017	.002
55.1	63.5	.135	.003	117.9	126.9	.014	.001
56.1	64.6	.142	.003	119.9	128.8	.012	.001
57.1	65.7	.130	.003	121.9	130.6	.013	.001
58.1	66.8	.127	.003	123.9	132.4	.012	.001
59.1	67.9	.108	.003	126.1	134.4	.015	.001
60.1	69.0	.107	.002	128.1	136.1	.012	.001
62.1	71.1	.098	.002	130.1	137.9	.011	.001
64.1	73.3	.092	.002	132.1	139.7	.010	.001
66.1	75.5	.089	.002	134.1	141.4	.011	.001
70.1	79.7	.092	.002	136.1	143.2	.012	.001
72.1	81.8	.086	.002	138.1	144.9	.013	.002
74.1	84.0	.079	.002	140.1	146.6	.012	.002
76.1	86.0	.070	.002				

(continued)

65.7 MeV (continued)

6.44 MeV 0+

θ_L (deg)	θ_{cm} (deg)	dσ/dΩ (mb/sr)	Δ (mb/sr)	θ_L (deg)	θ_{cm} (deg)	dσ/dΩ (mb/sr)	Δ (mb/sr)
16.1	18.9	1.113	.023	70.1	79.8	.038	.001
18.1	21.3	1.464	.026	74.1	84.0	.032	.001
20.1	23.6	.748	.019	76.1	86.1	.023	.001
22.1	26.0	.304	.007	78.1	88.2	.022	.001
22.1	26.0	.307	.007	80.1	90.2	.020	.001
24.1	28.3	.449	.008	82.1	92.3	.022	.001
24.1	28.3	.452	.009	84.1	94.3	.019	.001
26.1	30.6	.661	.010	86.1	96.4	.019	.001
26.1	30.6	.674	.011	88.1	98.4	.017	.001
28.1	32.9	.472	.008	90.1	100.4	.014	.001
30.1	35.2	.314	.005	92.1	102.4	.013	.001
32.1	37.6	.336	.005	94.1	104.4	.014	.001
34.1	39.9	.480	.006	96.1	106.3	.010	.001
38.1	44.4	.405	.005	98.1	108.3	.009	.001
40.1	46.7	.295	.004	100.1	110.2	.010	.001
42.1	49.0	.234	.004	102.1	112.2	.010	.001
44.1	51.2	.212	.004	104.1	114.1	.010	.001
46.1	53.5	.211	.004	106.1	116.0	.009	.001
48.1	55.7	.181	.003	108.1	117.9	.008	.001
50.1	58.0	.121	.003	110.1	119.8	.006	.001
52.1	60.2	.081	.002	110.1	119.8	.009	.001
53.1	61.3	.076	.002	112.1	121.6	.006	.001
54.1	62.4	.080	.002	114.1	123.5	.005	.001
55.1	63.5	.078	.002	116.1	125.3	.005	.001
56.1	64.6	.077	.002	116.1	125.3	.006	.001
57.1	65.7	.074	.002	117.9	127.0	.004	.001
58.1	66.8	.074	.002	119.9	128.8	.005	.001
59.1	67.9	.064	.002	121.9	130.6	.004	.001
60.1	69.0	.060	.002	123.9	132.4	.004	.001
62.1	71.2	.052	.001	126.1	134.4	.005	.001
64.1	73.4	.046	.001	128.1	136.2	.005	.001
66.1	75.5	.038	.001	130.1	137.9	.003	.001
68.1	77.6	.038	.001				

$Mg^{24}(\alpha,\alpha')$

81 MeV

Elastic

θ_L (deg)	θ_{cm} (deg)	$d\sigma/d\Omega$ (mb/sr)	Δ (mb/sr)	θ_L (deg)	θ_{cm} (deg)	$d\sigma/d\Omega$ (mb/sr)	Δ (mb/sr)
12.9	15.1	472.6	.6	41.9	48.4	2.366	.013
12.9	15.1	483.9	.4	45.9	52.9	1.569	.012
13.9	16.2	357.6	.4	47.9	55.1	1.413	.011
13.9	16.2	340.9	.4	49.9	57.3	1.164	.011
14.9	17.4	181.5	.4	51.9	59.5	.868	.009
14.9	17.4	191.7	.3	53.9	61.7	.607	.005
15.9	18.5	68.50	.16	55.9	63.9	.495	.005
16.4	19.1	35.15	.05	57.9	66.1	.408	.004
16.9	19.7	17.87	.08	59.9	68.3	.329	.004
17.9	20.9	20.96	.09	61.9	70.5	.281	.002
18.4	21.5	34.40	.05	63.9	72.6	.248	.002
18.9	22.0	47.02	.13	65.9	74.8	.167	.002
19.9	23.2	65.35	.08	67.9	76.9	.133	.002
20.4	23.8	72.23	.08	69.9	79.0	.112	.002
20.9	24.4	68.70	.07	71.9	81.1	.094	.002
21.9	25.5	56.93	.07	73.9	83.2	.078	.002
22.4	26.1	46.37	.06	75.9	85.3	.059	.001
22.9	26.7	37.68	.05	77.9	87.4	.052	.001
23.9	27.8	20.12	.06	79.9	89.4	.042	.001
24.9	29.0	10.41	.03	81.9	91.5	.035	.001
25.9	30.1	6.691	.024	83.9	93.5	.028	.001
26.9	31.3	8.440	.025	85.9	95.6	.025	.001
27.9	32.4	11.11	.03	87.9	97.6	.023	.001
28.9	33.6	11.80	.03	89.9	99.6	.019	.001
29.9	34.7	10.41	.03	91.9	101.6	.014	.001
30.9	35.9	8.752	.023	101.9	111.4	.0056	.0004
31.9	37.0	6.105	.021	103.9	113.3	.0048	.0004
32.9	38.2	4.341	.016	105.9	115.2	.0044	.0004
33.9	39.3	3.196	.015	107.9	117.1	.0030	.0003
34.9	40.4	3.054	.014	109.9	119.0	.0030	.0003
35.9	41.6	3.265	.015	111.9	120.9	.0026	.0003
37.9	43.8	3.819	.016	113.9	122.7	.0014	.0002
39.9	46.1	3.284	.016				

(continued)

81 MeV (continued)

1.368 MeV 2+

θ_L (deg)	θ_{cm} (deg)	dσ/dΩ (mb/sr)	Δ (mb/sr)	θ_L (deg)	θ_{cm} (deg)	dσ/dΩ (mb/sr)	Δ (mb/sr)
7.9	9.2	144.7	.2	45.9	52.9	3.404	.018
8.9	10.4	118.7	.3	47.9	55.2	2.842	.017
9.9	11.6	80.04	.17	49.9	57.4	2.524	.016
10.9	12.7	33.61	.16	51.9	59.6	2.207	.015
11.9	13.9	10.41	.06	53.9	61.8	1.867	.009
12.9	15.1	7.630	.075	55.9	64.0	1.621	.009
12.9	15.1	6.668	.049	57.9	66.2	1.337	.008
13.9	16.2	19.07	.09	59.9	68.4	1.052	.007
13.9	16.2	18.40	.09	61.9	70.5	.933	.004
14.9	17.4	36.21	.16	63.9	72.7	.902	.004
14.9	17.4	36.18	.12	65.9	74.8	.691	.004
15.9	18.6	43.53	.13	67.9	77.0	.555	.003
16.4	19.2	45.96	.06	69.9	79.1	.476	.004
19.9	23.2	10.48	.03	71.9	81.2	.384	.003
20.4	23.8	8.354	.026	73.9	83.3	.320	.003
20.9	24.4	7.410	.023	75.9	85.4	.255	.003
21.9	25.5	9.820	.026	77.9	87.5	.226	.003
22.4	26.1	12.32	.03	79.9	89.5	.184	.003
22.9	26.7	14.05	.03	81.9	91.6	.156	.002
28.9	33.6	4.407	.016	83.9	93.6	.125	.002
29.9	34.8	4.116	.017	85.9	95.7	.103	.002
30.9	35.9	4.853	.017	87.9	97.7	.091	.002
31.9	37.1	5.853	.020	89.9	99.7	.075	.002
32.9	38.2	6.271	.020	91.9	101.7	.062	.002
33.9	39.4	5.879	.021	101.9	111.5	.022	.001
34.9	40.5	5.295	.018	103.9	113.4	.020	.001
35.9	41.6	4.500	.017	105.9	115.3	.016	.001
37.9	43.9	3.590	.016	107.9	117.2	.013	.001
39.9	46.2	3.820	.018	109.9	119.1	.013	.001
41.9	48.4	4.163	.017	111.9	121.0	.011	.001
				113.9	122.8	.0059	.0005

(continued)

81 MeV (continued)

5.22 MeV 3+

θ_L (deg)	θ_{cm} (deg)	$d\sigma/d\Omega$ (mb/sr)	Δ (mb/sr)	θ_L (deg)	θ_{cm} (deg)	$d\sigma/d\Omega$ (mb/sr)	Δ (mb/sr)
8.9	10.5	.140	.012	45.9	53.1	.208	.004
9.9	11.6	.172	.008	47.9	55.4	.164	.004
10.9	12.8	.128	.010	49.9	57.6	.117	.003
11.9	14.0	.077	.005	51.9	59.8	.100	.003
15.9	18.7	.064	.005	57.9	66.4	.023	.001
16.9	19.8	.067	.005	59.9	68.6	.016	.001
17.9	21.0	.059	.005	61.9	70.8	.0083	.0004
18.4	21.6	.036	.002	63.9	73.0	.0084	.0006
18.9	22.2	.043	.004	65.9	75.1	.0061	.0003
19.9	23.3	.030	.002	67.9	77.2	.0092	.0004
20.4	23.9	.025	.001	69.9	79.4	.013	.001
21.9	25.7	.012	.001	71.9	81.5	.013	.001
22.4	26.2	.015	.001	73.9	83.6	.014	.001
22.9	26.8	.019	.001	75.9	85.7	.014	.001
23.9	28.0	.015	.001	77.9	87.8	.018	.001
24.9	29.1	.029	.001	79.9	89.8	.017	.001
25.9	30.3	.039	.002	81.9	91.9	.018	.001
26.9	31.5	.056	.002	83.9	93.9	.016	.001
27.9	32.6	.068	.002	85.9	96.0	.019	.001
28.9	33.8	.083	.002	87.9	98.0	.018	.001
29.9	34.9	.108	.003	89.9	100.0	.015	.001
30.9	36.1	.125	.003	91.9	102.0	.014	.001
31.9	37.2	.155	.003	101.9	111.8	.0073	.0005
32.9	38.4	.166	.003	103.9	113.7	.0076	.0005
33.9	39.5	.181	.004	105.9	115.6	.0075	.0005
34.9	40.7	.215	.004	107.9	117.5	.0062	.0004
35.9	41.8	.254	.004	109.9	119.4	.0065	.0005
37.9	44.1	.266	.004	111.9	121.2	.0042	.0004
39.9	46.4	.243	.004	113.9	123.1	.0028	.0003
41.9	48.6	.234	.004				

(continued)

81 MeV (continued)

6.00 MeV 4+

θ_L (deg)	θ_{cm} (deg)	$d\sigma/d\Omega$ (mb/sr)	Δ (mb/sr)	θ_L (deg)	θ_{cm} (deg)	$d\sigma/d\Omega$ (mb/sr)	Δ (mb/sr)
8.9	10.5	3.684	.052	34.9	40.7	.354	.005
9.9	11.6	4.676	.042	35.9	41.8	.310	.005
10.9	12.8	5.616	.064	37.9	44.1	.310	.005
11.9	14.0	5.627	.046	41.9	48.7	.258	.004
12.9	15.2	5.858	.065	45.9	53.2	.199	.004
12.9	15.2	5.250	.043	47.9	55.4	.196	.004
13.9	16.3	4.479	.041	49.9	57.7	.175	.004
13.9	16.3	4.268	.048	51.9	59.9	.161	.003
14.9	17.5	3.037	.047	53.9	62.1	.137	.002
14.9	17.5	3.016	.033	55.9	64.3	.118	.002
15.9	18.7	1.708	.026	61.9	70.8	.088	.001
16.4	19.3	1.160	.009	63.9	73.0	.079	.001
16.9	19.8	.862	.018	65.9	75.2	.063	.001
17.9	21.0	.596	.015	67.9	77.3	.050	.001
18.4	21.6	.653	.007	69.9	79.4	.044	.001
18.9	22.2	.850	.018	71.9	81.5	.037	.001
21.9	25.7	1.883	.011	73.9	83.6	.032	.001
22.4	26.3	1.692	.011	75.9	85.7	.026	.001
22.9	26.8	1.748	.011	77.9	87.8	.023	.001
23.9	28.0	1.424	.011	79.9	89.9	.019	.001
24.9	29.2	1.084	.009	81.9	91.9	.017	.001
25.9	30.3	.768	.009	83.9	94.0	.014	.001
26.9	31.5	.706	.007	85.9	96.0	.015	.001
27.9	32.6	.719	.007	87.9	98.0	.013	.001
28.9	33.8	.783	.007	89.9	100.0	.012	.001
29.9	34.9	.836	.008	91.9	102.0	.0091	.0006
30.9	36.1	.794	.007	101.9	111.8	.0046	.0004
31.9	37.2	.703	.007	103.9	113.7	.0057	.0004
32.9	38.4	.556	.006	105.9	115.6	.0053	.0004
33.9	39.5	.423	.005				

(continued)

81 MeV (continued)

θ_L (deg)	θ_{cm} (deg)	$d\sigma/d\Omega$ (mb/sr)	Δ (mb/sr)	θ_L (deg)	θ_{cm} (deg)	$d\sigma/d\Omega$ (mb/sr)	Δ (mb/sr)
6.44 MeV 0+							
15.9	18.7	1.359	.023	45.9	53.2	.071	.003
16.4	19.3	1.400	.010	47.9	55.4	.061	.003
16.9	19.9	1.233	.021	49.9	57.7	.067	.003
17.9	21.0	.752	.017	51.9	59.9	.061	.002
18.4	21.6	.557	.007	53.9	62.1	.054	.002
18.9	22.2	.401	.012	55.9	64.3	.045	.001
19.9	23.4	.419	.013	57.9	66.5	.038	.001
19.9	23.4	.387	.006	65.9	75.2	.026	.001
20.4	23.9	.495	.006	67.9	77.3	.023	.001
23.9	28.0	.869	.009	69.9	79.5	.019	.001
24.9	29.2	.806	.008	71.9	81.6	.018	.001
25.9	30.3	.586	.007	73.9	83.7	.016	.001
26.9	31.5	.457	.006	75.9	85.8	.015	.001
27.9	32.7	.389	.005	77.9	87.9	.012	.001
28.9	33.8	.386	.005	79.9	89.9	.011	.001
29.9	35.0	.433	.006	81.9	92.0	.0089	.0006
30.9	36.1	.437	.005	83.9	94.0	.0075	.0005
31.9	37.3	.417	.005	85.9	96.1	.0062	.0005
32.9	38.4	.372	.005	87.9	98.1	.0071	.0005
33.9	39.6	.273	.004	89.9	100.1	.0059	.0005
34.9	40.7	.210	.004	91.9	102.1	.0036	.0004
35.9	41.9	.176	.003	101.9	111.9	.0022	.0003
37.9	44.1	.130	.003	103.9	113.8	.0018	.0002
39.9	46.4	.133	.003	105.9	115.7	.0016	.0002

$Mg^{24}(\alpha,\alpha')$

119.7 MeV

Elastic

θ_L (deg)	θ_{cm} (deg)	$d\sigma/d\Omega$ (mb/sr)	Δ (mb/sr)	θ_L (deg)	θ_{cm} (deg)	$d\sigma/d\Omega$ (mb/sr)	Δ (mb/sr)
12.3	14.4	295.6	.6	38.3	44.3	1.955	.012
14.3	16.7	26.19	.09	39.3	45.5	1.755	.022
15.3	17.9	44.80	.10	40.3	46.6	1.566	.015
16.3	19.0	73.45	.16	41.3	47.7	1.153	.021
17.3	20.2	77.43	.13	43.3	50.0	.846	.011
18.3	21.4	62.95	.13	46.3	53.3	.439	.004
19.3	22.5	37.99	.11	48.3	55.6	.293	.003
20.3	23.7	22.56	.07	50.3	57.8	.206	.003
21.3	24.8	15.73	.06	51.4	59.0	.160	.007
22.3	26.0	17.82	.04	53.3	61.1	.102	.003
23.3	27.1	20.43	.08	54.3	62.2	.092	.003
24.3	28.3	20.86	.05	56.3	64.4	.056	.001
25.3	29.5	17.00	.09	58.3	66.6	.038	.001
26.3	30.6	17.12	.21	60.3	68.8	.028	.001
27.3	31.8	10.75	.04	62.3	70.9	.016	.001
28.3	32.9	9.663	.097	64.3	73.1	.011	.001
30.3	35.2	7.621	.045	66.3	75.2	.006	.001
31.3	36.4	7.226	.040	67.4	76.4	.007	.001
33.3	38.6	5.462	.033	69.3	78.4	.004	.001
34.3	39.8	4.617	.033	70.3	79.5	.002	.001
35.3	40.9	3.678	.032	72.3	81.6	.002	.001
36.3	42.1	2.987	.024	74.3	83.7	.001	.001
37.3	43.2	2.320	.013	76.3	85.8	.001	.001
37.3	43.2	2.442	.023	85.3	95.0	.0002	.0006
38.3	44.3	2.118	.014				

(continued)

119.7 MeV (continued)

1.368 MeV 2+

θ_L (deg)	θ_{cm} (deg)	$d\sigma/d\Omega$ (mb/sr)	Δ (mb/sr)	θ_L (deg)	θ_{cm} (deg)	$d\sigma/d\Omega$ (mb/sr)	Δ (mb/sr)
10.3	12.0	15.05	.21	40.3	46.6	2.451	.015
12.3	14.4	46.67	.22	41.3	47.8	1.873	.027
16.3	19.0	16.56	.07	43.3	50.0	1.555	.015
17.3	20.2	10.47	.05	46.3	53.4	.919	.006
18.3	21.4	15.35	.06	48.3	55.6	.639	.004
23.3	27.2	12.49	.06	50.3	57.8	.447	.004
24.3	28.3	10.76	.04	51.4	59.1	.353	.010
25.3	29.5	10.22	.07	53.3	61.2	.227	.004
26.3	30.6	12.63	.18	54.3	62.3	.231	.004
27.3	31.8	12.17	.04	56.3	64.5	.145	.002
28.3	32.9	12.32	.11	58.3	66.6	.104	.001
30.3	35.2	8.782	.049	60.3	68.8	.074	.001
31.3	36.4	7.379	.040	62.3	71.0	.049	.001
32.3	37.5	6.512	.045	64.3	73.1	.037	.001
33.3	38.7	5.836	.034	66.3	75.3	.025	.001
34.3	39.8	5.556	.036	67.4	76.5	.024	.003
35.3	41.0	5.103	.038	69.3	78.4	.015	.001
36.3	42.1	4.630	.030	70.3	79.5	.010	.001
37.3	43.2	3.762	.017	72.3	81.6	.008	.001
37.3	43.2	3.874	.028	74.3	83.7	.006	.001
38.3	44.4	3.431	.018	76.3	85.8	.005	.001
38.3	44.4	3.081	.015	85.3	95.1	.0010	.0001
39.3	45.5	2.797	.027				

(continued)

119.7 MeV (continued)

5.22 MeV 3+

θ_L (deg)	θ_{cm} (deg)	$d\sigma/d\Omega$ (mb/sr)	Δ (mb/sr)	θ_L (deg)	θ_{cm} (deg)	$d\sigma/d\Omega$ (mb/sr)	Δ (mb/sr)
15.3	17.9	.204	.007	38.3	44.5	.011	.001
16.3	19.1	.222	.009	39.3	45.6	.011	.002
17.3	20.3	.210	.007	40.3	46.8	.009	.001
18.3	21.4	.235	.008	41.3	47.9	.019	.003
19.3	22.6	.264	.009	46.3	53.5	.027	.001
20.3	23.8	.267	.008	48.3	55.8	.026	.001
21.3	24.9	.287	.008	50.3	58.0	.027	.001
22.3	26.1	.288	.006	53.3	61.3	.022	.001
23.3	27.2	.316	.009	54.3	62.4	.024	.001
24.3	28.4	.271	.005	56.3	64.6	.019	.001
25.3	29.6	.241	.010	58.3	66.8	.017	.001
26.3	30.7	.239	.025	60.3	69.0	.014	.001
27.3	31.9	.239	.006	62.3	71.2	.010	.001
28.3	33.0	.232	.015	64.3	73.3	.008	.001
31.3	36.5	.126	.005	66.3	75.5	.006	.001
32.3	37.6	.076	.005	69.3	78.7	.005	.001
33.3	38.8	.071	.004	70.3	79.7	.003	.001
34.3	39.9	.030	.003	72.3	81.8	.003	.001
35.3	41.1	.041	.003	74.3	83.9	.002	.001
36.3	42.2	.033	.003	76.3	86.0	.001	.001
37.3	43.3	.032	.002	85.3	95.2	.0007	.0001
37.3	43.3	.022	.002				

(continued)

119.7 MeV (continued)

6.00 MeV 4+

θ_L (deg)	θ_{cm} (deg)	dσ/dΩ (mb/sr)	Δ (mb/sr)	θ_L (deg)	θ_{cm} (deg)	dσ/dΩ (mb/sr)	Δ (mb/sr)
10.3	12.1	7.95	.15	35.3	41.1	.335	.010
12.3	14.4	4.404	.068	36.3	42.2	.268	.007
14.3	16.8	1.230	.019	37.3	43.4	.201	.004
18.3	21.4	1.802	.021	37.3	43.4	.219	.007
19.3	22.6	1.489	.021	38.3	44.5	.192	.004
20.3	23.8	.894	.014	38.3	44.5	.178	.004
21.3	24.9	.602	.012	39.3	45.6	.192	.007
22.3	26.1	.510	.007	40.3	46.8	.148	.004
23.3	27.3	.624	.013	41.3	47.9	.124	.007
24.3	28.4	.742	.009	43.3	50.2	.101	.004
25.3	29.6	.697	.017	50.3	58.0	.032	.001
26.3	30.7	.724	.044	53.3	61.3	.017	.001
27.3	31.9	.576	.009	54.3	62.4	.020	.001
28.3	33.1	.491	.022	56.3	64.6	.013	.001
30.3	35.4	.491	.011	58.3	66.8	.011	.001
31.3	36.5	.622	.012	70.3	79.8	.001	.001
34.3	39.9	.344	.009	72.3	81.9	.002	.001

(continued)

119.7 MeV (continued)

6.44 MeV 0+

θ_L (deg)	θ_{cm} (deg)	$d\sigma/d\Omega$ (mb/sr)	Δ (mb/sr)	θ_L (deg)	θ_{cm} (deg)	$d\sigma/d\Omega$ (mb/sr)	Δ (mb/sr)
10.3	12.1	3.57	.10	34.3	40.0	.204	.007
14.3	16.8	1.998	.024	35.3	41.1	.153	.006
15.3	17.9	1.156	.017	36.3	42.2	.126	.005
20.3	23.8	.654	.012	37.3	43.4	.081	.003
21.3	24.9	.418	.010	37.3	43.4	.088	.004
22.3	26.1	.211	.005	38.3	44.5	.083	.003
23.3	27.3	.158	.007	38.3	44.5	.060	.002
24.3	28.4	.140	.004	40.3	46.8	.069	.003
25.3	29.6	.188	.009	41.3	47.9	.056	.005
26.3	30.7	.259	.026	43.3	50.2	.059	.003
27.3	31.9	.216	.006	46.3	53.6	.026	.001
28.3	33.1	.244	.015	53.3	61.4	.010	.001
30.3	35.4	.152	.006	54.3	62.5	.010	.001
31.3	36.5	.167	.006	56.3	64.7	.002	.001

Ne^{20} (α,α') Ne^{20}

Beam Energy = 33.0 MeV

Elastic

θ_{cm} (deg)	dσ/dΩ (mb/sr)	Δ (mb/sr)	θ_{cm} (deg)	dσ/dΩ (mb/sr)	Δ (mb/sr)
12.5	3840	9	47.4	.181	.035
14.9	1070	5	47.9	.162	.010
17.2	209	3	48.0	.200	.012
18.8	149	1	49.8	1.39	.03
19.2	165	1	49.8	1.39	.03
19.2	161	1	50.2	1.57	.04
21.2	254	1	50.3	2.36	.05
22.0	290	2	52.1	4.33	.09
23.7	311	2	52.5	4.95	.05
24.0	275	1	52.7	5.18	.10
24.4	276	1	54.3	5.83	.10
26.1	171	1	54.3	5.94	.10
26.3	175	1	54.8	6.00	.07
26.3	169	1	55.6	5.41	.10
28.7	56.1	.1	56.6	5.11	.07
29.6	32.9	.3	56.6	5.43	.10
31.1	7.93	.09	56.6	4.95	.05
31.1	7.63	.08	57.5	4.68	.09
31.9	1.71	.09	58.9	3.26	.04
32.6	1.37	.14	59.7	2.87	.08
33.4	3.64	.07	61.1	1.69	.02
33.4	3.59	.04	61.8	1.49	.05
34.4	9.49	.22	62.6	1.15	.04
34.9	11.7	.3	63.4	.987	.030
36.8	23.4	.3	64.0	.910	.044
37.3	26.1	.4	64.8	.892	.028
38.7	29.4	.4	65.6	1.03	.07
39.6	27.2	.3	66.2	1.13	.03
41.1	21.6	.4	67.0	1.14	.04
42.0	19.6	.6	68.4	1.59	.04
42.8	15.6	.4	69.2	1.64	.04
42.8	13.8	.2	70.7	1.97	.05
42.8	14.0	.2	71.5	1.85	.04
43.3	12.7	.1	72.9	2.12	.05
43.5	9.52	.17	73.6	1.96	.04
44.3	7.88	.25	75.0	1.85	.05
45.6	3.25	.05	77.1	1.78	.05
46.4	1.69	.09	78.8	1.43	.03

(continued)

Beam Energy = 33.0 MeV

Elastic

θ_{cm} (deg)	$d\sigma/d\Omega$ (mb/sr)	Δ (mb/sr)	θ_{cm} (deg)	$d\sigma/d\Omega$ (mb/sr)	Δ (mb/sr)
79.4	1.27	.04	85.7	.218	.013
80.9	.964	.023	87.9	.194	.010
81.5	.701	.031	90.0	.261	.011
83.0	.524	.015	92.0	.373	.016
83.6	.395	.016	94.1	.394	.016
85.2	.261	.015	96.2	.421	.018

33.0 MeV (continued)

1.63 MeV 2^+

θ_{cm} (deg)	dσ/dΩ (mb/sr)	Δ (mb/sr)	θ_{cm} (deg)	dσ/dΩ (mb/sr)	Δ (mb/sr)
12.5	112	1	52.3	5.02	.09
15.0	111	1	52.7	5.10	.06
17.4	83.3	.4	53.0	4.07	.08
18.9	23.9	.3	54.6	2.48	.08
19.3	47.6	.3	54.6	2.39	.06
19.3	57.0	.5	55.0	1.92	.04
21.3	17.6	.3	55.8	1.75	.06
22.2	15.5	.3	56.9	1.59	.04
23.8	5.18	.2	56.9	1.66	.08
24.1	5.35	.18	56.9	1.53	.03
24.5	5.93	.16	57.2	1.87	.06
26.2	11.3	.3	59.2	2.47	.03
26.5	14.1	.1	59.4	3.16	.08
26.5	14.9	.2	61.4	3.71	.04
28.8	26.4	.2	62.1	4.25	.09
29.7	30.5	.4	62.9	4.06	.1
31.2	33.9	.2	63.7	4.33	.06
31.2	33.9	.1	64.3	4.34	.10
32.0	30.6	.4	65.1	4.22	.06
32.8	29.8	.6	65.9	4.35	.15
33.6	26.8	.2	66.5	3.92	.07
33.6	26.1	.2	67.3	3.54	.06
34.5	28.2	.4	68.7	3.15	.06
35.1	19.0	.3	69.6	2.56	.05
36.9	8.38	.10	71.0	2.43	.05
37.5	7.40	.17	71.8	1.88	.04
38.9	3.80	.19	73.2	1.92	.05
39.8	3.14	.11	74.0	1.66	.05
41.3	4.44	.12	75.3	2.19	.05
42.2	4.88	.28	77.5	2.58	.06
43.0	6.50	.26	79.1	2.64	.04
43.0	6.54	.02	79.7	2.78	.06
43.0	7.54	.02	81.3	3.05	.04
43.5	7.52	.07	81.9	2.58	.06
43.7	8.72	.16	83.4	2.90	.04
44.5	8.90	.26	83.9	2.65	.04
45.8	11.5	.1	85.5	2.63	.06
46.0	10.2	.2	86.0	2.28	.04
47.7	11.8	.3	88.2	1.88	.04
48.1	11.5	.1	90.3	1.42	.03
48.3	10.8	.1	92.2	1.11	.03
50.0	9.91	.15	94.3	.931	.026
50.0	9.62	.17	96.4	.811	.025
50.4	8.68	.08	98.5	.777	.024
50.6	7.71	.11			

33.0 MeV (continued)

4.25 MeV 4^+

θ_{cm} (deg)	dσ/dΩ (mb/sr)	Δ (mb/sr)	θ_{cm} (deg)	dσ/dΩ (mb/sr)	Δ (mb/sr)
15.1	4.27	.10	48.6	.727	.021
17.5	5.54	.11	50.4	.663	.039
19.5	5.55	.10	50.4	.586	.041
19.5	5.79	.16	50.9	.675	.021
22.4	7.05	.25	52.7	.800	.038
24.3	6.16	.17	53.2	.837	.021
24.8	6.36	.17	55.1	1.04	.04
26.7	4.66	.08	55.1	1.08	.04
26.7	4.39	.08	55.5	1.12	.03
29.1	2.80	.05	57.4	1.10	.03
31.5	1.35	.04	57.4	1.20	.05
31.5	1.19	.03	57.4	1.10	.02
33.1	1.02	.11	59.7	1.08	.02
33.9	.934	.033	61.9	.986	.019
33.9	.869	.022	63.4	.828	.026
35.5	.809	.068	64.2	.785	.030
37.8	1.24	.08	65.7	.612	.023
40.2	1.54	.08	66.5	.683	.061
42.6	1.67	.17	67.9	.565	.027
43.4	1.12	.10	70.2	.546	.023
43.4	1.55	.08	72.4	.589	.021
43.4	1.64	.08	74.6	.733	.027
43.9	1.52	.03	79.7	.761	.022
44.9	1.41	.11	81.9	.677	.018
46.2	1.07	.03	84.0	.575	.017
48.1	.777	.009	86.1	.542	.025

33.0 MeV (continued)

4.97 MeV 2^-

θ_{cm} (deg)	dσ/dΩ (mb/sr)	Δ (mb/sr)	θ_{cm} (deg)	dσ/dΩ (mb/sr)	Δ (mb/sr)
15.1	.823	.045	50.6	.410	.035
17.6	.647	.037	51.0	.397	.016
19.5	.787	.036	52.9	.410	.027
19.5	.771	.060	53.4	.408	.015
22.4	.763	.081	55.2	.377	.026
24.4	.580	.053	55.2	.408	.023
24.9	.418	.043	55.7	.398	.017
26.8	.118	.012	57.5	.267	.016
26.8	.234	.019	57.5	.332	.025
29.2	.160	.013	57.5	.294	.012
34.0	.248	.017	59.8	.231	.009
34.0	.219	.011	62.1	.258	.010
35.6	.212	.035	63.6	.225	.014
37.9	.152	.027	64.4	.261	.015
40.3	.189	.027	65.8	.327	.017
43.5	.169	.05	66.6	.348	.043
43.5	.126	.022	68.1	.372	.018
43.5	.124	.021	70.3	.347	.019
44.0	.165	.010	72.6	.284	.014
45.1	.139	.033	74.8	.143	.012
46.3	.234	.012	79.9	.053	.006
48.2	.164	.039	82.1	.108	.007
48.7	.369	.015	84.2	.150	.008
50.6	.393	.030	86.3	.140	.013

33.0 MeV (continued)

5.63 MeV 3^-

θ_{cm} (deg)	$d\sigma/d\Omega$ (mb/sr)	Δ (mb/sr)	θ_{cm} (deg)	$d\sigma/d\Omega$ (mb/sr)	Δ (mb/sr)
12.7	14.8	.3	48.9	1.92	.02
15.2	16.4	.2	50.7	1.61	.06
17.6	16.5	.2	50.7	1.82	.07
19.6	15.5	.4	51.2	1.54	.03
19.6	16.4	.3	53.0	1.65	.05
22.5	15.3	.4	53.5	1.63	.03
24.4	10.9	.2	55.3	1.21	.05
24.9	11.1	.2	55.3	1.75	.05
26.9	6.93	.09	55.8	1.76	.04
26.9	7.27	.11	57.7	1.63	.04
29.3	3.13	.06	57.7	1.73	.06
31.7	1.76	.04	57.7	1.85	.03
31.7	1.71	.04	60.0	1.82	.03
33.2	1.58	.15	62.2	1.63	.02
34.1	2.32	.05	63.7	1.30	.03
34.1	2.09	.03	64.5	1.49	.04
35.6	2.27	.11	66.0	1.39	.03
38.0	3.51	.13	66.8	1.15	.08
40.4	3.71	.12	68.3	1.11	.03
42.8	4.07	.26	70.5	.978	.030
43.6	2.97	.21	72.7	.973	.026
43.6	3.45	.11	74.9	.724	.027
43.6	3.51	.11	80.1	.610	.020
44.1	3.73	.05	82.2	.832	.020
45.2	3.12	.16	84.4	.717	.018
46.5	2.91	.04	86.5	.791	.030
48.3	1.78	.13			

33.0 MeV (continued)

5.80 MeV 1$^-$					
θ_{cm} (deg)	dσ/dΩ (mb/sr)	Δ (mb/sr)	θ_{cm} (deg)	dσ/dΩ (mb/sr)	Δ (mb/sr)
12.7	12.3	.2	48.8	1.33	.03
15.2	4.87	.11	50.7	1.74	.06
17.6	2.07	.07	50.7	1.63	.07
19.6	3.26	.07	51.2	1.71	.03
19.6	2.78	.11	53.1	1.77	.06
22.5	4.71	.20	53.5	1.65	.03
24.4	4.60	.15	55.4	2.20	.06
24.9	4.55	.14	55.4	1.51	.04
26.9	2.67	.06	55.8	1.23	.03
27.0	1.78	.05	57.7	1.04	.03
29.3	1.04	.03	57.7	.829	.040
31.7	1.38	.04	57.7	.716	.018
31.7	1.23	.03	60.0	.156	.008
33.3	1.72	.15	62.3	.120	.007
34.1	2.81	.06	63.8	.185	.012
34.1	2.84	.04	64.6	.227	.014
35.7	3.44	.14	66.0	.263	.015
38.1	3.18	.12	66.8	.563	.055
40.5	3.03	.11	68.3	.654	.025
42.8	1.46	.15	70.5	.591	.023
43.7	2.76	.20	72.8	.217	.013
43.7	1.69	.08	75.0	.207	.014
43.7	2.08	.08	80.1	.765	.022
44.1	1.45	.03	82.3	.978	.022
45.2	1.14	.10	84.4	1.24	.02
46.5	1.04	.03	86.6	1.17	.04
48.4	1.45	.13			

33.0 MeV (continued)

7.17 MeV 3^-

θ_{cm} (deg)	$d\sigma/d\Omega$ (mb/sr)	Δ (mb/sr)	θ_{cm} (deg)	$d\sigma/d\Omega$ (mb/sr)	Δ (mb/sr)
12.8	30.0	.4	49.1	1.80	.04
15.3	25.9	.2	51.0	1.98	.07
17.7	23.4	.2	51.0	1.63	.07
19.7	18.8	.2	51.5	1.92	.04
19.7	20.4	.3	53.4	1.47	.05
22.6	16.9	.3	53.8	1.57	.03
24.6	9.76	.22	55.7	1.26	.05
25.1	9.99	.20	55.7	1.31	.04
27.0	5.60	.08	56.1	1.24	.03
27.1	5.41	.09	58.0	.898	.029
29.5	3.61	.06	58.0	.942	.042
31.9	4.34	.07	58.0	1.02	.02
31.9	4.00	.05	60.3	.918	.019
33.5	4.72	.24	62.6	.951	.018
34.3	4.57	.07	64.1	1.20	.03
34.3	4.43	.05	64.9	1.01	.03
35.9	4.69	.16	66.4	.979	.029
38.2	4.77	.15	67.2	.662	.059
40.7	3.60	.11	68.6	.950	.029
43.1	3.06	.22	70.9	.827	.028
43.9	2.19	.18	73.1	.716	.024
43.9	1.86	.08	75.3	.618	.026
43.9	2.18	.09	80.5	.519	.018
44.4	2.11	.04	82.7	.503	.016
45.4	2.41	.15	84.9	.487	.015
46.7	1.88	.04	87.0	.441	.022
48.7	1.89	.13			

$Ne^{20}(\alpha,\alpha')$
33.0 MeV
Large angle data

	Elastic		1.63 MeV 2^+	
θ_L (deg)	θ_{cm} (deg)	dσ/dΩ (mb/sr)	θ_{cm} (deg)	dσ/dΩ (mb/sr)
86.7	98.1	.360	98.4	.832
88.7	100.3	.304	100.7	.934
90.7	102.3	.171	102.7	.800
92.7	104.3	.131	104.7	.844
94.7	106.3	.052	106.6	.564
96.7	108.2	.055	108.6	.578
98.7	110.2	.061	110.5	.446
100.7	112.1	.110	112.5	.484
102.7	114.0	.120	114.4	.264
104.7	115.9	.088	116.3	.233
106.7	117.8	.084	118.2	.229
108.7	119.7	.077	120.1	.301
110.7	121.6	.053	121.9	.308
112.7	123.4	.049	123.8	.437
114.7	125.3	.045	125.6	.441
116.7	127.1	.087	127.3	.553
118.7	128.9	.102	129.2	.313
120.7	130.7	.244	131.0	.294
122.7	132.5	.266	132.8	.215
124.7	134.3	.298	134.5	.278
126.7	136.1	.140	136.3	.293
128.7	137.6	.113	138.0	.596
130.7	139.3	.074	139.8	.662
132.7	141.0	.066	141.5	1.22
134.7	142.8	.110	143.2	.986
136.7	144.5	.230	144.9	1.13
138.7	146.2	.282	146.6	.901
140.7	147.9	.525	148.3	.873
142.7	149.5	.319	150.0	.558
144.7	151.2	.387	151.6	.737
146.7	152.9	.291	153.3	1.01
148.7	154.5	.323	154.9	1.81
150.7	156.2	.206	156.5	1.54

(continued)

33.0 MeV (continued) Large angle data

		4.25 MeV 4^+			4.97 MeV 2^-	
θ_L (deg)	θ_{cm} (deg)	$d\sigma/d\Omega$ (mb/sr)	Δ (mb/sr)	θ_{cm} (deg)	$d\sigma/d\Omega$ (mb/sr)	Δ (mb/sr)
	97.2	1.07	.03	97.6	.147	.010
86.7	99.4	1.01	.03	99.6	.094	.008
88.7	101.3	1.17	.03	101.5	.069	.006
90.7	103.3	1.07	.02	103.5	.082	.007
92.7	105.4	1.21	.03	105.6	.090	.007
94.7	107.4	.853	.023	107.6	.131	.009
96.7	109.2	.855	.017	109.4	.110	.006
98.7	111.1	.718	.016	111.3	.171	.008
100.7	113.2	.873	.018	113.4	.234	.009
102.7	115.1	.768	.017	115.3	.098	.006
104.7	116.9	.994	.019	117.1	.121	.007
106.7	118.8	1.01	.019	119.0	.062	.005
108.7	120.7	1.55	.024			
110.7	122.6	1.12	.020	122.8	.061	.005
112.7	124.3	1.28	.021	124.5	.104	.006
114.7	126.1	1.07	.02	126.3	.089	.006
116.7	128.0	1.10	.02	128.2	.109	.006
118.7	129.8	.697	.016	130.0	.227	.009
120.7	131.5	.557	.010	131.7	.227	.007
122.7	133.3	.439	.009	133.5	.248	.007
124.7	135.1	.578	.010	135.3	.083	.004
126.7	136.9	.683	.011	137.0	.071	.004
128.7	138.5	1.89	.03	138.7	.145	.007
130.7	140.2	2.45	.03	140.4	.376	.011
132.7	142.0	3.25	.03	142.2	.497	.013
134.7	143.7	2.61	.03	143.9	.523	.013
136.7	145.3	1.48	.01	145.5	.284	.006
138.7	147.0	1.14	.01	147.1	.266	.006
140.7	148.7	1.07	.01	148.9	.234	.005
142.7	150.4	.664	.008	150.5	.117	.004
144.7	151.9	.744	.007	152.1	.080	.002
146.7	153.6	.727	.007			
148.7						
150.7						
	88.9	.560	.021	89.1	.088	.008
	91.0	.639	.022	91.2	.062	.007
	92.9	.755	.022	93.1	.048	.006
	95.0	.967	.024	95.4	.047	.005

$Ne^{20}(\alpha,\alpha')$

50.9 MeV

Elastic

θ_L (deg)	θ_{cm} (deg)	$d\sigma/d\Omega$ (mb/sr)	θ_L (deg)	θ_{cm} (deg)	$d\sigma/d\Omega$ (mb/sr)
36.7	43.6	9.94	94.7	106.3	.103
38.7	45.9	8.88	96.6	108.1	.092
40.6	48.2	6.56	98.6	110.1	.059
42.6	50.5	3.59	100.7	112.1	.047
44.7	52.9	1.84	102.7	114.0	.024
46.7	55.2	1.23	104.6	115.8	.013
48.6	57.3	1.24	106.6	117.7	.011
50.6	59.0	1.28	108.7	119.7	.0092
52.7	61.9	1.04	110.7	121.6	.0066
54.7	64.2	.590	112.6	123.3	.0046
56.6	66.3	.418	114.6	125.7	.0030
56.6	66.3	.398	116.7	127.1	.0056
58.6	68.5	.362	118.7	128.9	.0054
58.6	68.5	.362	120.6	130.6	.0068
60.7	70.8	.436	122.6	132.4	.0055
60.7	70.8	.482	124.7	134.3	.0025
62.7	73.0	.483	126.7	136.0	.0085
62.7	73.0	.489	128.6	137.7	.022
64.6	75.1	.546	129.3	138.3	.024
64.6	75.1	.538	130.6	139.4	.035
66.6	77.3	.535	131.4	140.1	.035
66.6	77.3	.518	132.7	141.3	.037
68.7	79.5	.497	133.4	141.8	.040
68.7	79.5	.528	134.7	143.0	.030
70.7	81.7	.411	135.4	143.5	.031
70.7	81.7	.424	137.3	145.1	.016
72.6	83.7	.386	139.4	146.9	.0104
74.6	85.8	.370	141.4	148.6	.022
76.7	88.0	.299	143.4	150.4	.048
78.7	90.1	.319	145.3	151.9	.065
80.6	92.1	.335	147.4	153.7	.079
82.6	94.1	.329	149.4	155.3	.062
84.7	96.3	.220	151.4	157.1	.038
86.7	98.3	.205	153.3	158.5	.017
88.6	100.2	.170	155.4	160.2	.036
90.6	102.2	.158	157.4	161.8	.075
92.7	104.3	.125	159.4	163.4	.124

(continued)

50.9 MeV (continued)

1.63 MeV 2^+

θ_L (deg)	θ_{cm} (deg)	dσ/dΩ (mb/sr)	θ_L (deg)	θ_{cm} (deg)	dσ/dΩ (mb/sr)
36.7	43.7	3.89	94.7	106.5	.740
38.7	46.1	3.23	96.6	108.4	.628
40.6	48.3	4.35	98.6	110.3	.542
42.6	50.6	4.76	100.7	112.4	.522
44.7	53.0	4.37	102.7	114.3	.458
46.7	55.3	2.54	104.6	116.1	.445
48.6	57.5	1.71	106.6	118.0	.452
50.6	59.8	1.18	108.7	119.9	.465
52.7	62.1	1.18	110.7	121.8	.387
54.7	64.4	1.19	112.6	123.6	.394
56.6	66.5	1.27	114.6	125.4	.378
56.6	66.5	1.31	116.7	127.3	.331
58.6	68.7	1.08	118.7	129.1	.265
58.6	68.7	1.07	120.6	130.8	.206
60.7	71.0	.837	122.6	132.6	.180
60.7	71.0	.848	124.7	134.5	.160
62.7	73.2	.629	126.7	136.2	.170
62.7	73.2	.629	128.6	137.9	.201
64.6	75.3	.615	129.3	138.4	.212
64.6	75.3	.598	130.6	139.6	.239
66.6	77.5	.785	131.4	140.3	.241
66.6	77.5	.729	132.7	141.4	.239
68.7	79.7	.966	133.4	142.0	.236
68.7	79.7	.875	134.7	143.1	.194
70.7	81.9	1.04	135.4	143.7	.199
70.7	81.9	.906	137.3	145.3	.152
72.6	83.9	1.05	139.4	147.0	.140
74.6	86.1	1.08	141.4	148.7	.135
76.7	88.2	.986	143.4	150.4	.170
78.7	90.2	.894	145.3	152.0	.180
80.6	92.3	.894	147.4	153.8	.248
82.6	94.4	.894	149.4	155.4	.229
84.7	96.5	1.00	151.4	157.1	.177
86.7	98.6	.909	153.3	158.6	.114
88.6	100.4	.947	155.4	160.3	.109
90.6	102.4	.932	157.4	161.9	.159
92.7	104.6	.879	159.4	163.5	.234

(continued)

50.9 MeV (continued)

4.25 MeV 4^+

θ_L (deg)	θ_{cm} (deg)	$d\sigma/d\Omega$ (mb/sr)	Δ (mb/sr)	θ_L (deg)	θ_{cm} (deg)	$d\sigma/d\Omega$ (mb/sr)	Δ (mb/sr)
74.6	86.4	.393	.026	122.6	132.9	.216	.029
76.7	88.6	.403	.026	124.7	134.8	.237	.028
78.7	90.6	.425	.026	126.7	136.5	.229	.028
80.6	92.7	.423	.026	128.6	138.2	.265	.026
84.7	96.9	.408	.026	129.3	138.8	.242	.019
86.7	99.0	.437	.026	130.6	139.9	.256	.026
88.6	100.9	.454	.026	131.4	140.5	.253	.018
90.6	102.9	.467	.026	132.7	141.7	.229	.027
92.7	105.0	.498	.025	133.4	142.3	.211	.020
94.7	106.9	.460	.026	134.7	143.4	.159	.032
96.6	108.8	.450	.020	135.4	144.0	.161	.023
98.6	110.7	.449	.020	137.3	145.6	.130	.029
100.7	112.8	.422	.021	139.4	147.2	.129	.028
102.7	114.7	.352	.023	141.4	149.0	.175	.024
104.6	116.5	.319	.024	143.4	150.7	.242	.020
106.6	118.4	.313	.024	145.3	152.3	.308	.017
108.7	120.3	.312	.024	147.4	153.9	.166	.023
110.7	122.2	.290	.025	149.4	155.6	.095	.030
112.6	123.9	.300	.025	151.4	157.2	.438	.014
114.6	125.8	.296	.025	153.3	158.8	.409	.017
116.7	127.7	.272	.026	155.4	160.4	.391	.016
118.7	129.4	.240	.027	157.4	162.1	.314	.018
120.6	131.2	.208	.029	159.4	163.6	.251	.018

(continued)

50.9 MeV (continued)

4.97 MeV 2$^-$

θ_L (deg)	θ_{cm} (deg)	dσ/dΩ (mb/sr)	Δ (mb/sr)	θ_L (deg)	θ_{cm} (deg)	dσ/dΩ (mb/sr)	Δ (mb/sr)
76.7	88.7	.188	.038	124.7	134.9	.069	.051
78.7	90.8	.198	.038	126.7	136.6	.061	.054
80.6	92.8	.185	.039	128.6	138.3	.050	.060
84.7	97.0	.167	.042	129.3	138.9	.038	.048
86.7	99.1	.174	.041	130.6	140.0	.048	.060
88.6	101.0	.140	.046	131.4	140.7	.051	.041
90.6	103.0	.164	.043	132.7	141.8	.061	.053
92.7	105.1	.168	.043	133.4	142.4	.056	.039
94.7	107.1	.153	.045	134.7	143.5	.069	.049
96.6	108.9	.133	.037	135.4	144.1	.069	.034
98.6	110.9	.130	.037	137.3	145.6	.074	.038
100.7	112.9	.131	.038	139.4	147.3	.076	.037
102.7	114.8	.129	.038	141.4	149.1	.066	.038
104.6	116.6	.142	.036	143.4	150.7	.043	.048
106.6	118.5	.156	.034	145.3	152.3	.025	.061
108.7	120.4	.142	.036	147.4	153.9	.069	.036
110.7	122.3	.125	.039	151.4	157.3	.070	.034
112.6	124.0	.117	.040	153.3	158.8	.083	.035
114.6	125.8	.114	.041	155.4	160.4	.085	.035
118.7	129.5	.079	.048	157.4	162.1	.074	.036
120.6	131.3	.081	.048	159.4	163.7	.060	.039
122.6	133.0	.077	.049				

(continued)

50.9 MeV (continued)

4.25 MeV 4^+			4.97 MeV 2^-		
θ_L (deg)	θ_{cm} (deg)	$d\sigma/d\Omega$ (mb/sr)	θ_L (deg)	θ_{cm} (deg)	$d\sigma/d\Omega$ (mb/sr)
40.0	47.9	1.05	40.0	48.0	.034
42	50.2	.953	42	50.3	.025
44	52.5	.909	44	52.6	.019
46	54.8	.863	46	54.9	.020
48	57.1	.866	48	57.2	.024
50	59.4	.865	50	59.5	.040
52	61.7	.651	52	61.8	.070
54	63.9	.676	54	64.0	.072
60	70.6	.476	60	70.7	.108
62	72.8	.494	62	72.9	.109
64	75.0	.490	64	75.1	.126
66	77.2	.419	66	77.3	.160
68	79.4	.356	68	79.5	.180
70	81.5	.318	70	81.7	.211
72	83.7	.279	72	83.8	.171
74	85.8	.286	74	85.9	.176

(continued)

50.9 MeV (continued)

5.63 MeV 3^-			5.80 MeV 1^-			7.17 MeV 3^-		
θ_L (deg)	θ_{cm} (deg)	$d\sigma/d\Omega$ (mb/sr)	θ_L (deg)	θ_{cm} (deg)	$d\sigma/d\Omega$ (mb/sr)	θ_L (deg)	θ_{cm} (deg)	$d\sigma/d\Omega$ (mb/sr)
40.0	48.0	1.01	40.0	48.0	.685	40.0	48.2	.448
42	50.4	.795	42	50.4	.772	42	50.5	.387
44	52.7	.747	44	52.7	.721	44	52.9	.356
46	55.0	.480	46	55.0	.699	46	55.2	.321
48	57.3	.578	48	57.3	.405	48	57.5	.222
50	59.6	.580	50	59.6	.276			
52	61.8	.535	52	61.9	.117			
60	70.8	.276	54	64.1	.122			
62	73.0	.222	60	70.9	.095			
64	75.2	.192	62	73.1	.033			
66	77.4	.123	64	75.3	.024			
68	79.6	.166	66	77.5	.050			
70	81.8	.130	68	79.6	.011			
72	83.9	.062	70	81.8	.019			

$Ne^{20}(\alpha,\alpha')$

80.8 MeV

Elastic

θ_L (deg)	θ_{cm} (deg)	dσ/dΩ (mb/sr)	Δ (mb/sr)	θ_L (deg)	θ_{cm} (deg)	dσ/dΩ (mb/sr)	Δ (mb/sr)
11.9	14.3	322.1	1.5	43.9	52.0	2.530	.036
13	15.6	402.6	1.8	45.9	54.2	1.951	.028
14	16.8	348.0	.7	47.8	56.4	1.516	.049
15.9	19.1	125.6	.3	47.8	56.4	1.467	.025
18	21.6	17.45	.06	49.8	58.7	1.322	.024
20	24.0	36.49	.08	51.8	61.0	1.101	.022
22	26.3	49.89	.14	53.8	63.2	.832	.020
24	28.7	26.32	.09	57.8	67.6	.476	.018
26	31.1	7.793	.044	57.9	67.8	.496	.017
28	33.5	5.267	.075	57.9	67.8	.449	.013
30	35.8	7.985	.048	61.9	72.2	.297	.009
30.9	36.9	7.96	.31	69.9	80.8	.087	.005
31.8	37.9	7.54	.36	77.8	89.2	.031	.005
32	38.2	7.117	.047	77.8	89.2	.030	.004
32.9	39.2	5.57	.32	81.8	93.3	.035	.003
33.9	40.4	4.607	.119	83.9	95.5	.0174	.0023
34	40.5	4.431	.038	85.9	97.5	.0106	.0024
35.8	42.6	3.179	.074	89.8	101.5	.0080	.0017
36	42.8	3.229	.027	97.9	109.4	.0074	.0015
37.9	45.0	3.269	.033	103.8	115.1	.0042	.0011
38	45.2	3.296	.040	105.8	117.0	.0049	.0016
39.9	47.4	3.514	.035	117.8	128.1	.0006	.0004
41.9	49.7	3.182	.048				

(continued)

80.8 MeV (continued)

1.63 MeV 2^+

θ_L (deg)	θ_{cm} (deg)	$d\sigma/d\Omega$ (mb/sr)	Δ (mb/sr)	θ_L (deg)	θ_{cm} (deg)	$d\sigma/d\Omega$ (mb/sr)	Δ (mb/sr)
11	13.2	54.19	.50	45.9	54.4	3.237	.036
11.9	14.3	18.60	.36	47.8	56.5	2.737	.066
13	15.6	6.77	.23	47.8	56.5	2.701	.034
14	16.8	14.23	.14	49.8	58.8	2.188	.031
15.9	19.1	39.88	.18	51.8	61.1	1.921	.029
18	21.6	34.64	.08	53.8	63.3	1.664	.028
20	24.0	13.20	.05	57.8	67.8	1.280	.029
24	28.8	13.77	.07	57.9	67.9	1.310	.027
26	31.2	14.37	.06	57.9	67.9	1.298	.022
30	35.9	4.742	.037	61.9	72.3	.891	.016
30.9	37.0	4.26	.22	77.8	89.3	.210	.012
31.8	38.0	4.79	.29	77.8	89.3	.214	.010
32	38.2	4.917	.039	81.8	93.5	.148	.007
32.9	39.3	6.07	.33	83.9	95.6	.113	.006
33.9	40.5	5.74	.13	85.9	97.7	.106	.007
36	42.9	5.32	.08	89.8	101.6	.078	.005
38	45.2	4.07	.05	97.9	109.6	.031	.003
39.9	47.5	3.31	.04	103.8	115.2	.021	.003
41.9	49.8	3.311	.049	105.8	117.1	.021	.003
43.9	52.1	3.396	.042	117.8	128.2	.0091	.0017

(continued)

80.8 MeV (continued)

4.25 MeV 4^+

θ_L (deg)	θ_{cm} (deg)	$d\sigma/d\Omega$ (mb/sr)	Δ (mb/sr)	θ_L (deg)	θ_{cm} (deg)	$d\sigma/d\Omega$ (mb/sr)	Δ (mb/sr)
11	13.3	5.99	.16	43.9	52.2	.852	.021
11.9	14.4	6.203	.21	45.9	54.5	.841	.018
13	15.7	5.63	.21	47.8	56.7	.760	.018
14	16.9	4.426	.078	49.8	59.0	.711	.018
15.9	19.2	1.585	.036	51.8	61.3	.621	.017
18	21.7	.981	.013	53.8	63.5	.535	.016
20	24.1	2.411	.021	57.9	68.1	.453	.016
22	26.5	3.079	.036	57.9	68.1	.418	.012
24	28.9	2.094	.025	61.9	72.5	.331	.010
26	31.3	1.496	.019	69.9	81.2	.201	.008
28	33.6	1.629	.042	77.8	89.5	.093	.008
30	36.0	1.742	.022	77.8	89.5	.090	.006
30.9	37.1	1.75	.15	81.8	93.7	.069	.005
31.8	38.1	1.53	.16	83.9	95.9	.065	.004
32	38.4	1.409	.021	85.9	97.9	.052	.005
32.9	39.4	1.02	.13	89.8	101.8	.047	.004
33.9	40.6	1.089	.058	97.9	109.8	.027	.003
34	40.7	1.064	.019	103.8	115.5	.024	.003
35.8	42.8	.844	.038	105.8	117.4	.0152	.0029
36	43.1	.945	.015	117.8	128.4	.0064	.0014
39.9	47.6	.971	.018				
41.9	49.9	.962	.026				

(continued)

80.8 MeV (continued)

4.97 MeV 2^-

θ_L (deg)	θ_{cm} (deg)	$d\sigma/d\Omega$ (mb/sr)	Δ (mb/sr)	θ_L (deg)	θ_{cm} (deg)	$d\sigma/d\Omega$ (mb/sr)	Δ (mb/sr)
11	13.3	.793	.061	41.9	50.0	.199	.012
11.9	14.4	.380	.052	43.9	52.3	.243	.011
14	16.9	.305	.020	45.9	54.6	.244	.010
18	21.7	.118	.004	47.8	56.8	.179	.017
20	24.1	.105	.004	47.8	56.8	.192	.009
22	26.5	.111	.007	49.8	59.0	.156	.008
24	28.9	.196	.008	51.8	61.3	.160	.008
26	31.3	.258	.008	53.8	63.6	.100	.007
28	33.7	.277	.017	57.9	68.1	.077	.007
30	36.0	.371	.010	57.9	68.1	.088	.006
30.9	37.1	.324	.062	61.9	72.6	.075	.005
31.8	38.2	.310	.073	69.9	81.3	.037	.003
32	38.4	.402	.011	77.8	89.6	.024	.003
32.9	39.5	.445	.089	81.8	93.8	.0126	.0021
33.9	40.6	.415	.036	83.9	95.9	.0103	.0017
34	40.7	.414	.012	85.9	98.0	.0090	.0022
35.8	42.8	.399	.026	89.8	101.9	.0062	.0015
36	43.1	.401	.010	97.9	109.9	.0045	.0012
37.9	45.3	.378	.011	103.8	115.6	.0012	.0006
38	45.4	.343	.013	105.8	117.4	.0027	.0012
39.9	47.6	.317	.010	117.8	128.5	.0015	.0007

(continued)

80.8 MeV (continued)

5.63/5.80 MeV $3^-/1^-$

θ_L (deg)	θ_{cm} (deg)	dσ/dΩ (mb/sr)	Δ (mb/sr)	θ_L (deg)	θ_{cm} (deg)	dσ/dΩ (mb/sr)	Δ (mb/sr)
11	13.3	24.42	.34	38	45.5	.701	.018
11.9	14.4	19.31	.37	39.9	47.7	.709	.016
13	15.7	13.61	.32	41.9	50.0	.765	.024
14	16.9	9.34	.11	43.9	52.3	.753	.020
15.9	19.2	3.55	.05	45.9	54.6	.716	.017
18	21.7	6.23	.06	47.8	56.8	.660	.032
22	26.5	5.81	.06	47.8	56.8	.613	.016
24	28.9	4.382	.037	49.8	59.1	.546	.015
26	31.3	3.570	.030	51.8	61.4	.552	.016
28	33.7	3.032	.057	53.8	63.6	.483	.015
30	36.1	2.414	.026	61.9	72.6	.241	.008
30.9	37.2	2.26	.16	69.9	81.3	.114	.006
31.8	38.2	1.48	.16	77.8	89.7	.043	.004
32	38.4	1.746	.023	81.8	93.9	.043	.004
32.9	39.5	1.44	.16	83.9	96.0	.028	.003
33.9	40.7	1.174	.060	85.9	98.1	.024	.004
34	40.8	1.177	.019	89.8	102.0	.0127	.0022
35.8	42.9	.857	.038	97.9	110.0	.0065	.0015
36	43.1	.849	.014	103.8	115.6	.0055	.0013
37.9	45.4	.676	.015	117.8	128.5	.0018	.0008

(continued)

$O^{16}(\alpha,\alpha')$

50 MeV

Elastic

θ_L (deg)	θ_{cm} (deg)	$d\sigma/d\Omega$ (mb/sr)	θ_L (deg)	θ_{cm} (deg)	$d\sigma/d\Omega$ (mb/sr)
8.3	9.8	235.5	24.3	30.3	13.7
9.3	11.6	373.9	25.3	31.5	31.0
10.3	12.8	662.8	26.3	32.8	37.7
11.3	14.1	169.8	28.3	35.2	47.4
12.3	15.3	16.9	30.3	37.7	36.1
13.2	16.5	14.7	32.2	39.9	22.2
13.3	16.6	36.2	32.3	40.1	2.52
14.3	17.8	133.4	33.7	41.7	14.2
15.2	19.0	162.7	34.2	42.3	6.50
15.3	19.1	447.0	38.5	47.6	16.3
16.3	20.3	235.5	40.2	49.6	17.5
17.3	21.5	226.9	42.2	51.9	14.4
18.2	22.7	187.9	44.2	54.3	9.61
18.3	22.8	184.8	46.2	56.7	5.48
19.3	24.0	125.8	50.2	61.4	2.41
20.2	25.2	82.4	52.2	63.7	2.07
20.3	25.3	69.6	54.2	66.0	1.58
21.3	26.6	25.3	58.2	70.6	.762
22.2	27.7	12.9	64.7	77.9	1.074
22.3	27.8	6.88	66.7	80.6	1.25
23.3	29.1	6.44	68.7	82.3	1.55

(continued)

50 MeV (continued)

6.137 MeV 3^-

θ_L (deg)	θ_{cm} (deg)	$d\sigma/d\Omega$ (mb/sr)	θ_L (deg)	θ_{cm} (deg)	$d\sigma/d\Omega$ (mb/sr)
9.3	11.7	16.7	26.3	33.2	8.15
11.3	14.4	21.3	28.3	35.6	6.92
12.3	15.7	23.6	30.3	38.1	4.55
13.2	16.8	22.4	32.2	40.6	2.87
14.3	18.2	23.9	32.3	40.6	2.82
15.2	19.3	22.2	33.7	42.4	2.18
15.3	19.5	42.7	34.2	43.0	1.02
16.3	20.7	19.3	38.5	48.1	3.12
17.3	22.0	16.3	40.2	50.4	3.62
18.2	23.1	13.5	42.2	52.8	3.23
18.3	23.2	13.0	44.2	55.2	2.58
19.3	24.5	9.92	46.2	57.6	2.02
20.2	25.6	7.79	50.2	62.3	1.72
20.3	25.8	7.76	52.2	64.7	1.70
21.3	27.0	6.22	54.2	67.0	1.57
22.2	28.1	5.40	58.2	71.6	1.40
22.3	28.3	6.00	64.7	79.0	1.00
23.3	29.5	6.49	66.7	81.3	1.03
24.3	30.8	7.30	68.7	83.5	1.02
25.3	32.0	7.84			

(continued)

50 MeV (continued)

6.918 MeV 2^+			7.118 MeV 1^-			8.876 MeV 2^-		
θ_L (deg)	θ_{cm} (deg)	$d\sigma/d\Omega$ (mb/sr)	θ_L (deg)	θ_{cm} (deg)	$d\sigma/d\Omega$ (mb/sr)	θ_L (deg)	θ_{cm} (deg)	$d\sigma/d\Omega$ (mb/sr)
9.3	11.7	14.6	9.3	11.8	3.29	9.3	11.8	1.82
11.3	14.4	12.3	11.3	14.4	.005	10.3	13.2	1.45
12.3	15.7	9.94	12.3	15.7	1.15	12.3	15.7	1.63
13.2	16.9	7.87	13.2	16.8	1.50	13.2	16.9	1.41
14.3	18.2	2.91	14.3	18.2	3.80	14.3	18.4	1.26
15.2	19.4	4.04	15.2	19.4	2.85	15.2	19.5	1.29
15.3	19.5	6.84	15.3	19.5	6.28	15.3	19.6	2.38
16.3	20.8	2.85	16.3	20.8	3.16	16.3	20.9	.946
17.3	22.0	2.87	17.3	22.1	2.96	17.3	22.2	.793
18.2	23.2	2.95	18.2	23.2	2.97	18.2	23.3	.678
18.3	23.3	3.40	18.3	23.3	2.88	18.3	23.4	.393
19.3	24.6	4.20	19.3	24.6	2.37	19.3	24.7	.402
20.2	25.7	3.87	20.2	25.7	2.00	20.2	25.9	.377
20.3	25.8	4.48	20.3	25.8	2.05	20.3	26.0	.320
21.3	27.0	4.45	21.3	27.1	1.77	21.3	27.3	.257
22.2	28.2	3.88	22.2	28.2	1.72	22.3	28.5	.243
22.3	28.4	4.26	22.3	28.4	1.82	23.3	29.8	.239
23.3	29.6	3.55	23.3	29.6	2.05	24.3	31.1	.348
24.3	30.9	3.02	24.3	30.9	2.28	25.3	32.3	.329
25.3	32.1	1.94	25.3	32.1	2.48	26.3	33.5	.392
26.3	33.2	1.46	26.3	33.3	2.53	28.3	36.1	.383
28.3	35.9	.968	28.3	35.9	2.15	30.3	38.6	.293
30.3	38.4	1.27	30.3	38.4	1.40	32.2	40.9	.154
32.2	40.7	1.31	32.2	40.7	.838	32.3	41.1	.203
32.3	40.8	1.82	32.3	40.9	.597	33.7	42.8	.140
33.7	42.5	1.38	33.7	42.6	.611	34.2	43.3	.062
38.5	48.4	1.01	38.5	48.5	.699	38.5	48.7	.208
40.2	50.5	.924	40.2	50.5	.817	40.2	50.8	.340
42.2	52.9	.827	42.2	53.0	1.04	42.2	53.3	.392
44.2	55.3	.915	44.2	55.4	.983	44.2	55.7	.417
50.2	62.5	.535	50.2	62.5	1.43	46.2	58.1	.405
54.2	67.2	.254	54.2	67.2	1.39	50.2	62.9	.378
						52.2	65.2	.385
						54.2	67.6	.384
						58.2	72.2	.332
						64.7	79.7	.328
						66.7	81.9	.300
						68.7	84.1	.265

$O^{16}(\alpha,\alpha')$

80.7 MeV

g.s. 0^+

θ_L (deg)	θ_{cm} (deg)	$d\sigma/d\Omega$ (mb/sr)	Δ (mb/sr)	θ_L (deg)	θ_{cm} (deg)	$d\sigma/d\Omega$ (mb/sr)	Δ (mb/sr)
10	12.5	24.07	.76	32	39.7	10.62	.14
11	13.8	82.08	.20	32	39.7	10.67	.08
12	15.0	180.5	2.1	32	39.7	9.800	.064
12	15.0	299.7	.3	33	40.9	10.73	.13
12	15.0	228.8	.9	33	40.9	9.944	.081
13	16.3	350.9	1.9	34	42.1	9.69	.13
13	16.3	323.2	.4	34	42.1	9.153	.064
14	17.5	277.7	2.6	35	43.3	9.22	.12
14	17.5	315.7	1.1	35	43.3	8.330	.062
14	17.5	324.0	.4	36	44.5	7.625	.051
15	18.8	321.5	1.9	36	44.5	7.626	.060
15	18.8	247.2	.3	37	45.8	7.488	.085
16	20.0	163.3	2.0	38	47.0	7.692	.053
16	20.0	150.1	.8	38	47.0	7.495	.077
16	20.0	167.7	.3	38	47.0	7.20	.06
17	21.2	111.8	1.1	38	47.0	7.57	.11
18	22.5	39.32	.39	39	48.2	7.609	.086
18	22.5	41.83	.14	40	49.4	8.290	.056
19	23.7	32.51	.59	40	49.4	8.518	.083
20	25.0	34.56	.29	40	49.4	7.617	.062
20	25.0	35.13	.14	41	50.5	8.226	.090
21	26.2	43.35	.26	41	50.5	7.935	.056
21	26.2	45.53	.14	42	51.7	8.822	.057
22	27.4	52.46	.37	42	51.7	8.751	.085
23	28.7	49.07	.27	42	51.7	8.085	.057
24	29.9	39.48	.32	43	52.9	8.553	.093
24	29.9	41.66	.14	44	54.1	8.337	.089
25	31.1	30.53	.21	44	54.1	8.358	.083
26	32.4	16.74	.21	44	54.1	8.39	.13
26	32.4	17.20	.10	44	54.1	7.950	.058
27	33.6	10.87	.14	46	56.5	7.349	.082
28	34.8	6.82	.11	46	56.5	7.41	.12
29	36.0	6.67	.10	46	56.5	7.217	.056
30	37.3	8.18	.12	48	58.8	6.227	.078
30	37.3	7.989	.070	48	58.8	6.21	.11
31	38.5	9.38	.12	48	58.8	6.035	.053
31	38.5	9.004	.074	50	61.2	5.003	.069

(continued)

80.7 MeV (continued)

g.s. 0^+							
θ_L (deg)	θ_{cm} (deg)	$d\sigma/d\Omega$ (mb/sr)	Δ (mb/sr)	θ_L (deg)	θ_{cm} (deg)	$d\sigma/d\Omega$ (mb/sr)	Δ (mb/sr)
50	61.2	5.11	.10	68	81.5	.781	.013
50	61.2	5.062	.049	68	81.5	.745	.025
52	63.5	4.471	.088	70	83.7	.648	.012
52	63.5	4.368	.047	72	85.9	.511	.012
54	65.8	3.938	.084	74	88.0	.419	.010
56	68.1	3.262	.077	76	90.2	.343	.014
58	70.4	2.767	.071	78	92.3	.243	.012
60	72.6	2.266	.034	80	94.4	.187	.011
62	74.9	1.716	.030	82	96.5	.165	.010
64	77.1	1.277	.026	84	98.5	.116	.011
64	77.1	1.278	.031	86	100.6	.109	.010
66	79.3	1.007	.023	88	102.6	.0692	.0083
66	79.3	1.007	.029	90	104.6	.0787	.0090

(continued)

80.7 MeV (continued)

θ_L (deg)	θ_{cm} (deg)	$d\sigma/d\Omega$ (mb/sr)	Δ (mb/sr)	θ_L (deg)	θ_{cm} (deg)	$d\sigma/d\Omega$ (mb/sr)	Δ (mb/sr)
			6.137 MeV 3^-				
10	12.6	25.06	.76	34	42.5	2.749	.035
11	13.9	28.10	.11	35	43.8	2.108	.057
12	15.2	21.81	.71	35	43.8	2.353	.033
12	15.2	24.99	.09	36	45.0	2.130	.029
12	15.2	22.88	.30	36	45.0	2.139	.031
13	16.4	24.02	.49	37	46.2	2.112	.045
13	16.4	19.41	.10	38	47.4	2.046	.027
14	17.7	13.35	.56	38	47.4	2.025	.040
14	17.7	13.96	.23	38	47.4	1.81	.03
14	17.7	13.75	.07	38	47.4	2.114	.057
15	18.9	11.30	.35	39	48.6	2.110	.045
15	18.9	8.294	.059	40	49.8	2.202	.028
16	20.2	4.46	.32	40	49.8	2.240	.042
16	20.2	4.64	.13	40	49.8	2.021	.032
16	20.2	4.937	.046	41	51.0	2.008	.044
17	21.5	4.02	.20	41	51.0	2.032	.028
18	22.7	4.35	.12	42	52.2	2.244	.029
18	22.7	4.026	.044	42	52.2	2.080	.029
19	24.0	6.45	.26	44	54.6	2.187	.045
20	25.2	7.32	.13	44	54.6	2.133	.063
20	25.2	7.335	.062	44	54.6	2.039	.029
21	26.5	8.26	.11	46	57.0	2.124	.045
21	26.5	8.319	.059	46	57.0	2.001	.062
22	27.7	8.63	.15	46	57.0	1.935	.029
22	27.7	7.975	.059	48	59.4	1.868	.041
23	29.0	7.73	.11	48	59.4	1.904	.061
24	30.2	6.15	.12	48	59.4	1.708	.028
24	30.2	6.049	.054	50	61.7	1.603	.040
25	31.4	5.290	.089	50	61.7	1.650	.057
26	32.7	4.552	.107	50	61.7	1.589	.027
26	32.7	3.984	.045	52	64.1	1.515	.051
30	37.6	3.817	.048	52	64.1	1.451	.027
31	38.9	3.580	.046	54	66.4	1.383	.049
32	40.1	3.554	.048	56	68.7	1.166	.046
32	40.1	3.334	.037	58	71.0	.946	.042
33	41.3	3.078	.045	66	80.0	.579	.017
34	42.5	2.488	.049	66	80.0	.491	.019
34	42.5	2.461	.066	68	82.2	.460	.010

(continued)

80.7 MeV (continued)

6.137 MeV 3^-

θ_L (deg)	θ_{cm} (deg)	dσ/dΩ (mb/sr)	Δ (mb/sr)	θ_L (deg)	θ_{cm} (deg)	dσ/dΩ (mb/sr)	Δ (mb/sr)
68	82.2	.481	.019	80	95.1	.176	.010
70	84.4	.412	.010	82	97.2	.153	.010
72	86.7	.326	.008	84	99.3	.117	.011
74	88.8	.283	.008	86	101.3	.120	.011
76	90.9	.267	.013	88	103.4	.089	.009
78	93.0	.209	.011	90	105.4	.0748	.0088

(continued)

80.7 MeV (continued)

6.916/7.115 MeV $2^+/1^-$

θ_L (deg)	θ_{cm} (deg)	$d\sigma/d\Omega$ (mb/sr)	Δ (mb/sr)	θ_L (deg)	θ_{cm} (deg)	$d\sigma/d\Omega$ (mb/sr)	Δ (mb/sr)
10	12.7	15.07	.59	34	42.6	1.410	.037
12	15.2	6.96	.40	34	42.6	1.630	.054
12	15.2	6.61	.23	38	47.5	1.004	.039
13	16.5	6.05	.25	40	49.9	.620	.022
14	17.7	4.25	.32	41	51.1	.693	.026
14	17.7	5.00	.21	42	52.3	.684	.016
15	19.0	6.52	.26	42	52.3	.651	.023
16	20.2	5.51	.36	43	53.5	.616	.025
16	20.2	5.96	.17	44	54.7	.674	.025
17	21.5	6.99	.27	44	54.7	.644	.023
18	22.7	6.09	.15	44	54.7	.666	.035
19	24.0	6.84	.27	46	57.1	.664	.025
20	25.3	4.82	.11	46	57.1	.657	.036
20	25.3	5.009	.051	48	59.5	.674	.025
21	26.5	4.279	.079	48	59.5	.691	.037
21	26.5	4.225	.042	50	61.8	.675	.025
22	27.8	3.848	.098	50	61.8	.664	.036
23	29.0	3.704	.073	52	64.2	.597	.032
24	30.3	3.703	.096	54	66.5	.625	.033
24	30.3	3.820	.043	56	68.8	.540	.031
25	31.5	3.816	.076	58	71.1	.476	.029
26	32.7	3.748	.097	60	73.4	.451	.015
26	32.7	3.956	.045	62	75.7	.422	.015
27	34.0	3.535	.083	64	77.9	.329	.013
28	35.2	3.368	.055	72	86.7	.326	.008
28	35.2	3.466	.077	74	88.9	.169	.006
29	36.5	3.332	.071	76	91.0	.153	.010
30	37.7	2.861	.070	78	93.2	.126	.009
30	37.7	2.829	.041	80	95.3	.107	.008
31	38.9	2.441	.061	82	97.3	.0731	.0068
32	40.2	2.094	.044	84	99.4	.0636	.0078
32	40.2	2.093	.060	86	101.5	.0680	.0082
32	40.2	2.064	.036	88	103.5	.0591	.0077
33	41.4	1.835	.053	90	105.5	.0424	.0066

(continued)

80.7 MeV (continued)

8.876 MeV 2^-

θ_L (deg)	θ_{cm} (deg)	$d\sigma/d\Omega$ (mb/sr)	Δ (mb/sr)	θ_L (deg)	θ_{cm} (deg)	$d\sigma/d\Omega$ (mb/sr)	Δ (mb/sr)
11	14.0	.446	.014	41	51.3	.127	.007
12	15.2	.328	.010	42	52.5	.190	.009
13	16.5	.303	.013	44	54.9	.173	.008
14	17.8	.260	.010	46	57.3	.154	.008
15	19.0	.211	.009	48	59.7	.127	.008
16	20.3	.155	.008	50	62.0	.111	.007
18	22.8	.164	.009	52	64.4	.093	.007
20	25.3	.291	.012	56	69.0	.0464	.0091
21	26.6	.346	.012	58	71.3	.0390	.0084
22	27.9	.323	.012	60	73.6	.0351	.0042
24	30.4	.374	.013	62	75.9	.0326	.0041
26	32.9	.333	.013	64	78.1	.0209	.0033
30	37.8	.211	.011	64	78.1	.0231	.0043
31	39.1	.314	.014	66	80.4	.0237	.0035
32	40.3	.223	.012	66	80.4	.0188	.0039
32	40.3	.272	.011	68	82.6	.0153	.0020
33	41.5	.283	.014	68	82.6	.0079	.0026
34	42.8	.220	.010	74	89.1	.0147	.0020
35	44.0	.245	.010	76	91.3	.0105	.0025
36	45.2	.216	.010	86	101.7	.0094	.0030
38	47.6	.21	.01	88	103.7	.0064	.0025
38	47.6	.153	.015	90	105.8	.0090	.0030
40	50.1	.202	.010				

REFERENCES

1. W. W. Eidson and J. G. Cramer, Phys. Rev. Letters 9, 497 (1962).
2. W. J. Braithwaite, J. G. Cramer and R. A. Hinrichs, Inelastic Excitation of Unnatural-Parity States, in Nuclear Physics Laboratory Annual Report, University of Washington, June 1966, p. 18.
3. F. W. Bingham, Phys. Rev. 145, 901 (1966).
4. J. Kokame, K. Fukunaga, N. Inoue and H. Nakamura, Phys. Letters 8, 342 (1964).
5. J. S. Vincent, E. T. Boschitz and J. R. Priest, Bull. Am. Phys. Soc. 11, 333 (1966).
6. J. S. Vincent, E. T. Boschitz and J. R. Priest, Phys. Letters 25B, 81 (1967).
7. R. E. Malmin, P. P. Singh, D. W. Devins, J. G. Wills, C. R. Bingham and M. L. Halbert, Bull. Am. Phys. Soc. 13, 117 (1968).
8. J. S. Blair, N. Cue and D. Shreve, Inelastic α-Particle Scattering from ^{16}O, in Nuclear Physics Laboratory Annual Report, University of Washington, June 1965, p. 3.
9. J. S. Blair, Phys. Rev. 115, 928 (1959).
10. S. I. Drozdov, J. Exptl. Theoret. Phys. (U. S. S. R.) 28, 734 (1955); 28, 736 (1955). (Translation: Soviet Phys. JETP 1, 591, 588 (1955)).
11. E. V. Inopin, J. Exptl. Theoret. Phys. (U. S. S. R.) 31, 901 (1956). (Translation: Soviet Phys. JETP 4, 764 (1957)).
12. N. Austern and J. S. Blair, Ann. of Phys. 33, 15 (1965).
13. E. Rost and N. Austern, Phys. Rev. 120, 1375 (1960).
14. R. H. Bassel, G. R. Satchler, R. M. Drisko and E. Rost, Phys. Rev. 128, 2693 (1962).
15. B. L. Cohen, Phys. Rev. 116, 426(1959).
16. B. G. Harvey, D. L. Hendrie, O. N. Jarvis, J. Mahoney and J. Valentin, Excitation of Rotational Levels in ^{152}Sm and ^{154}Sm, UCRL-17303, 1966.
17. D. K. McDaniels, J. S. Blair, S. W. Chen, and G. W. Farwell, Nucl. Phys. 17, 614(1960).
18. M. A. Preston, Physics of the Nucleus (Addison-Wesley Publishing Company, Inc., Reading, Mass., 1962).

19. T. Honda and H. Ui, Nucl. Phys. 34, 593 (1962).
20. F. Ajzenberg-Selove and T. Lauritsen, Nucl. Phys. 11, 1 (1959).
21. P. M. Endt and C. Van Der Leun, Nucl. Phys. A105, 1 (1967).
22. E. L. Kelly, General Description and Operating Characteristics of the Berkeley 88-Inch Cyclotron in Proceedings of the International Conference on Sector-Focused Cyclotrons, Los Angeles, April 1962, Nucl. Instr. Methods 18, 19, 33 (1962).
23. B. G. Harvey, unpublished magnet notes.
24. A. Septier, Focusing of Charged Particles (Academic Press, New York, 1967).
25. D. Judd, Brobeck Associates Report, "Study of Ion Optical Theory and Design for the University of Colorado," Report No. 200-57-R1, July 1960.
26. C. F. Williamson, J-P. Boujot and J. Picard, Tables of Range and Stopping Power of Chemical Elements for Charged Particles of Energy 0.05 to 500 MeV, CEA-R3042, 1966.
27. G. Dearnaley and D. C. Northrop, Semiconductor Counters for Nuclear Radiations (John Wiley Inc., New York, 1963).
28. F. S. Goulding, Semiconductors for Nuclear Spectrometry. UCRL-16231, July 1965.
29. F. S. Goulding and W. L. Hansen, An Automatic Lithium Drifting Apparatus for Silicon and Germanium Detectors, UCRL-11261, Feb. 1964.
30. F. S. Goulding and D. Landis, Linear Amplifier, Gating and Timing System, in Instrumentation Techniques in Nuclear Pulse Analysis (National Academy of Sciences, Publication 1184, 1964).
31. E. A. Silverstein, Nucl. Instr. Methods 4, 53 (1959).
32. A. Springer, Scattering of 50.9 MeV α Particles from ^{20}Ne and ^{40}Ca. (Ph.D. thesis), UCRL-11681, May 1965.
33. J. Moss and G. C. Ball, Energy Resolution in Cyclotron Experiments, UCRL-17124, Sept. 1966.
34. C. M. Lederer, J. M. Hollander and I. Perlman, Table of Isotopes (John Wiley and Sons, Inc., New York, 1967).
35. P. M. Endt and C. Van Der Leurs, Nucl. Phys. 34, 1 (1962).

36. D. L. Hendrie, B. G. Harvey, J. Mahoney, and J. R. Meriwether, The $^{24}Mg(\alpha,\alpha')$ Reaction at 50 MeV in Nuclear Chemistry Annual Report UCRL-17299, January 1967.

37. J. A. Kuehner and J. D. Pearson, Canadian Journal of Phys. 43, 477 (1964).

38. A. Springer and B. G. Harvey, Phys. Rev. Letters 14, 316 (1965).

39. B. G. Harvey, J. R. Meriwether, J. Mahoney, A. Bussiere de Nercy and D. J. Horen, Phys. Rev. 146, 712 (1966).

40. B. G. Harvey, E. J-M. Rivet, A. Springer, J. R. Meriwether, W. B. Jones, J. H. Elliott and P. Darruilat, Nucl. Phys. 52, 465 (1964).

41. J. A. Kuehner and E. Almqvist, Bull. Am. Phys. Soc. 10, 37 (1965).

42. A. V. Cohen and J. A. Cookson, Nucl. Phys. 29, 604 (1962).

43. A. E. Litherland, J. A. Kuehner, H. E. Grove, M. A. Clark and E. Almqvist, Phys. Rev. Letters 7, 98 (1961).

44. D. M. Brink and G. F. Nash, Nucl. Phys. 40, 608 (1963).

45. J. P. Elliott and B. H. Flowers, Proc. Roy. Soc. 242, 57 (1957).

46. P. H. Stelson and L. Grodzins, Nucl. Data 1, 21 (1965).

47. W. Hauser and H. Feshbach, Phys. Rev. 87, 366 (1952).

48. W. R. Smith, A General Hauser-Feshbach Nuclear-Scattering Computer Program, ORNL-TM-1117, May 1965.

49. W. R. Smith, The Hauser-Feshbach Nuclear Scattering Computer Code LIANA, ORNL-TM-1234, Sept. 1965.

50. H. Feshbach, M. M. Shapiro and V. F. Weisskopf, Tables of Penetrabilities for Charged Particle Reaction, NYO-3077, June 1953.

51. J. M. Blatt and V. F. Weisskopf, Theoretical Nuclear Physics (John Wiley and Sons, Inc., New York 1952) p. 371.

52. N. K. Glendenning, Lectures: Inelastic Scattering and Nuclear Structure, UCRL-17503, 1967.

53. T. Tamura, Reviews Mod. Phys. 37, 679 (1965).

54. A. K. Kerman, Nuclear Rotational Motion, in Nuclear Reactions, vol. I, edited by P. M. Endt and M. Demeur (North-Holland Publishing Company, Amsterdam, 1959).

55. M. A. Melkanoff, T. Swada and J. Raynal, SEEK: A Fortran Program for

Automatic Searches in Elastic Scattering Analyses with the Nuclear Optical Model, UCLA Report 66-10, 1966.

56. H. H. Duhm, Private Communication.

57. I. M. Naqib, Excitation of Nuclear Levels in ^{24}Mg, ^{27}Al and ^{12}C through Inelastic Scattering of α Particles, Ph.D. Thesis, University of Washington, 1962.

58. T. Tamura, Nucl. Phys. 73, 241 (1965).

59. C. R. Gruhn and N. S. Wall, Nucl. Phys. 81, 161 (1966).